MECHANICAL STRATIGRAPHIC MODEL OF THE EAGLE FORD FORMATION, SOUTH AND WEST TEXAS

A Dissertation

by

GUANGJIAN XU

Submitted to the Office of Graduate and Professional Studies of
Texas A&M University
in partial fulfillment of the requirements for the degree of

DOCTOR OF PHILOSOPHY

Chair of Committee,	Judith S. Chester
Committee Members,	Frederick M. Chester
	Hiroko Kitajima
	Mukul Bhatia
	Michael Pope
	Daniel Hill
Head of Department,	Michael Pope

August 2019

Major Subject: Geology

ABSTRACT

Mechanical stratigraphy strongly impacts the growth of hydraulic fractures in shale reservoirs. Without a complete understanding of the properties of the target and surrounding intervals, it is hard to predict the bulk mechanical response of these zones, including the surrounding layers. Due to limited access to the core from productive fields, a complete mechanical characterization often is lacking. Outcrop and core from a condensate producing reservoir provide a great opportunity to characterize the geomechanical properties of individual and composite lithologic units of the Cretaceous carbonaceous Eagle Ford Formation over length scales of a decimeter to tens of meters. This study employs extensive triaxial deformation experiments on samples of the Eagle Ford Formation, as well as detailed lithostratigraphic characterizations of the sampled outcrop and subsurface well site, to define the elastic and inelastic properties and relate them to lithologic characteristics.

The Eagle Ford Formation exhibits a wide variation in elastic modulus as a function of carbonate facies. The reservoir rock samples also show a moderate pressure dependency when compared to the outcrop samples, especially under low-pressure conditions. The latter difference is likely related to crack-like pores and microcracks in the reservoir rocks that result from decompression. Under reservoir conditions, Young's modulus and Poisson's ratio increase by a factor of 4 and 1.5, respectively. Young's modulus and Poison's ratio increase similarly with an increase in carbonate content, and a decrease in organic matter and clay mineral fraction. Young's modulus also increases with an increase in the ratio of grains to mud-size particles, quantified by the grain

fraction. This latter relation is most significant for the mudstone and wackestone facies with relatively large mud matrix. Both Young's modulus and Poisson's ratio of the Eagle Ford Formation can display anisotropy with a directional variation of ~40%, most notably in micro-laminated and clay-rich rocks. The degree of anisotropy is positively correlated with clay mineral content, with the greatest change occurring in mud-supported facies.

The inelastic strength properties of yield strength, ultimate strength, and coefficient of sliding friction are determined as a function of confining pressure to quantify failure criteria and a fracture mode criterion appropriate to hydrofracture. The ultimate strength increases by a factor of 2 from the mudstone to packstone/grainstone facies. Ultimate strength increases gradually with confining pressure. All carbonate facies deformed by formation of brittle failure macroscopic faulting displaying the greatest localization under low-stress conditions. The angle of the failure plane is not sensitive to facies type, yet it does increase with confining pressure. Clay minerals have a significant impact on ultimate strength and decrease by 50% for clay contents ranging from 0 to ~10%. Yet increasing clay mineral content does not promote an increase in ductility over the conditions tested. The ultimate strength increases with increasing grain fraction for samples with 0-50% grain fraction with more subtle changes above 50%.

Based on the laboratory mechanical data, six brittleness indices are derived and compared with the mechanical properties. Most of the brittleness indices increase from the mud-supported to grain-supported facies. Young's modulus and ultimate strength show a positive trend with the composition-based brittleness and pre-fracture strain

based brittleness indices, suggesting that Young's modulus could be used to estimate brittleness of the formation if the rock fails in a predominantly brittle manner.

A mechanical stratigraphic model of the Eagle Ford Formation is constructed based on detailed lithostratigraphic descriptions of the Eagle Ford Formation using visual observations and a relatively simple lithologic classification scheme, and then applying average mechanical properties for each lithology, combined with simple averaging schemes, to determine the effective behavior of the multilayered formation. The mechanical properties of the Eagle Ford Formation vary systematically with mineralogy, composition, and textural characteristics (i.e., recrystallized grains, grain fraction), and effective confining pressure, which can be expressed with quantitative relationships. The experimental data also supports robust quantitative relationships between elastic and inelastic mechanical properties. Accordingly, a mechanical stratigraphic model describing inelastic behaviors including brittleness can be constructed indirectly from geophysical and rock physics interpretation of logging data.

DEDICATION

I dedicate my dissertation work to my family and many friends.

ACKNOWLEDGEMENTS

I would like to thank my committee chair, Prof. Judith Chester, and my committee members, Prof. Fred Chester, Prof. Hiroko Kitajima, Prof. Mukul Bhatia, Prof. Mike Pope, and Prof. Dan Hill, for their guidance, patience, and support throughout the course of this research.

Thanks also go to my friends and colleagues and the department faculty and staff for making my time at Texas A&M University a great experience.

Finally, thanks to my parents and husband for their encouragement and love.

CONTRIBUTORS AND FUNDING SOURCES

Contributors

This work was supervised by a dissertation committee consisting of Prof. Judith Chester, Prof. Fred Chester, Prof. Hiroko Kitajima, Prof. Mukul Bhatia, and Prof. Michael Pope of the Department of Geology and Geophysics and Professor Daniel Hill of the Department of Petroleum Engineering.

The borehole data of the Eagle Ford Formation in Lozier Canyon, West Texas analyzed for Section 4 was provided by BP America. The sample from the Eagle Ford reservoir rock and the corresponding well log data are provided by Professor Michael Tice. All other work conducted for the dissertation was completed by the student independently.

Funding Sources

Graduate study was supported by Berg-Hughes Center at Texas A&M University. This work was also made possible in part by AAPG graduate aid program and GCAGS scholarship.

TABLE OF CONTENTS

LIST OF FIGURES

LIST OF TABLES

Page

1. INTRODUCTION

1.1. Research Motivation

Successful and economically viable production from the Eagle Ford Formation relies on horizontal drilling and hydraulic fracturing. Shale gas reservoir typically consists of layered sequences with varying layer thicknesses, compositions, and textures. Composition and texture are significant factors that contribute to differences in physical properties (e.g., relative ductility) within a stratigraphic succession of shale rocks can be important to the development, extent, and complexity of fracturing during hydraulic stimulation (Teufel and Clark, 1984; Gu et al., 2006). Advanced geomechanical modeling of hydrofracture fracture processes in shale reservoir rocks can help us understand the effects of layering and variations in mechanical properties

One obstacle to the practical application of such models to guide completion in unconventional shale reservoirs, however, is the paucity of data defining the mechanical properties of distinct lithostratigraphic units and a mechanical definition of layering spanning scales important to fracture-propagation and reservoir models. The focus of this research is to develop a mechanical stratigraphic model for the Eagle Ford Formation on the basis of detailed descriptions of lithostratigraphy, and direct laboratory testing of distinct, representative lithostratigraphic units in order to determine the elastic and inelastic mechanical properties.

The basis and utility of developing mechanical stratigraphic models was demonstrated by numerous field and laboratory studies that identify relationships between styles of deformation in sedimentary rock (folding, faulting, and fracturing) to relative mechanical properties and layering characteristics of the stratigraphic sequences (e.g., Corbett et al., 1987; Chester et al., 1991; Helgeson and Aydin, 1991; Narr and Suppe, 1991; Gross et al., 1995; Goff et al., 1996; Rijken and Cooke, 2001; Lorenz et al. 2002; Chester, 2003; Ferrill and Morris, 2008; Morris et al., 2009; Ferrill et al., 2017). Relevant to unconventional reservoirs such as the Eagle Ford Formation, is that fracture characteristics (e.g., fracture-spacing, fracture lengths both parallel and perpendicular to layering and fracture orientation) often vary within a succession of interlayered rocks of different lithology (e.g., McGinnis et al., 2017). This concept is clearly illustrated in Eagle Ford Formation exposures along Antonio Creek of West Texas (Ferrill et al., 2014), where the regional fracture set clearly displays local differences in fracture-spacing and fracture-height between the interbedded organic-rich laminated mudstones and more massive-bedded foraminifera packstone (Fig. 1.1). The variation in fracture spacing with rock type reflects differences in layer thickness, layer interface friction, and elastic and inelastic properties of the layers (e.g., Papanastasiou et al., 1995; Engelder et al., 2009; Laubach et al., 2009; Ferrill et al., 2014).

To date, few published comprehensive studies have defined the relationship between mechanical properties and rock characteristics (e.g., composition, texture, and layering) of the Eagle Ford Formation. Experimental rock deformation tests are

performed to determine both elastic and inelastic mechanical properties as a function of confining pressure for a suite of Eagle Ford Formation samples representing distinct lithostratigraphic units defined in earlier works (e.g., Donovan et al. 2012, 2015, 2016; Gardner et al., 2013). The impact of pressure, rock type, mineralogy, and microstructure on rock mechanical behavior are investigated using controlled triaxial cyclic loading conditions to define elastic behavior of single lithologic units and composite layers. These data are augmented with geophysical log data from both locations to build a quantitative mechanical stratigraphic model for the Eagle Ford Formation that characterizes geomechanical properties for individual and composite lithologic units over a range of length scales from decimeter to tens of meters.

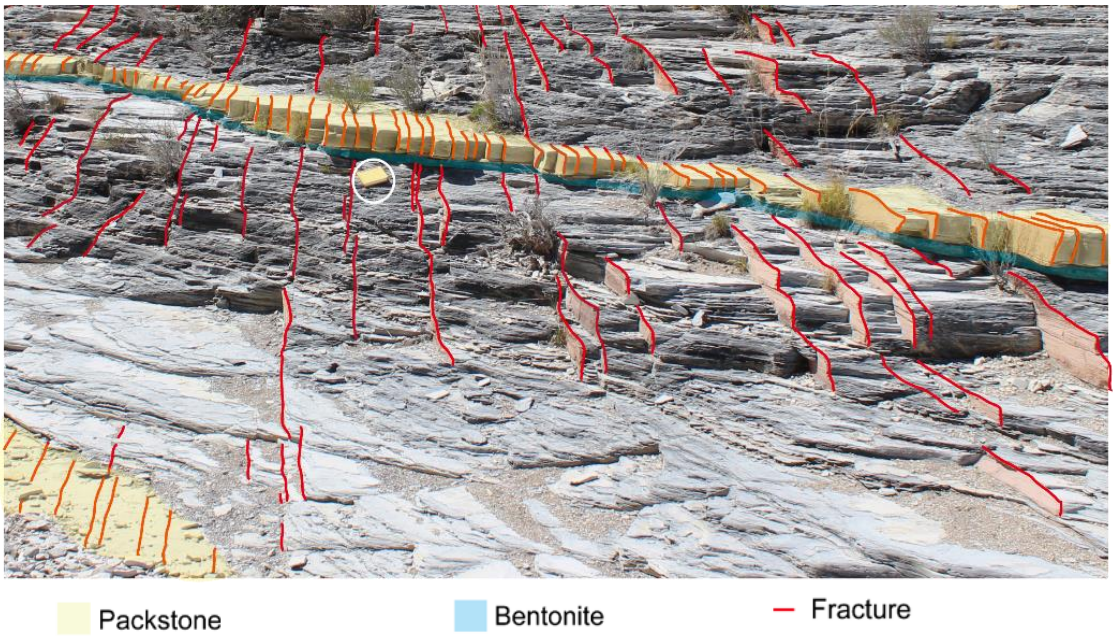

Figure 1.1 Eagle Ford Formation Outcrop in Antonio Creek (~22 km west of Langtry, TX) from Terrell County, West Texas. A variation in fracture intensity of a regional set of joints in interlayered packstone, mudstone, and bentonite beds is shown. Field notebook circled for scale. The photo was taken looking southwest.

The calcareous Eagle Ford Formation is one of the main prolific shale gas reservoirs in the United States, with calcite content ranging from 30 to 95% (Mcallister, 2017). This study focuses on two Eagle Ford Formation stratigraphic sections from outcrop and reservoir (Fig. 1.2). The variation in sedimentary facies, mineralogy, texture, geochemistry, and geophysical borehole signatures of the exposed Eagle Ford outcrop in West Texas has been extensively studied (e.g., Donovan et al., 2012, 2015, 2016; Gardner et al., 2013). The core samples are from a condensate liquid producing reservoir in McMullen County, South Texas, located 320 km east of the outcrop. Representative samples from main carbonate rock types were collected based on the

detailed stratigraphic characterization. Major facies identified in the Eagle Ford Formation outcrop include organic-rich mudstone, packstone, and packstone-grainstone, and , foraminiferal-wackestone, -packstone, and -grainstone (Fig. 1.3). Types of carbonate facies in the producing core are similar to those in outcrop, but the producing core is missing diagenesis-related facies, i.e., the packstone with dispersed pyrite nodules and the dolomitic packstone/grainstone. Abundant ash beds occur in both the outcrop and productive core sequences, with ash thicknesses ranging from a few mm to 15 cm. Overall, the producing subsurface section preserves greater amount of dark, calcareous organic-rich mudstone and less packstone to grainstone facies as the rocks were deposited in anoxia conditions on the distal portion of the carbonate platform and were buried to a greater depth than the outcrop section in Lozier Canyon. The thermal maturation of the Eagle Ford Formation is measured by vitrinite reflectance. The immature samples from the outcrop have an RO% around 0.6, and the maximum burial depth of the outcrop was interpreted to be ~ 2.8 km based on source rock evaluation (Tmax = 180 ℃) (Rose, 2016). The samples from the producing reservoir have thermal maturation (RO%) varying from 0.6 to 1.0. A burial history model (Gong and Rodriguez, 2017) suggests that the Eagle Ford Formation in this region was buried to a maximum depth of ~3.8 km during a rapid period of sedimentation.

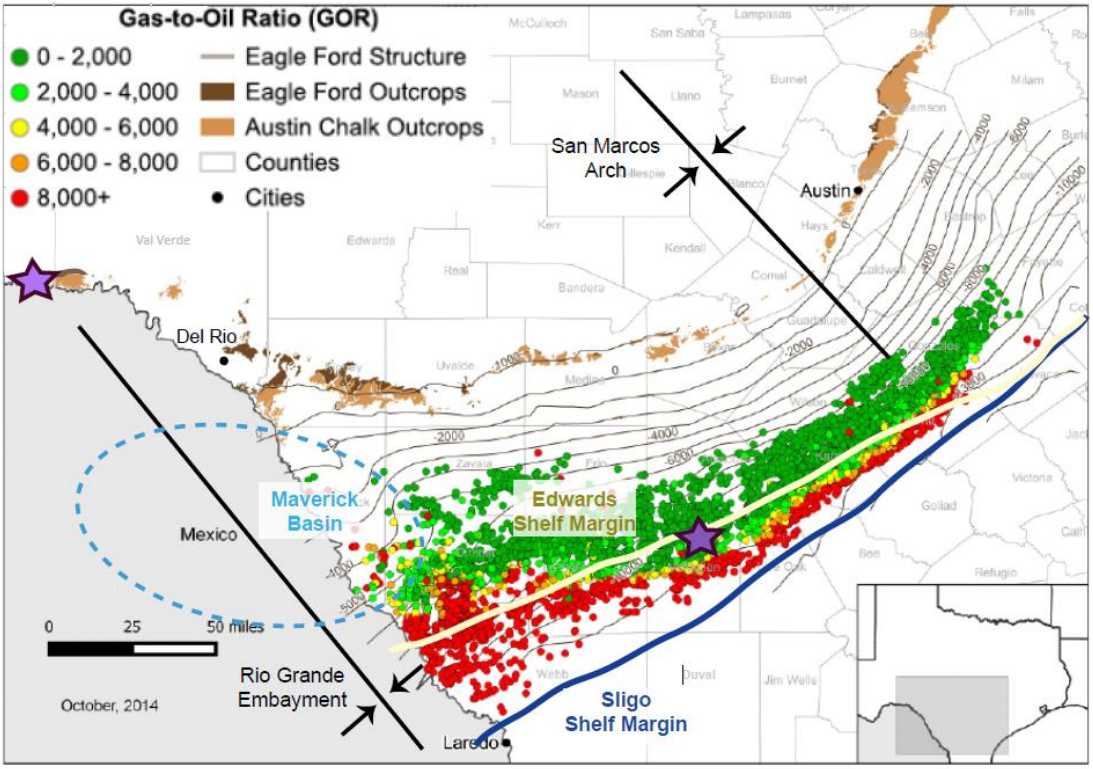

Figure 1.2 Gas-to-Oil ratio map for the Eagle Ford Formation. The outcrop and associated borehole samples for this study were collected at sites in Terrell and Val Verde Counties, Texas (blue star). Samples from the producing borehole are from McMullen County, Texas (black star). Figure is modified after the U.S. Energy Information Administration map (Jan. 21, 2015).

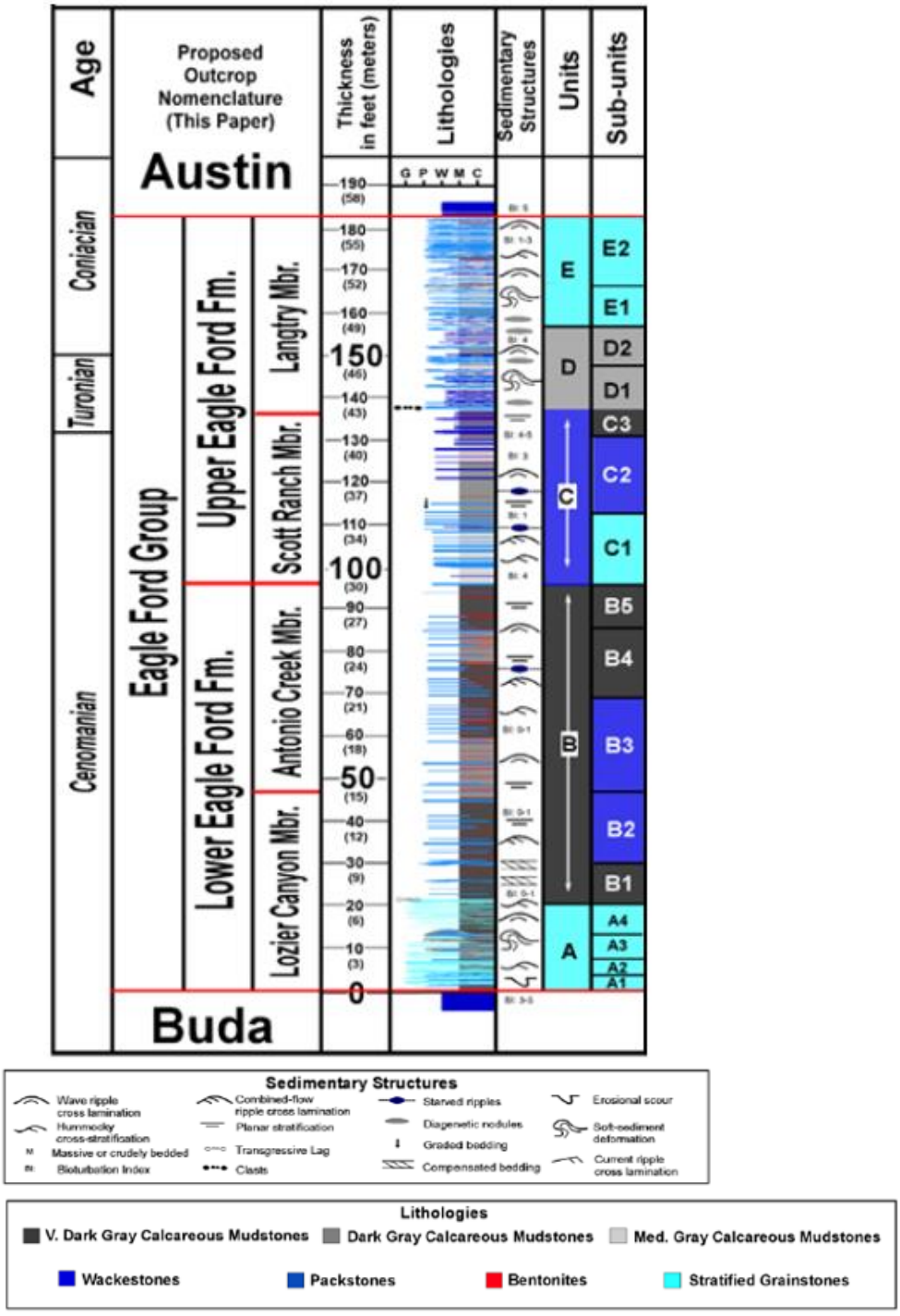

Figure 1.3 Lithostratigraphic description of the Eagle Ford section from the outcrop in Terrell County, West Texas. Figure from Gardner et al. (2013).

From the analysis of the data identified above, I will address the following questions and objectives.

1. What is the relationship between the mechanical properties and the composition and texture of the Eagle Ford Formation?

2. Is there an abrupt change in mechanical properties with grain fraction, representing a change from a matrix-supported to a grain-supported framework?

3. Do correlative outcrop and core samples show differences in mechanical behavior, and if so, what is the likely origin of the differences?

4. Can anisotropic elastic properties determined in experiments be explained in terms of a sample's textural and compositional laminations?

5. Can a mechanical stratigraphic model constructed on the basis of detailed lithostratigraphic sequences and informed by the mechanical properties determined through rock mechanics testing be used to upscale behaviors to a variety of length scales?

6. How does brittleness depend on confining pressure, and do brittleness indices determined from compositional data, pre-failure elastic properties, or dynamic elastic properties determined from logging, compare with brittleness determined directly through mechanical testing?

1.2. Thesis Outline

This thesis covers three topics through three Sections: correlation between rock composition, texture, and elastic properties of the Eagle Ford Formation under triaxial compression using outcrop and core samples (Section 2), triaxial inelastic deformation and brittleness of the Eagle Ford Formation as a function of composition and grain structure (Section 3), and application of laboratory rock geomechanical properties in reservoir exploration and production (Section 4)

In Section 2, elastic moduli (Young's modulus and Poisson's ratio) of the Eagle Ford Formation is determined through a series of triaxial compression tests. The elastic moduli are correlated with lithology, mineralogy, texture (grain fraction), and pressure. The carbonaceous Eagle Ford Formation shows a wide range in Young's modulus and Poisson's ratio. Elastic moduli increases from mud-supported facies to grain-supported carbonate facies. A positive relationship is found between rock carbonate minerals and elastic moduli. A negative relationship is found between clay content and QFP (quartz, feldspar, and pyrite) of the samples. The textural character of the rock estimated by grain fraction shows a great impact on Young's modulus, especially for mud-supported facies. Young's modulus stiffening is observed in reservoir samples and is found related to lithology, yet it is not obvious in the outcrop samples.

In Section 3, we measured and determined inelastic properties of the Eagle Ford samples including yield strength, ultimate strength, frictional sliding strength, ductility (plastic yielding prior to failure), uniaxial compressive strength (UCS), and failure

envelope. The relationship between mineralogy, texture, pressure and failure properties are analyzed. The Eagle Ford samples show a wide variation in rock strength under various confining pressures. With increasing confining pressure, the strength of the rock increases. The strength of the rock increases as an increase in the content of carbonate minerals and a decrease in clay content. Rock strength also shows a positive relationship with the numbers of grains (grain fraction) in the sample. In addition, failure properties are used to derive brittleness indices that show a similar relationship with rock composition and texture as rock strength.

In Section 4, based on laboratory geomechanical properties, a mechanical stratigraphic model on elastic and inelastic properties of the Eagle Ford Formation is created for outcrop and core sections. The model is upscaled and shows a good agreement with a mechanical model based on geophysical log data. Different brittleness indices of the Eagle Ford Formation are also assessed based on laboratory mechanical tests, geochemical, or wireline logs. These indices are well correlated with geomechanical properties (e.g., Young's modulus) and geophysical properties of the log. By quantifying the relationships between geomechanical properties and brittleness indices (e.g., Young's modulus vs. brittleness) and relationship among different brittleness indices, rock properties, especially inelastic properties can be estimated from geophysical logs.

1.3. References

Chester, J. S., Logan, J. M., and Spang, J.H., 1991. Influence of layering and boundary conditions on fault-bend and fault-propagation folding, Geol. Soc. Am. Bull., 103, 1059 – 1072.

Chester, F.M., Chester, J.S., Evans, J. P., Kirschner, D.L., Schulz, S.E., and Evans, J.P., 2003. Structure of large-displacement, strike-slip fault zones in the brittle continental crust. In: Karner, G., Garry, D., Taylor, B., Driscoll, N., Kohlstedt, D.L. (Eds.). Rheology and Deformation of the Lithosphere at Continental Margins, Columbia University Press, New York, MARGINS Theoretical and Experimental Earth Science Series I.

Corbett, K., Friedman, M. and Spang, J., 1987. Fracture development and mechanical stratigraphy of Austin Chalk, Texas. AAPG Bulletin, 71(1), pp.17-28.

Donovan, A. D., Staerker, T. S., Pramudito, A., Li, W., Corbett, M. J., Lowery, C. M., Romero, AA.M., and Gardner, R. D., 2012. The Eagle Ford outcrops of West Texas: A laboratory for understanding heterogeneities within unconventional mudstone reservoirs, GCAGS Journal, v. 1, p. 162-185.

Donovan, A. D., Gardner, R. D., Pramudito, A., Staerker, T. S., Wehner, M., Corbett, M. J., and Boling, K. S., 2015. Chronostratigraphic relationships of the woodbine and Eagle Ford Groups across Texas. GCAGS Journal. 4. 67-87.

Donovan, A.D., Staerker T.S., Gardner R., Pope M., Pramudito A., and Wehner M., 2016. Findings from the Eagle Ford outcrops of west Texas and implications to the subsurface of south Texas: in J. A. Breyer, ed., The Eagle Ford Shale: A renaissance in U.S. oil production: AAPG Memoir 110, p. 301–336.

Engelder, T., Lash, G.G. and Uzcátegui, R.S., 2009. Joint sets that enhance production from Middle and Upper Devonian gas shales of the Appalachian Basin. AAPG bulletin, 93(7), pp.857-889.

Ferrill, D. A., and Morris, A. P., 2008. Fault zone deformation controlled by carbonate mechanical stratigraphy, Balcones fault system, Texas. AAPG bulletin, 92(3), 359-380.

Ferrill, D.A., McGinnis, R.N., Morris, A.P., Smart, K.J., Sickmann, Z.T., Bentz, M., Lehrmann, D. and Evans, M.A., 2014. Control of mechanical stratigraphy on bed-restricted jointing and normal faulting: Eagle Ford Formation, south-central Texas. AAPG Bulletin, 98(11), pp.2477-2506.

Ferrill, D. A., Morris, A. P., McGinnis, R. N., Smart, K. J., Wigginton, S. S., and Hill, N. J., 2017. Mechanical stratigraphy and normal faulting. Journal of Structural Geology, 94, 275-302.

Gardner, R.D., Pope, M.C., Wehner, M.P., and Donovan, A., 2013. Comparative Stratigraphy of the Eagle Ford Group Strata in Lozier Canyon and Antonio Creek, Terrell County, Texas. GCAGS Journal, v. 2, p. 42–52.

Goff, F., 1996. Vesicle cylinders in vapor-differentiated basalt flows. Journal of Volcanology and Geothermal Research, 71(2-4), 167-185.

Gong C., and Rodriguez L., 2017. Challenges in Pore Pressure Prediction for Unconventional Petroleum Systems. Oral presentation given at AAPG Hedberg Conference, The Future of Basin and Petroleum Systems Modeling, Santa Barbara, California

Gross, M.R., Fischer, M.P., Engelder, T. and Greenfield, R.J., 1995. Factors controlling joint spacing in interbedded sedimentary rocks: integrating numerical models with field observations from the Monterey Formation, USA. Geological Society, London, Special Publications, 92(1), pp.215-233.'

Gu, H., and Siebrits, E., 2006. Effect of formation modulus contrast on hydraulic fracture height containment. In International Oil and Gas Conference and Exhibition in China. Society of Petroleum Engineers. 10.2523/103822-MS.

Helgeson, D. E., and Aydin, A., 1991. Characteristics of joint propagation across layer interfaces in sedimentary rocks. Journal of Structural Geology, 13(8), 897-911.

Laubach, S.E., Olson, J.E. and Gross, M.R., 2009. Mechanical and fracture stratigraphy. AAPG bulletin, 93(11), pp.1413-1426.

Lorenz, J.C., Sterling, J.L., Schechter, D.S., Whigham, C.L. and Jensen, J.L., 2002. Natural fractures in the Spraberry Formation, Midland basin, Texas: The effects of mechanical stratigraphy on fracture variability and reservoir behavior. AAPG bulletin, 86(3), pp.505-524.

McGinnis, R. N., Ferrill, D. A., Morris, A. P., Smart, K. J., and Lehrmann, D., 2017. Mechanical stratigraphic controls on natural fracture spacing and penetration. Journal of Structural Geology, 95, 160-170.

Mcallister, R. 2017. Diagenetic modifications of the Eagle Ford Formation: implications on chemical and physical properties. Doctoral dissertation, University of Manchester.

Morris, A.P., Ferrill, D.A. and McGinnis, R.N., 2009. Mechanical stratigraphy and faulting in Cretaceous carbonates. AAPG bulletin, 93(11), pp.1459-1470.

Narr, W., and Suppe, J., 1991. Joint spacing in sedimentary rocks. Journal of Structural Geology, 13(9), 1037-1048.

Papanastasiou, P., Thiercelin, M., Cook, J., and Durban, D., 1995. The influence of plastic yielding on breakdown pressure in hydraulic fracturing. In Rock mechanics, Proc. 35th US Symposium. pp. 281-286.

Rijken, P. and Cooke, M.L., 2001. Role of shale thickness on vertical connectivity of fractures: application of crack-bridging theory to the Austin Chalk, Texas. Tectonophysics, 337(1), pp.117-133.

Rose, Peter R, 2016. Late Cretaceous and Tertiary Burial History, Central Texas. GCAGS Journal 5: 141-179.

Teufel, L. W., Hart, C. M., Sattler, A. R., and Clark, J. A., 1984. Determination of hydraulic fracture azimuth by geophysical, geological, and oriented-core methods at the Multiwell Experiment Site, Rifle, CO. In SPE Annual Technical Conference and Exhibition. Society of Petroleum Engineers. SPE 13226.

2. CORRELATING COMPOSITION, TEXTURE, AND ELASTIC PROPERTIES OF THE EAGLE FORD FORMATION UNDER TRIAXIAL COMPRESSION USING OUTCROP AND CORE SAMPLES

2.1. Introduction

Successful and economically viable production from a shale gas reservoir relies on horizontal drilling and hydraulic fracturing. Shale gas reservoirs often are thick, heterogeneous sequences of mudrocks with varying mineralogy, organic carbon, bed thickness, and sedimentary structures at multiple scales. These compositional and textural variations can be significant and contribute to notable variations in mechanical properties (e.g., Young's modulus, Poissons's ratio), and can affect the formation, extent, and complexity of fracture, as well as fracture reactivation during hydraulic stimulation (e.g., Teufel and Clark, 1984; Gu et al., 2006; Suarez-Rivera et al., 2006; Li et al., 2015, Ma and Zoback, 2017).

Extensive laboratory studies have investigated the influence of pressure, temperature, and strain rate on the mechanical properties of shale rocks (e.g., Altowairqi et al., 2015; Bourg, 2015; Ibanez and Kronenberg, 1993; Josh et al. 2012; Kwon et al. 2001; Li et al., 2015; Li et al., 2016; Masri et al., 2014; Mokhtari et al., 2016; Niandou et al., 1997; Sone and Zoback, 2013a, b). These studies have evaluated different types of shale rocks from specific shale formations, and documented notable variability in behavior, especially in elastic properties. For example, Eagle Ford Formation samples with different carbonate content (60-80% versus 45-55%) display clear differences in

mechanical properties (e.g., static Young's modulus) that can vary by a factor of three (Sone and Zoback, 2013a and b). In addition to mineralogical variations, textural characteristics can impart a significant mechanical anisotropic response to loading. In a carbonate-rich rock like the Eagle Ford Formation, the distribution of grains, matrix, pores, stiff inclusions, and recrystallized zones can be significant in defining the response to loading. For instance, Young's modulus can increase significantly with an increase in the average number of grain-to-grain contacts if the grains serve as the stiff load-bearing framework relative to the matrix (e.g., Plumb, 1994). Bourg (2015) proposed that a threshold matrix content of 35% distinguishes a grain-supported texture from a mud-supported texture in shale rocks. The distribution of clay particles and organic matter in the form of laminae can strongly impact the degree of mechanical anisotropy at small length-scales (Sone and Zoback, 2013a; Mokhtari et al., 2016; Wu et al., 2016), and contribute to producing an anisotropic mechanical response at larger length-scales associated with bedding sequences.

The goal of this Section is to define the elastic mechanical properties of the Eagle Ford Formation for a specific suite of samples representing distinct lithostratigraphic units defined in earlier works (e.g., Donovan and Staerker, 2010, Donovan et al. 2012, 2016; Gardner et al. 2013). This sample suite is further distinguished on the basis of key characteristics (e.g., composition, texture and layering). These key characteristics are determined via mineralogy, texture, and microstructure analyses and are analyzed in terms of the role they play in defining the mechanical behavior and geophysical

properties at the individual layer scale. At the micron to mm scale, the distribution and packing of grains with different compositions and grain sizes often produce laminations that may serve as planes or zones of weakness. Stiff inclusions can serve as sites nucleation sites of deformation. Post-depositional processes such as diagenesis, organic-matter maturation, lithification, exhumation, and weathering also contribute to the heterogeneity of shale rocks and affect mechanical properties.

This study will focus on two stratigraphic sections of the Eagle Ford Formation, (1) the outcropping section exposed in Lozier Canyon and Antonio Creek, Terrell County, TX, that was measured and described in detail by Donovan et al. (2012; 2015) and Gardner et al. (2013), and the equivalent stratigraphic section captured in a continuous core also collected in Lozier Canyon (Donovan et al., 2015), and (2) a nearly complete stratigraphic section exposed in core provided by Apache Oil that was taken from the Swenson #1 borehole, a condensate-producing well in McMullen County (Donavan et al., 2015) (Fig. 2.1a).

2.2. Methods

2.2.1. Sample Selection

Previous studies provide detailed lithostratigraphic characterizations of the Eagle Ford Formation outcrops in Antonio Creek and Lozier Canyon (Donovan et al., 2012; Gardner et al., 2013). Bed lithology and thickness, fossil content, ichnofabric index (BI), sedimentary structures, and color were recorded at a ~30 cm scale interval in Antonio

Creek. The Antonio Creek section is correlated laterally with the outcrops in Lozier Canyon (Gardner et al., 2013).

The lithology of the Eagle Ford Formation from the Swenson core was described based on Dunham's (1962) carbonate rock classification, and sedimentary structures were described following Campbell's (1967) classification. The subsurface core characterization includes descriptions of lithology, bedding and lamination thicknesses, color, and sedimentary structures at the cm-scale. High-resolution XRF was performed on the core at a 5 mm resolution (Zeng et al., 2018). Samples to determine total organic carbon through Rock-Eval pyrolysis were collected every 30 cm, and kerogen type and maturity were determined every 1.8 m (Zeng et al., 2018).

The samples used for this study were chosen based on the data described above, and on available petrophysical logs. These samples represent the variation in composition, texture, and thermal maturation observed in outcrop and the Swenson core. The major carbonate facies identified in outcrop and the core include mudstone, foraminifera or skeletal wackestone, packstone, and grainstone. These facies are further distinguished by grain type (e.g., foraminifera tests, coccolith, skeletal grains) and sedimentary structures (e.g., laminated, bioturbated). The full suite of samples that were selected from the two geographic locations was further characterized in terms of mineralogy and texture through XRD, and optical and scanning electron microscopy.

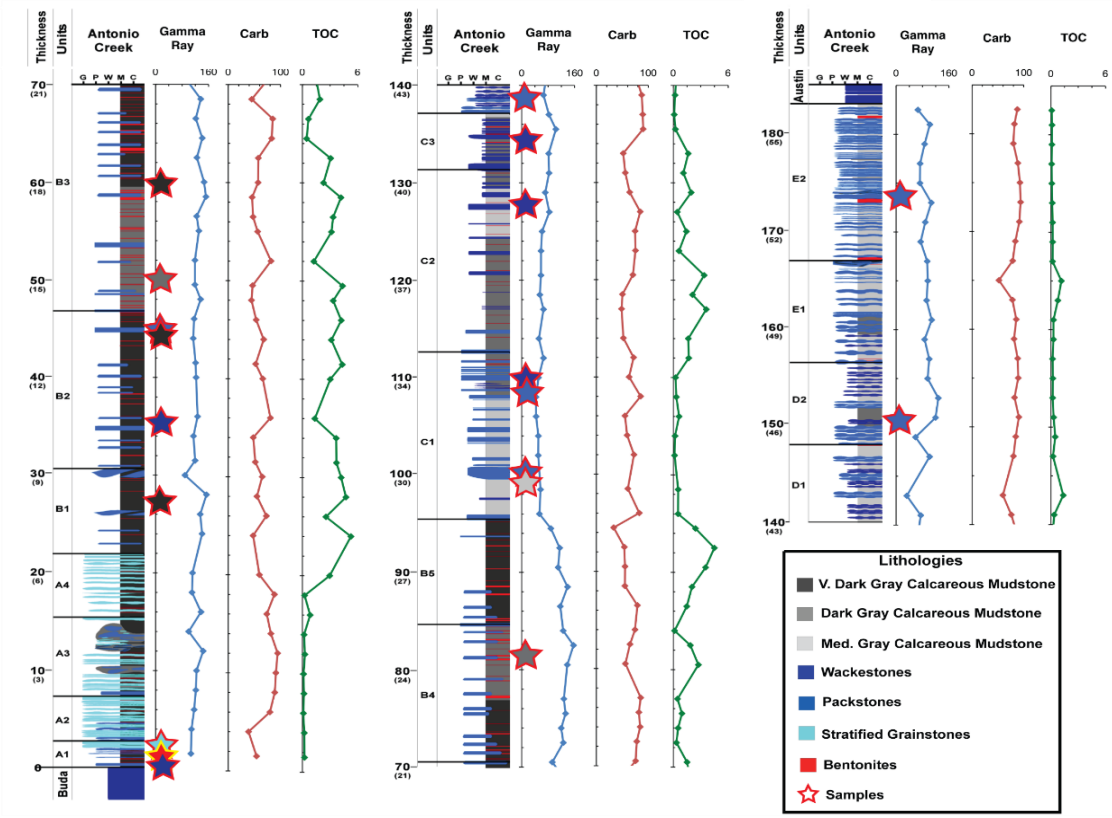

Figure 2.1 A detailed lithologic description of the Eagle Ford Formation outcrop in Antonio Creek, Terrell County, West Texas. Figure from Gardner et al. (2013). Colored stars indicate sample locations for the rock deformation tests. One of the samples collected at a road cut along highway 90, ~30 km away from the Antonio Creek is equivalent to B1/B2 unit.

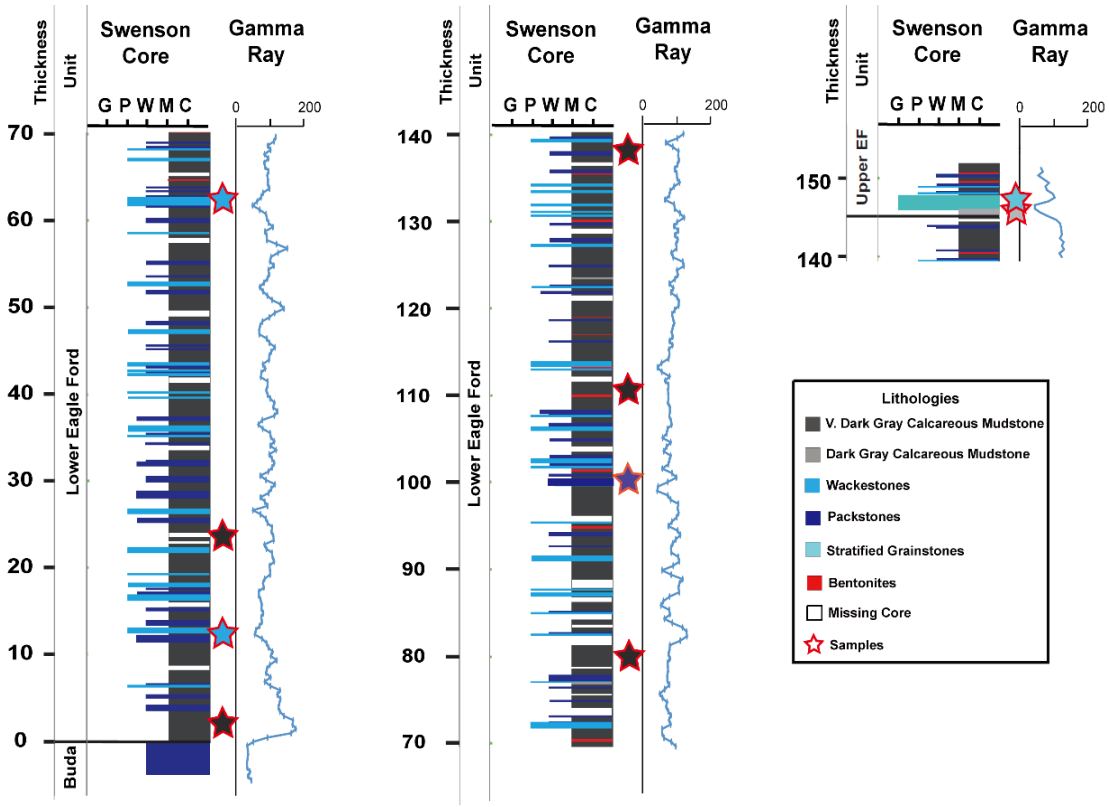

Figure 2.2 A detailed lithologic description of the Eagle Ford Formation Swenson #1 core in McMullen County, South Texas. Gamma Ray profile is plotted based on wireline log data. Colored stars indicate sample locations for the rock deformation tests.

2.2.2. Triaxial Experiments to Determine Elastic Properties

Multiple adjacent sub-cores were taken at specific horizons from each representative Eagle Ford Formation rock type. The right-circular cylinder sub-cores used for the elastic properties tests were 19 mm in diameter with a length to diameter ratio of approximately 2.25:1; this ratio minimizes end-effects during sample loading. A prism-shaped sample was cut from the host block for one of the delicate mudstones (an equivalent diameter of 15mm; sample 387; Table 2.3) because a cylindrical-shaped

sample could not be obtained. Sub-core samples were cut both perpendicular and parallel to laminations to allow quantification of anisotropic elastic behavior.

To determine elastic properties, a linear and a rosette strain gauge were used. These strain gauges were positioned across the central portion of each sample, spaced 180 °apart (Fig. 2.2). The linear strain gauge measured the Young's modulus of the middle 1/3 of the sub-core, parallel to the axial load. The rosette strain gauge measured both Young's modulus and Poisson's ratio of the same central area of the sample. Mechanical data was recorded at 10 Hz and recorded digitally at 1 Hz. The triaxial compression experiments were conducted using a modified variable strain-rate triaxial apparatus (MVSR) that is particularly well suited for testing fine-grained rocks. All samples were deformed at room-humidity, room temperature, and at a constant strain rate of 10^{-5} s^{-1}. In this apparatus, force is measured internal to the pressure vessel, and the strain was determined directly with strain gauges that were glued on the outside of the samples (Fig. 2.2).

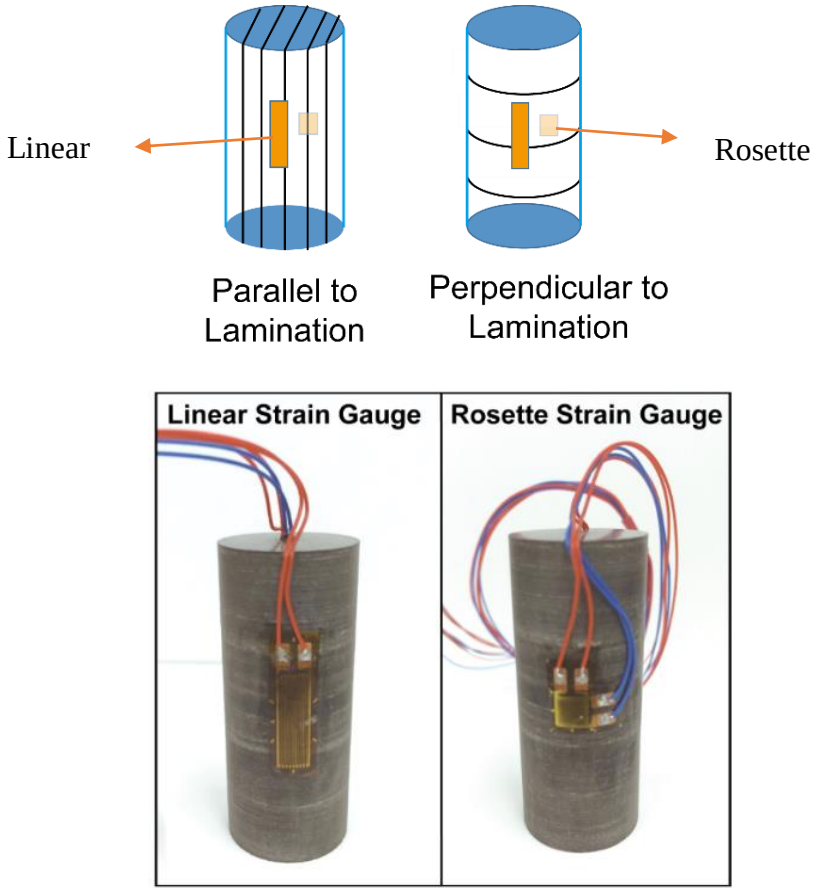

Figure 2.3 Setup for laboratory cylinder sample for elastic property testing. Two strain gauges are attached to the sample to determine elastic moduli.

Confining pressures between 1 MPa and 40 MPa were employed so as not to exceed analogous reservoir conditions, and to simulate lower effective pressure conditions appropriate for the hydrofracture treatments. Each sub-core was subjected to cyclic loading (Fig. 2.4) where the confining pressure was increased from 1, 3, 7, 15, and 40 MPa and then decreased back down to 1 MPa. Each sample was subjected to two load-unload cycles at each confining pressure step during increasing pressure steps, and one load-unload cycle during decreasing pressure steps. This load path was designed to

close pre-existing cracks during the first load cycle and therefore minimize the effect of pre-existing microcracks on the subsequent measurements (e.g., Sone and Zoback, 2013a). For each loading cycle, the elastic properties were determined by linear fitting over the differential stress range between 10 MPa and 30 MPa to eliminate the non-linear portion at low differential stress from the closure of soft crack-like pores. The Young's modulus of the sample was averaged from measurements provided by the linear and rosette strain gauges. At each pressure step, the reported elastic moduli of the samples were averaged from multiple load-unload cycles. When the elastic moduli from a loading cycle were more than 5% different than the other cycles it is excluded from the averaging step; this 5% difference typically occurs at the first loading cycle.

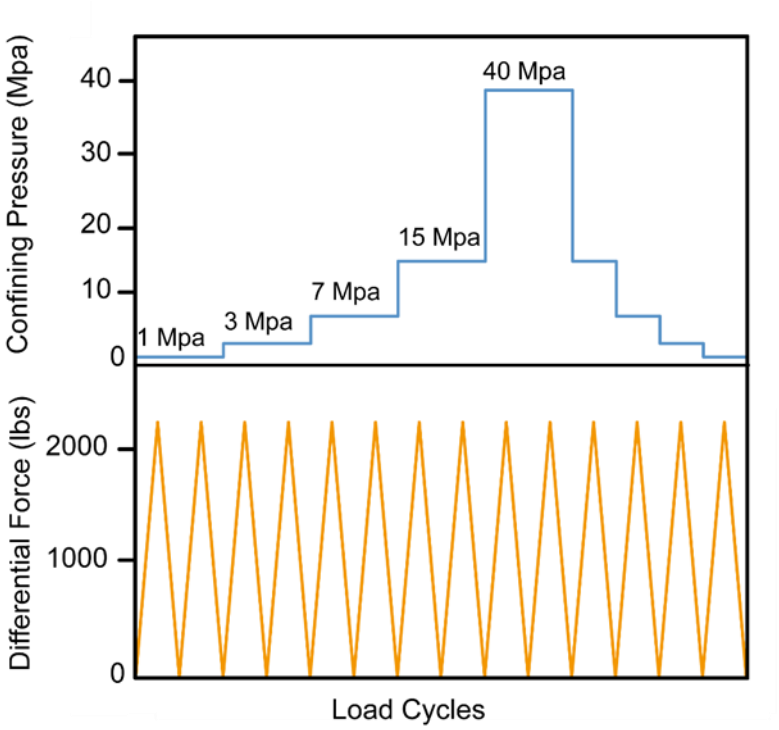

Figure 2.4 Load path used for elastic property tests. Two loading and unloading cycles are applied as confining pressure is increased and one cycle is applied during decreasing confining pressure step.

2.2.3. Triaxial Experiments to Determine Elastic Properties

A second set of sub-cores was collected adjacent to those used for the mechanical properties tests, over the exact same horizons. This second set of sub-cores was used to provide sample material for XRD analyses, and to make thin sections that were analyzed with optical and electron microscopy for composition, mineralogy, and textural characterizations.

The XRD analyses were run to provide bulk compositions of the representative sample horizons. Two grams of rock was taken from each sub-core across the exact

same horizon measured by the linear strain gauge. This sub-sample was ground to powder using a mortar and pestle, passed through a 63 μm sieve, and then further ground to a uniform powder with a particle size of 1-4 mm using a McCrone micronizing mill. The bulk mineralogy analyses were performed in the Petroleum Engineering Department at Texas A&M University.

Microstructural fabric analysis of the mudrock samples includes characterization of depositional features (e.g., laminations), spatial distributions of grains (larger than 30 μm) and mud particles. Minerals and phases were determined optically and through scanning electron microscopy, employing ImageJ ® to filter and threshold grey-scale plain-polarized micrographs (Fig. 2.5).

On each thin section, a sequence of 14 plane-polarized photomicrographs (34mm x 27mm) was taken under 4x magnification with the same light intensity using a Zeiss light microscope (Fig. 2.5). Neighboring micrographs are stitched together to create a mosaic micrograph with ~1/5 to 1/4 overlapping areas. A series of digital image processing steps were performed on each micrograph, including a background correction for light and a correction for thickness variations between thin sections. Due to the nature of the light source, the center of the micrograph was always brighter than the corners. The uneven distribution of brightness in each micrograph can create a large difference in light intensity level for the same phase/mineral in an image and impact the image analysis. To correct for this problem, a background image that captured the distribution of the light source was thus taken, under the same imaging conditions,

through a plain glass slide. To remove the uneven illumination, both the background images and plane-polarized micrographs were converted to gray-scale images. The plane-polarized micrograph was corrected by subtracting the background image to achieve a similar intensity level for each phase throughout the micrograph. The thin sections with variable thickness across the slide, resulting during preparation, were corrected by (1) taking intensity profiles across each micrograph in different orientations, (2) quantifying the intensity levels of a single phase (e.g., matrix) along each profile and determining the orientation of the fastest intensity variation, and (3) applying a background image which assumes a linear reduction of section thickness. After all corrections, 14 corrected gray-scale micrographs were then stitched together to create a mosaic image that covers the strain-gauged horizon of each sample.

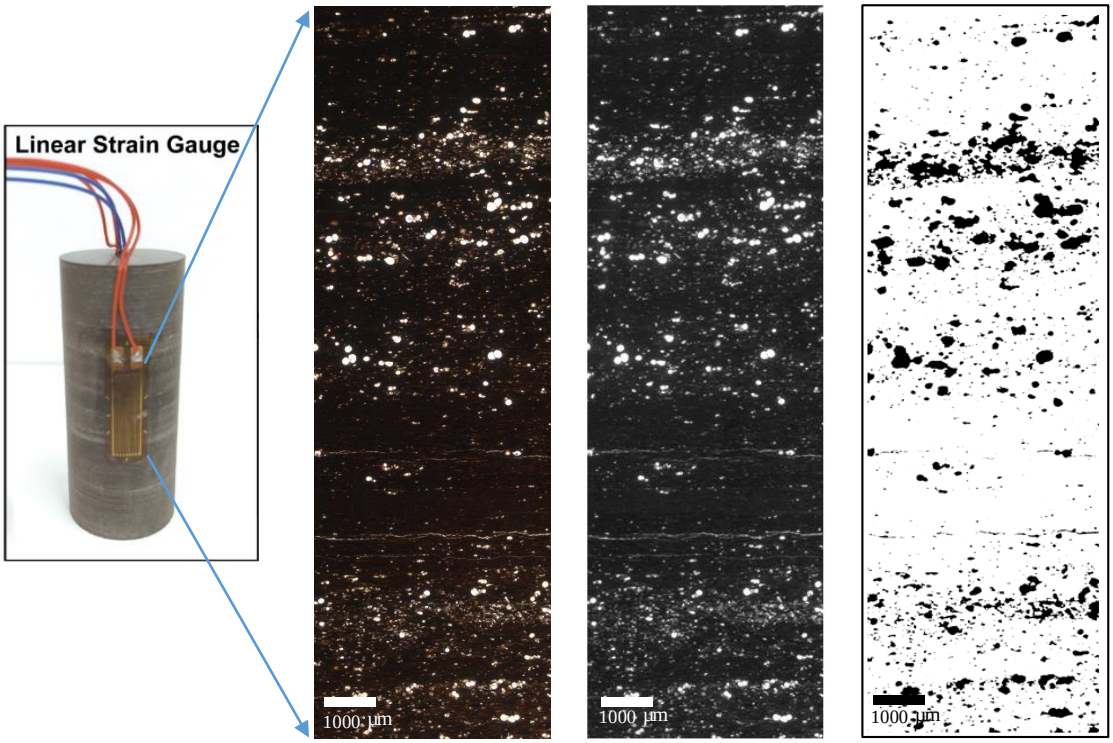

Figure 2.5 Example of micrographs for microstructure grain fraction analyses. A plane-polarized micrograph of a mosaic image is composed of 14 images. The corresponding gray-scale image after correction is created through Matlab and a threshold image distinguished grain vs. mud is created using ImageJ. The area of the mosaic image is equivalent to the area of linear strain gauge on the deformed sample.

Taking advantage of the density contrast among different components under plane-polarized light, the fraction of grains (>30 µm) relative to mud (fine silt and clay particles) was determined through digital image analysis with ImageJ ®. In a plane-polarized image of the Eagle Ford sample, calcite is present as bright, white grains that fill in foraminifera tests and is present as microcrystalline or sparry cement. Quartz typically is present as authigenic, microcrystalline cement that is light gray to white.

Clay and organic matter are the darkest phases in the thin sections that usually occur as lamina with a low aspect ratio.

The fraction of the grains in each sample was estimated based on image analyses on a gray-scale mosaic micrograph with an area equivalent to the linear strain-gauged area of each sample. The mosaic micrograph stitched by 14 separate images is converted to an 8-bit grey-scale image after correction. All components in the rock correspond to a distinct intensity value within a range from 0 to 255. Zero is taken to be black, and 255 is taken to be white. Three to four intensity profiles perpendicular and parallel to bedding that cut through both grains and mud in the mosaic image were plotted to analyze the color intensity of different phases. Brighter particles, such as calcite filling foraminifera tests, show high intensity, and dark particles, such as clay, organic matter, or matrix mixed with clay, show low intensity. Based on several intensity profiles, the lower limit of the intensity, the upper limit of the intensity, and the difference of the two limits that represent different shades of grey within the sample can be determined. In order to differentiate grains from mud matrix, an intensity threshold is determined to separate brighter grains and dark matrix. Considering the variation in color intensity of clay matrix, the threshold value that separates grains and mud are selected by the lower limit of the intensity plus an additional 15% of the difference between the upper and the lower limit of the intensity. In a mosaic micrograph, components with an intensity below the threshold values are the common soft phase (clay, organic matter, or phyllosilicate matrix mixed with microcrystalline cement) and the area with the intensity above the

threshold are typically stiff phases such as calcite, quartz, and pyrite minerals. The grain fraction estimates the total areas of each phase with grey intensity above the threshold. The mud fraction is estimates the total areas of each phase with grey intensity below the threshold. Since the petrographic thin section is typically around 30 μm, any grains that are less than 30 μm are excluded in the image analyses through a filter function to avoid scenarios of vertically overlapping particles in the thin section. The filtered grain fraction and mud fraction of a gray-scale mosaic micrograph, ignoring grains <30 μm. are then normalized as the sum of grain fraction and mud fraction, should be 1. Normalized grain fraction is used for texture analysis for the Eagle Ford Formation samples.

Secondary electron (SE) and backscattered secondary electron (BSE) micrographs images also were taken of the thin sections using a Tescan FERA-3 FIB-SEM (scanning electron microprobe with focused ion beam) to resolve the fabric of fine-grained samples such as and the location of bitumen, different types of clay, and occurrence of fine-grained cement such as recrystallized calcite or quartz. The images cover an area 1000 μm (wide) x 750 μm (tall) and have a resolution of 0.5 μm. A mosaic composed of seven vertically stitched micrographs covering the vertical length of the strain-gauged area was analyzed as done in the optical images. SEM energy dispersive X-ray spectroscopy (EDS) maps were collected for Ca, Mg, Fe, Si, Al, C, and S. Although the samples are carbon coated, concentrations of organic matter can still be recognized (Ko et al. 2016). The % area of mud-size particles, their shapes and

orientation, and their distribution with respect to stiff, large grains were determined through image analysis as these fine-grained, soft component are important to deformation behavior of shales (e.g., strain partitioning) (Sone and Zoback, 2013b).

2.3. Results

2.3.1. Starting Material

The main facies of the outcrop and subsurface calcareous Eagle Ford Formation samples used in this study are described according to the carbonate classification scheme of Dunham (1962) and Embry and Klovan (1971). The concept of grain/mud supported texture focuses on the continuity of the grains versus mud (i.e., particles of clay and fine silt size less than 30 μm in diameter). A mudstone is defined as having less than 10% grains floating in the continuum of mud matrix. A mud-supported carbonate rock containing more than 10% grains is defined as a wackestone. If the grains are touching each other and the mud is filling the gaps, the carbonate rock is called a packstone; Rocks with no mud are grainstones. The percentage of mud/grains at which there is a switch between a mud-supported and grain-supported texture depends on the microtextural characteristics of the carbonate rock. The major carbonate facies identified in Eagle Ford Formation samples used in this study include mudstone, wackestone, packstone, and grainstone. These are further distinguished by grain type (e.g., foraminifera tests, coccolith, skeletal grains) and sedimentary structures (e.g., laminated, bioturbated) (e.g., Donovan et al., 2016).

Based on the powder X-ray diffraction analyses, the main minerals identified in the Eagle Ford Formation samples chosen for this study include calcite, quartz, kaolinite, pyrite, muscovite, dolomite, illite, albite, and smectite (Fig. 2.6, Table 2.1). Overall, the outcrop and subsurface samples contain 52%-96 vol% carbonates (calcite + dolomite), 3-35 vol% QFP (quartz + feldspar + pyrite), and 0-28 vol% clay content. For all facies investigated, carbonate (calcite + dolomite) minerals are dominant and account for half of the rock volume. Quartz-feldspar-pyrite make up the next most abundant group. Clay minerals are the minor phase group. Carbonate content increases and clay content decreases from mud-supported facies to grain-supported facies.

In addition to mineralogy, a semi-quantitative estimation of the grain fraction in a sample was determined using the mosaic micrograph of each thin section using ImageJ ® to quantify texture of the Eagle Ford Formation samples (Table 2.2). The grain/mud supported texture is characterized by the volume of grains in a sample in which grains are defined as 30 μm or larger in diameter, except for the recrystallized carbonate facies. With an increasing fraction of grains in a sample, the spatial distribution of grains in the rock changes from isolated, to patches of grain clusters, to connected grains, to laminae of grains.

Table 2.1 Quantitative X-ray Diffraction results (reported values are in volume %).[a]

Location [b]	Name	facies	Calcite (Vol%)	Quartz (Vol%)	kaolinite (Vol%)	pyrite (Vol%)	muscovite (Vol%)	dolomite (Vol%)	illite (Vol%)	albite (Vol%)	smectite (Vol%)
H1	H1B1-2	mudstone	63.8	28.1	7	1.1	0	0	0	0	0
AC	B70'	mudstone	59.7	33.4	5.8	1.1	0	0	0	0	0
AC	B1-27	wackestone	79.1	17	3.4	0.5	0	0	0	0	0
AC	B4-83'	packstone	89.4	5.3	4.9	0.4	0	0	0	0	0
AC	D-139	packstone	94.3	3	1.4	0	1.3	0	0	0	0
AC	B-60	packstone	81.4	15.3	3	0.4	0	0	0	0	0
AC	E2	packstone	94.9	2.7	2.4	0	0	0	0	0	0
AC	C98	packstone	74.7	21.2	2.5	0.2	0	1.5	0	0	0
AC	B-35	packstone	90.6	9.4	0	0	0	0	0	0	0
AC	C-110	grainstone	84.2	13.6	1.4	0.3	0	0.4	0	0	0
AC	B-50	grainstone	90.8	9.2	0	0	0	0	0	0	0
AC	A-1	grainstone	74.9	7.4	7.4	0	0	10.3	0	0	0
SC	SC473	mudstone	53.4	30.9	6.2	2.4	7.1	0	0	0	0
SC	SC387	mudstone	59.1	20.3	4.9	2.4	13.4	0	0	0	0
SC	SC506	mudstone	53.1	15.7	22.6	2.5	0	0	5.8	0	0.3
SC	SC513	wackestone	71.2	16.3	11	1.5	0	0	0	0	0
SC	SC427	wackestone	92	7.7	0	0.4	0	0	0	0	0
SC	SC477	packstone	84.5	13.7	0.7	1.2	0	0	0	0	0
SC	SC430	packstone	90.6	8.8	0.6	0	0	0	0	0	0
SC	SC423	packstone	96.2	3.2	0	0.6	0	0	0	0	0

a. The ground powder used for each sample analysis was derived from the same interval recorded by the linear strain gauges for the sample.

b. H1 refers to U.S. Highway 90 road-cut samples taken just north of Del Rio, TX
AC refers to Antonio Creek outcrop samples; SC refers to Swenson Core samples

Table 2.2 Grain fraction of samples from outcrop and core determined from image analysis. [a]

Location	Name	Facies	Grain fraction (Vol%)
H1	H1B1-2	mudstone	9.3
AC	AC_B70	mudstone	17.3
AC	AC_B1-27	wackestone	39.0
AC	AC_B4-83	packstone	73.3
AC	AC_B-47	packstone	72.9
AC	AC_D-139	packstone	90.9
AC	AC_B-60	packstone	57.9
AC	AC_E2	packstone	91.9
AC	AC_C-109	packstone	59.5
AC	AC_C98	packstone	99.2
AC	AC_B-35	packstone	73.9
AC	AC_C-110	grainstone	72.2
AC	AC_B-50	grainstone	72.4
AC	AC_A-1	grainstone	84.8
SC	SC473	mudstone	4.4
SC	SC387	mudstone	16.0
SC	SC506	mudstone	10.1
SC	SC513	wackestone	32.8
SC	SC427	wackestone	22.6
SC	SC477	packstone	45.9
SC	SC430	packstone	42.4
SC	SC423	packstone	56.0

a. H1 refers to U.S. Highway 90 road-cut samples taken just north of Del Rio, TX
   AC refers to Antonio Creek outcrop samples
   SC refers to Swenson Core samples
b. Grain and mud fraction are normalized values based on image analysis (see text).

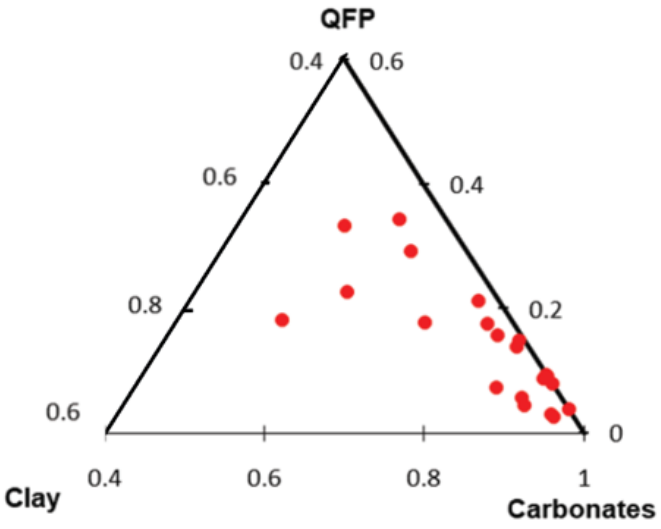

Figure 2.6 Ternary plot of compositions of samples from outcrop and core. Data obtained by X-ray diffraction analysis.

Mudstone facies in the Eagle Ford Formation includes argillaceous mudstone and weakly laminated mudstone. Overall, mudstones contain 53-64 vol% carbonates, 18-34 vol% QFP, and 6-29 vol% clay content (Table 2.1). The mudstone facies overall contains 4-6 wt% total organic carbon. Yet, mudstone facies only contains 6-13 vol% grains (Table 2). Based on the petrographic analysis, the argillaceous mudstone (Fig. 2.7a) is dark brown to black in color. The grains (>30 μm) are mostly planktonic foraminifera tests filled with calcite or kaolinite minerals. Few detrital quartz grains also are observed. Pyrite minerals are present as framboids or fragments infilling biogenic debris. Sparse grains are isolated and dispersed through the matrix. Although more than half of the rock is made up of carbonate minerals, SEM microscopy indicates most calcite is present as calcite cement that replaces coccolith debris and most of these are

recrystallized. The matrix of the mudstone sample is composed of calcite cement and quartz cement which are typically less than 10 μm, and clay particles. Clay minerals typically occur in lenticular or tabular shapes with low aspect ratios and are parallel to bedding. Weakly laminated mudstone (Fig. 2.7b) is similar to argillaceous mudstone in terms of color, presence of grains, and grain distribution. The difference is that the foraminifera grains in the weakly laminated mudstones are typically larger; the tests are mostly filled with calcite cement, with only a few grains that are filed with kaolinite. Sub-millimeter scale wavy laminae in this facies are formed by aligned lenticular shaped clay particles or organic-rich mud drapes. Millimeter-scale laminae are found in zones with a high concentration of foraminifera tests and grains in the mud matrix.

a)

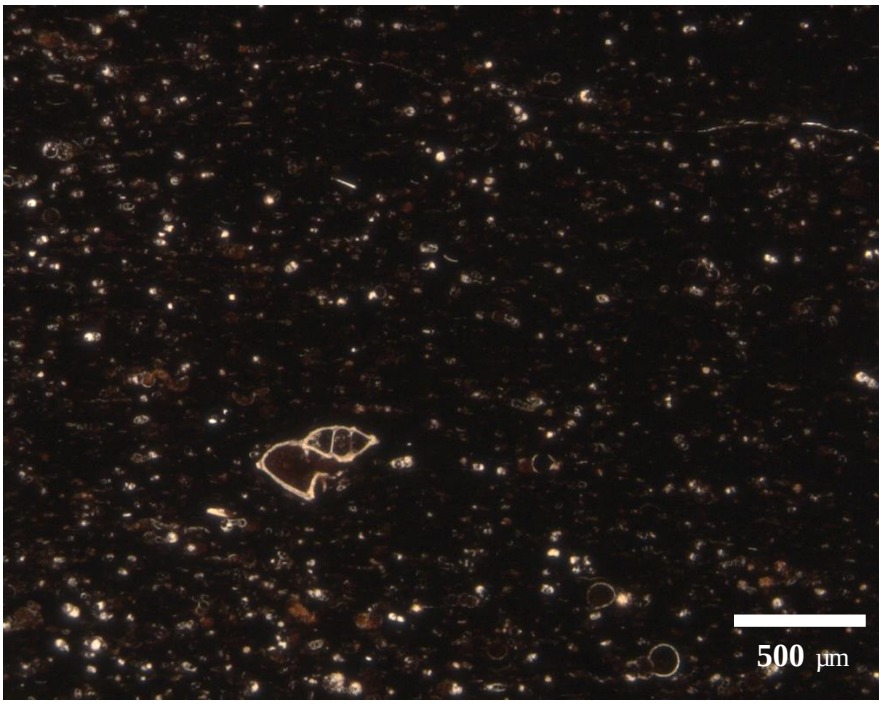

Figure 2.7 Optical and scanning electron micrographs of mudstone. **a.** A plane-polarized image of an argillaceous mudstone facies (sample SC506). **b.** A backscattered electron (BSE) micrograph of an argillaceous mudstone facies showing the distribution of different minerals (cal-calcite, qtz-quartz, pry-pyrite, kao-kaolinite). The image is representative of sample SC506. **c.** A plane-polarized image of a weakly laminated mudstone facies (sample H1B1). **d.** SE, BSE images, and elemental maps of Ca, Si, Al, and Mg of a foraminiferal mudstone sample (7c) showing distributions of different minerals using SEM-EDX. Calcite minerals concentrated in Ca are present as cement filling foraminifera tests and small cement grains in the matrix. Quartz minerals concentrated in Si are present as microcrystalline cement in the sample. Clay minerals concentrated in Al are present as a matrix (sample H1B1).

b)

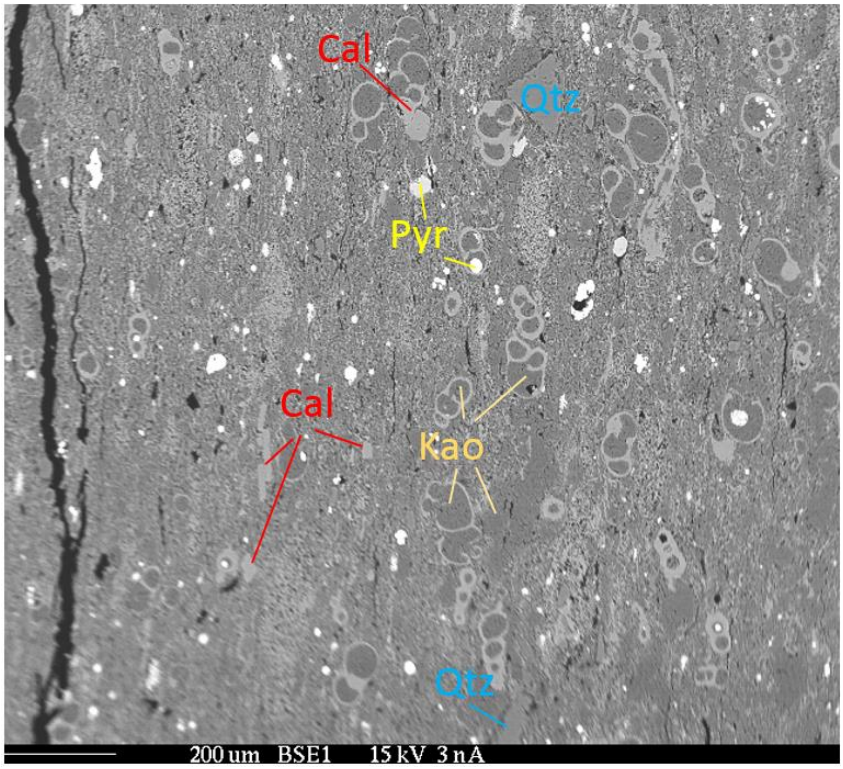

c)

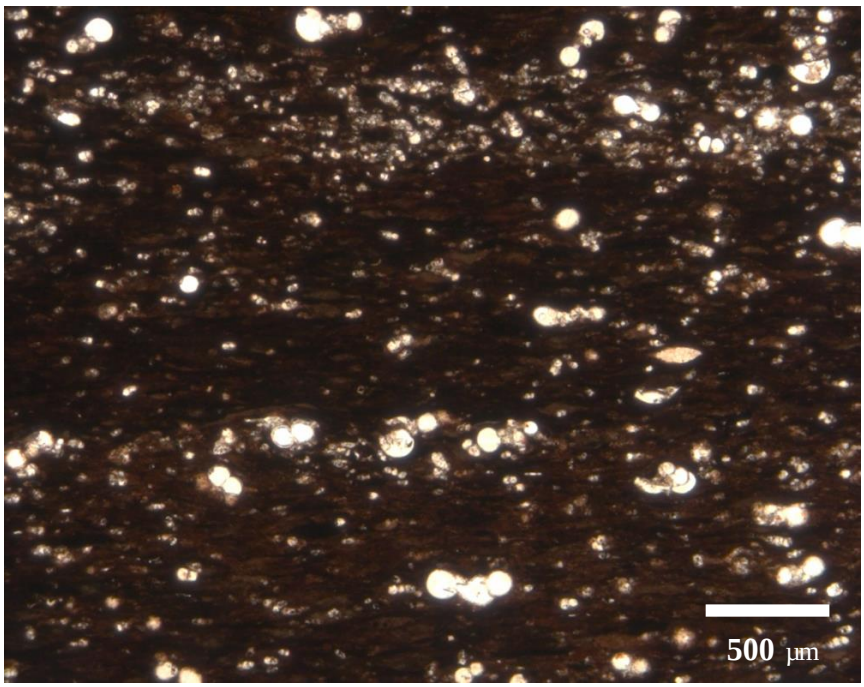

Figure 2.7 Continued

d)

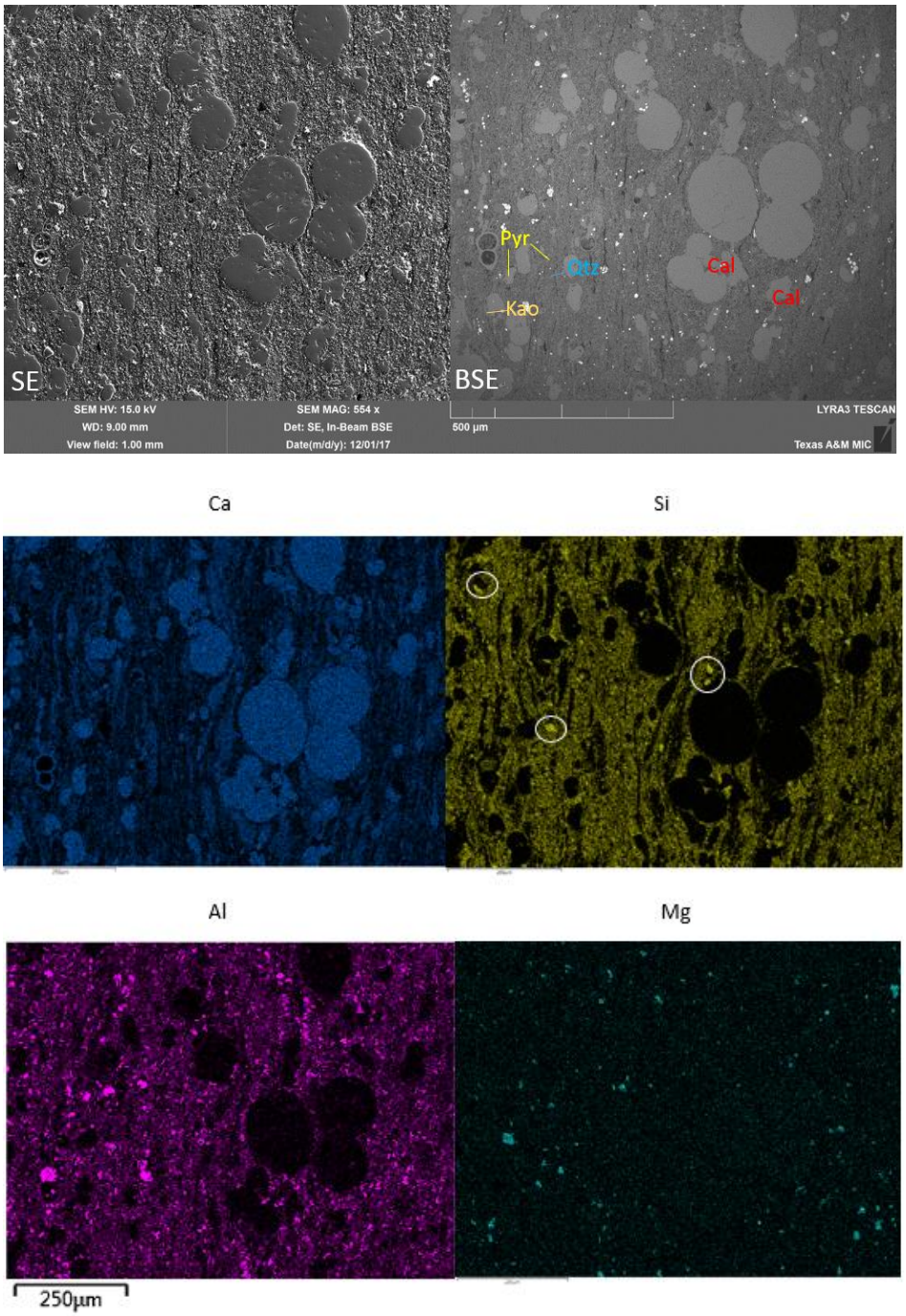

Figure 2.7 Continued

The wackestone facies contains laminated foraminifera wackestones and recrystallized wackestones. The wackestone facies contains 71-92 vol% carbonates, 8-18 vol% QFP, and 0-11 vol% clay content. The grain percentage varies from 13 to 28% (Table 1,2). Laminated foraminifera wackestone (Fig. 2.8a, 2.8b) is grey to black in color. In this facies, carbonate minerals are present as calcite cement infilling benthic or planktonic foraminifera chambers or skeletal debris, and as authigenic calcite surrounding foraminifera grains. Some foraminifera grains are recrystallized and the boundary between adjacent foram tests are connected. Concentrations of these foraminifera tests and skeletal debris are present as microcrystalline cement. Only a few are detrital grains were noted. Pyrite is less abundant in the wackestone facies compared to mudstones and is present as framboids. Clay minerals in this facies mostly occur as matrix and do not have lenticular shapes as seen in the mudstones. No clay minerals are observed within foraminifera tests in the wackestone facies. The recrystallized wackestone (Fig. 2.8c) contains a higher carbonate content than the laminated foraminifera wackestone facies. The recrystallized facies exhibits homogeneous texture and is mostly made up of recrystallized, angular shape, diagenetic calcite grains. The size of the cement depends on the degree of recrystallization. Since the wackestone is mud-supported, grains are partially connected. Grain size reduction associated with recrystallization results in a lower estimated grain fraction, as isolated grains less than 30 μm are not included.

a)

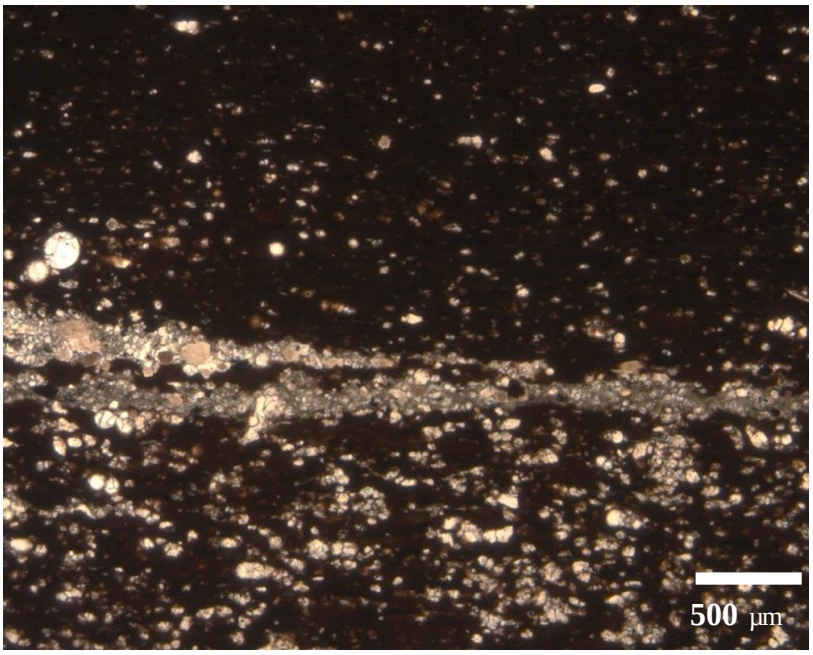

b)

Figure 2.8 Optical and scanning electron micrographs of wackestone. **a.** A plane-polarized micrograph of a laminated foraminifera wackestone (sample AC_B27). **b.** A BSE micrograph of a laminated foraminifera wackestone showing distributions of grains and calcareous rich matrix (sample AC_B27). **c.** A plane-polarized micrograph of a recrystallized wackestone facies (sample SC_427).

c)

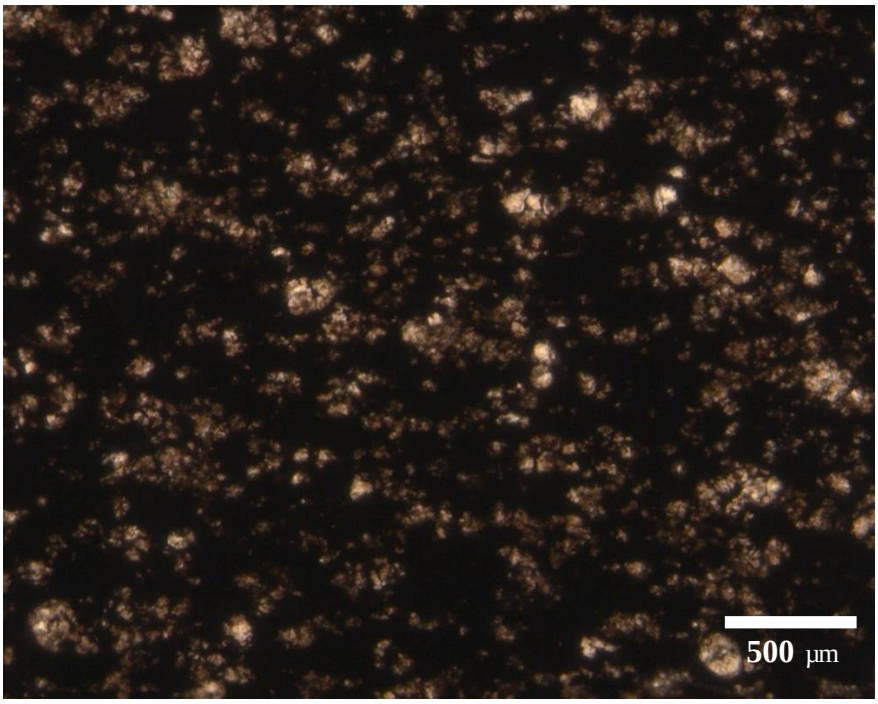

Figure 2.8 Continued

The most common packstone facies are foraminiferal rich or skeletal packstones. The packstones overall contain 76-95 vol% carbonates, 3-21 vol% QFP, and 1-5 vol% clay content. The packstone has a wide range of grain fractions, varying from 68% to almost 100 vol% (Table 1, 2). The packstone is typically light grey to dark grey in color. The dominant foraminifera grains in the packstone facies are filled by calcite (Fig. 2.9a). The matrix of the rock consists of microcrystalline calcite cement, quart cement, and clay minerals. Clay is much less abundant in the grain-supported facies than it in mud-supported facies. The overall texture of the foraminifera packstone is homogeneous. Laminations occur where foraminiferal tests are concentrated. The skeletal packstone is

similar to the foraminifera rich packstone as calcite minerals infill the predominant grains in the rock. On the other hand, the rock is heterogeneous compared to the foraminiferal packstone as large skeletal debris are randomly distributed in the rock.

The grainstone is typically light grey in color. It is very similar to the packstone except that clay minerals are rare in this facies. Grainstones in the Eagle Ford Formation contain 75-96 vol% carbonates, 4-14 vol% QFP, and 0-7 vol% clay content (Table 1). The grainstone facies has the highest carbonate content and lowest QFP and clay content among all carbonate facies. Texture analysis shows grainstones vary from 66% to almost 100% in grain fraction (Table 2). The grainstone, in general, lacks a sedimentary structure and is dominated by isopachous calcite cement. Bioturbation is also observed in the grain-supported facies. Recrystallization is a very common diagenetic feature in the packstone and grainstone facies. It destroys the original depositional character of the sample. The size of calcite cement grains varies from 10 μm to 100 μm, and depends on the degree of recrystallization. In some cases, the matrix is wholly composed of micrite. Recrystallized particles less than 30 μm are still counted as grains when the large grains (>30 μm) and recrystallized grains are connected to one another to create a stiff framework and no obvious boundaries between the two can be distinguished in the sample based on color contrast or texture.

a)

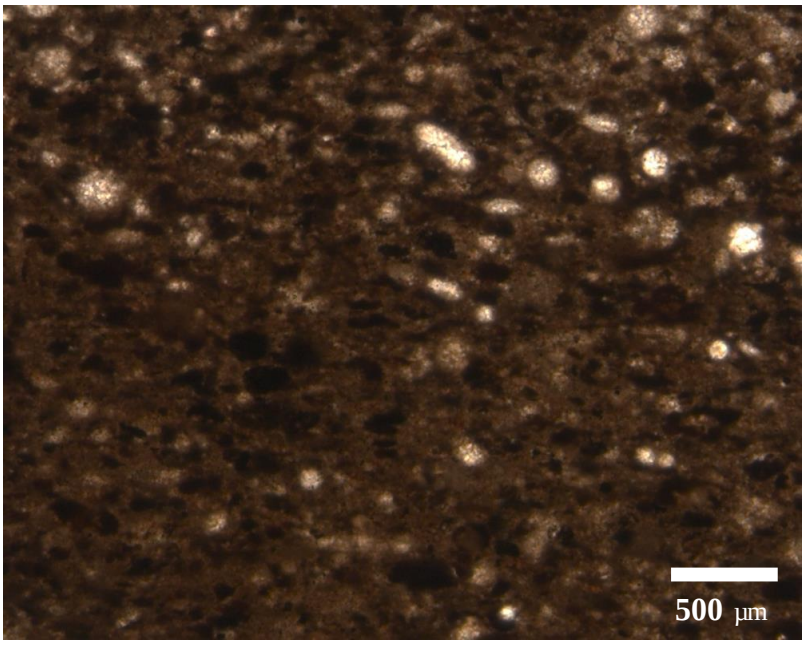

b)

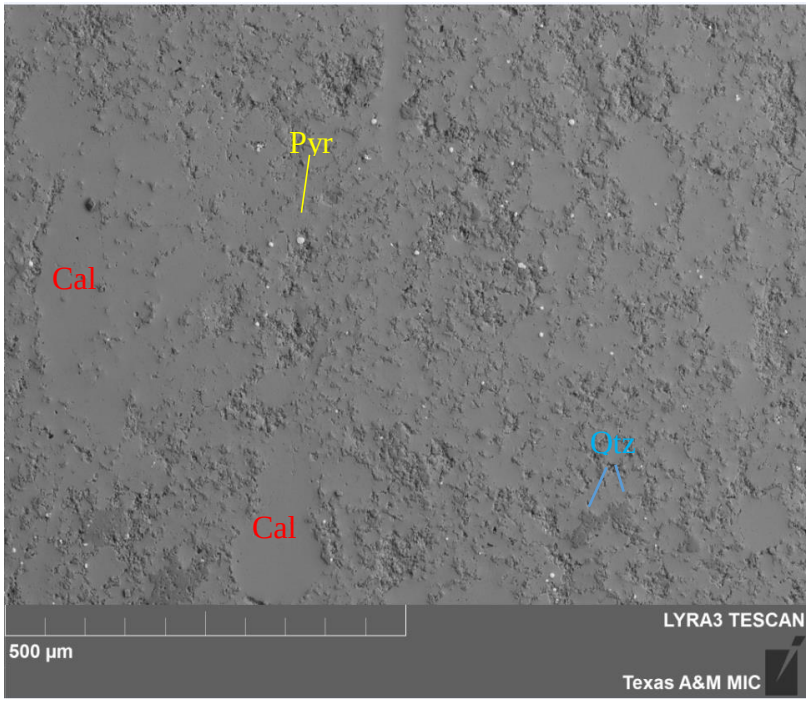

Figure 2.9 Optical and scanning electron micrographs of packstone and grainstone. **a.** A plane-polarized micrograph of a foraminiferal packstone (sample AC_B60). **b.** A BSE micrograph of a foraminiferal packstone showing connected foraminifera grains and recrystallized calcite grains (sample AC_B60). c. A plane-polarized micrograph of a grainstone facies (sample AC_A1).

c)

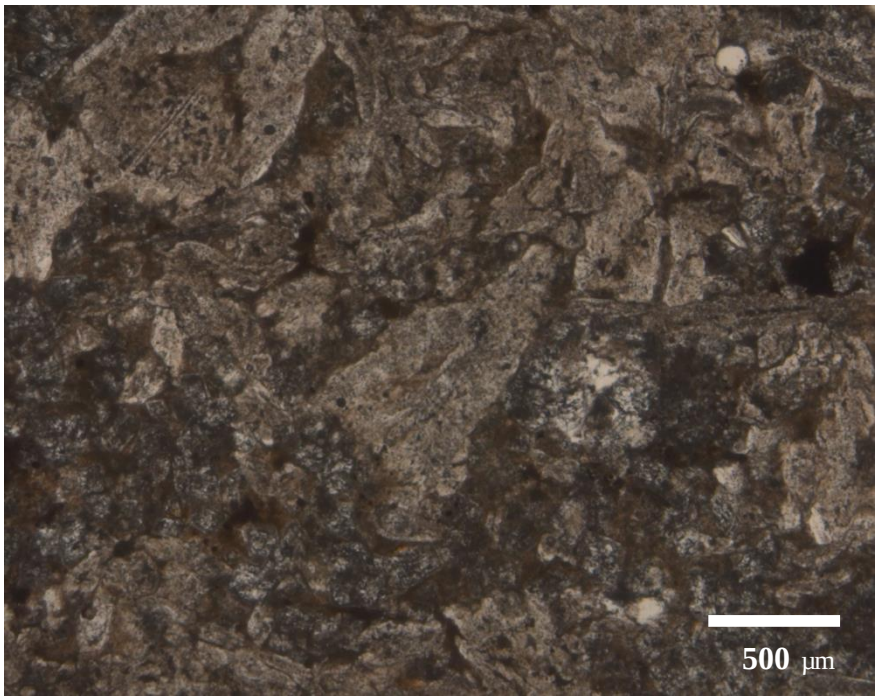

Figure 2.9 Continued

Overall, the carbonate content of the rock increases with carbonate facies. The boundary between wackestone and packstone or packstone and grainstone are not easy to distinguish at the sample scale as the concentration of grains varies at even a finer scale. The grain fraction of the samples, in general, shows a power-law relation with carbonate content (Fig. 2.10). Carbonate content increases rapidly with grain fraction for the mud-supported facies, indicating a transition from isolated grains to patches of calcareous grains. The transition from mud-supported facies to grain-supported facies corresponds to a grain fraction of ~ 40%. In the grain-supported facies, the grain fraction of the rock varies a lot yet the carbonate content does not vary as much, suggesting the

presence of isolated tiny calcite grains and cement. The grain fraction distinguishes the packstone and grainstone facies that have a similar carbonate content (>80%) but a different grain distribution. A packstone with grain fraction of 44% contains abundant isolated mud-size calcite grains and cement, yet a packstone with a grain fraction of 90% displays interconnected calcite grains and/or recrystallized calcite cement. Based on the petrographic observations, SEM microscopy, and composition analyses, the samples can be separated into three categories: (1) granular carbonates with more than 1% clay minerals, (2) granular carbonates with less than 1% clay minerals, and (3) coarse-grained, recrystallized carbonates (Table 2.2; Fig. 2.10).

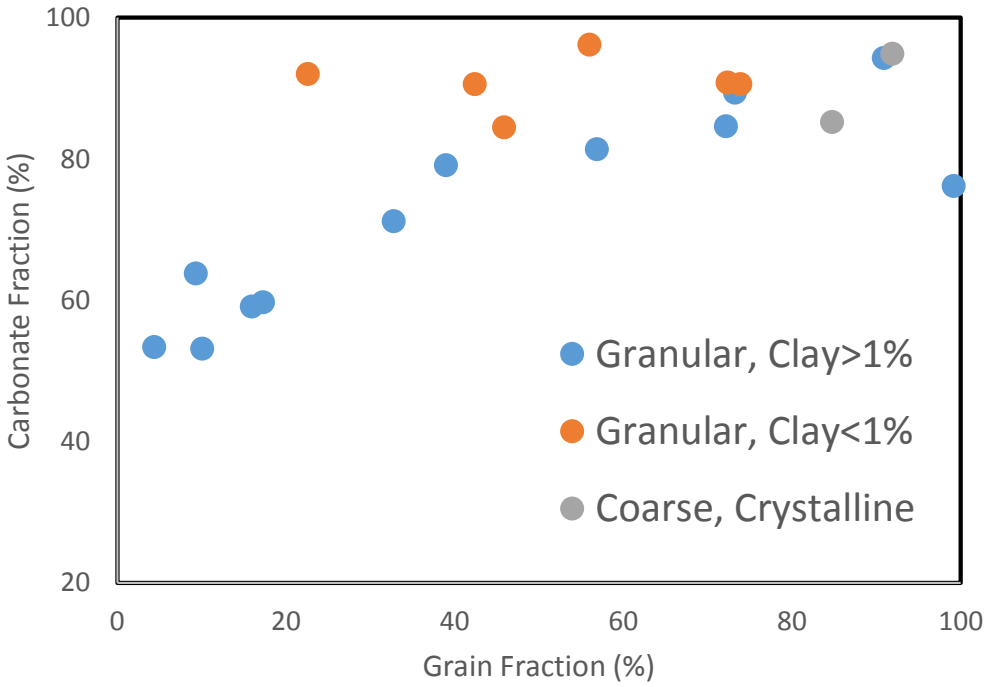

Figure 2.10 Relationship between grain fraction and carbonate fraction of samples.

2.3.2. Elastic Behavior and relation with mineralogy and texture

Stress-strain relations of representative carbonate facies show that the mudstone facies is the most compliant facies among the Eagle Ford Formation samples. Grainstone facies is the strongest facies. Under a certain stress condition, rock axial strain, radial strain, and volumetric strain decrease from mudstone to grainstone. The difference in elastic strain between mudstone and wackestone is large yet the difference between packstone and grainstone is small. Stress-strain curves of all carbonate facies are overall linear under low stress, suggesting the samples have low porosity and crack density under reservoir conditions (15 MPa confining pressure) (Fig. 2.11a). Based on elastic property tests on 23 samples, a large variation in Young's modulus is observed for the Eagle Ford Formation (Table 2.3). For example, Young's modulus of the Eagle Ford Formation samples measured under 15 MPa confining pressure vary from 15 GPa to 65 GPa, corresponding to a carbonate facies change from mudstone to grainstone (Fig. 2.11b). The organic-rich mudstone facies has the lowest Young's modulus, varying from 15 GPa to 31 GPa. With an increase in grain-supported character, carbonate content, and a decrease in clay and organic matter, Young's modulus of the rock increases greatly. The Young's modulus of grain-supported carbonate rocks packstone and grainstone is the highest, varying from ~ 45 GPa to 65 GPa. The grainstone/packstone facies can reach up to 4-5 times stiffer than mudstone facies, depending on the confinement pressure (Table 2.3). Under all pressure conditions, greater variation of Young's modulus is observed for samples from outcrop locality compared to the reservoir core

samples. In addition, the mature samples from the reservoir are overall weaker than the immature outcrop samples for the same types of carbonate rocks. Poisson's ratio of the Eagle Ford Formation increases gradually from 0.18 to 0.28, with an increase in mud/grain ratio of the rock. From mudstone to grainstone facies, Poisson's ratio of the rock increases by up to 67% (Fig. 2.11b). Overall, Young's modulus shows a positive relationship with Poisson's ratio. Among the Eagle Ford Formation samples, mudstone facies typically has the lowest Young's modulus of ~20 GPa and the lowest Poisson's ratio of ~0.2; The packstone/grainstone facies on average has a higher Young's modulus and Poisson's ratio of ~ 60 GPa and ~0.3, respectively.

Table 2.3 Elastic moduli determined from samples at three confining pressures. [a]

				Pc = 1 MPa		Pc = 3 MPa		Pc = 7 MPa		Pc = 15 MPa		Pc = 40 MPa	
Outcrop	Facies	Sample diameter (mm)	sample length (mm)	*E*	v	*E*	v	*E*	v	*E*	v	*E*	v
H1B1-2	mudstone	19	45	21.7	0.18	21.6	0.18	21.8	0.18	22.2	0.18	23.6	0.20
H1B1//	mudstone	19	44	28.2	0.28	27.1	0.28	27.2	0.28	28.7	0.19	28.9	0.26
AC_B70	mudstone	19	43	32.8	0.15	24.4	0.16	33.1	0.17	33.0	0.18	33.1	0.18
AC_B1-27	wackestone	19	45	35.1	0.23	35.2	0.23	35.5	0.22	35.9	0.22	35.6	0.22
AC_B1-27//	wackestone	19	45	41.9	0.31	41.9	0.31	41.9	0.31	41.9	0.30		
AC_B4-83	packstone	19	45	54.0	0.28	53.8	0.28	54.0	0.28	54.2	0.28	55.3	0.28
AC_B-47	packstone	19	45	60.0	0.30	59.4	0.33	58.1	0.30	57.7	0.28	57.7	0.28
AC_D-139	packstone	19	45	45.7	0.26	45.4	0.26	45.5	0.26	45.9	0.27	47.2	0.27
AC_D-139//	packstone	19	45	33.1	0.24	33.5	0.24	34.1	0.25	34.9	0.25	37.1	0.30
AC_B-60	packstone	19	45	55.1	0.26	55.3	0.26	56.2	0.26	56.5	0.26	57.5	0.26
AC_E2	packstone	19	46	60.4	0.28	60.2	0.28	60.3	0.28	60.8	0.28	61.0	0.28
AC_E2//	packstone	19	41	64.6	0.28	64.8	0.28	64.8	0.28	65.2	0.28	65.2	0.28
AC_C-109	packstone	19	44	62.7	0.27	62.3	0.27	62.7	0.27	62.6	0.27	61.7	0.27
AC_C98	packstone	19	44	50.9	0.24	51.0	0.24	51.3	0.24	51.5	0.24	52.2	0.25
AC_C98//	packstone	19	40							53.2	0.25		
AC_C-110	packstone	19	46	63.9	0.28	62.8	0.28	62.2	0.28	61.6	0.28	63.0	0.28
AC_C-110//	packstone	19	44	62.9	0.26	63.0	0.28	63.2	0.28	62.8	0.28	64.1	0.28
AC_B-50	grainstone	19	45	63.4	0.28	63.6	0.28	63.9	0.29	63.8	0.29	63.5	0.28
AC_B-50//	grainstone	19	45	63.2	0.28	62.4	0.28	62.4	0.28	62.8	0.28	61.2	0.28
AC_A-1	grainstone	19	45	55.5	0.27	55.3	0.27	56.4	0.27	56.4	0.27	56.5	0.28
AC_A-1//	grainstone	19	44	53.0	0.25	53.5	0.26	54.2	0.26	54.1	0.27	54.9	0.27
AC_B-35	grainstone	19	45	53.6	0.27	53.3	0.27	53.6	0.27	53.7	0.27	53.2	0.28
AC_B35//	grainstone	19	45	64.1	0.30	64.1	0.30	64.1	0.30	64.2	0.30	64.8	0.30

Table 2.3 Continued

				Pc = 1 MPa		Pc = 3 MPa		Pc = 7 MPa		Pc = 15 MPa		Pc = 40 MPa	
Core	Facies	Sample diameter (mm)	sample length (mm)	*E*	ν	*E*	ν	*E*	ν	*E*	ν	*E*	ν
SC473	mudstone	19	44	18.3	0.16	19.4	0.17	20.5	0.18	21.9	0.19	22.8	0.19
SC473//	mudstone	19	45	35.5						37.0	0.27		
SC387	mudstone	19	44	12.2	0.16	12.9	0.17	13.9	0.18	15.5	0.19	18.3	0.21
SC387//	mudstone	15	44	27.5	0.28	27.7	0.29	27.8	0.27				
SC506	mudstone	19	45	26.3	0.19	27.7	0.20	29.5	0.22	30.7	0.22	31.6	0.23
SC513	wackestone	19	41	26.4	0.18	28.3	0.19	31.7	0.27	34.4	0.27	37.2	0.25
SC427	wackestone	19	45	32.7	0.17	33.9	0.18	35.8	0.19	38.5	0.19	41.6	0.20
SC477	packstone	19	45	33.3	0.19	34.0	0.19	34.7	0.19	37.4	0.21	42.4	0.23
SC430	packstone	19	39	47.6	0.24	47.7	0.24	47.8	0.24	48.4	0.24	50.1	0.26
SC423	grainstone	19	43	49.0	0.26	50.3	0.26	51.8	0.27	53.8	0.27	55.7	0.27
SC423//	grainstone	19	42	55.2	0.26	55.6	0.26	55.8	0.26	56.3	0.26	57.0	0.26

a. H1 refers to U.S. Highway 90 road-cut samples taken just north of Del Rio, TX
AC refers to Antonio Creek outcrop samples
SC refers to Swenson Core samples

E is Young's modulus; ν is Poisson's ratio; Pc is confining pressure

Sample SC387// is cut as a prism

a)

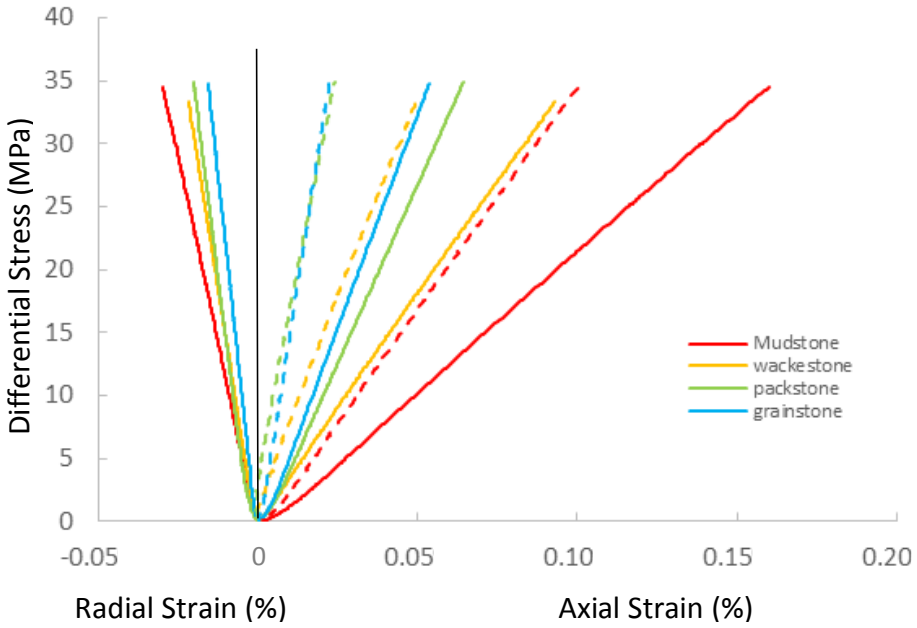

b)

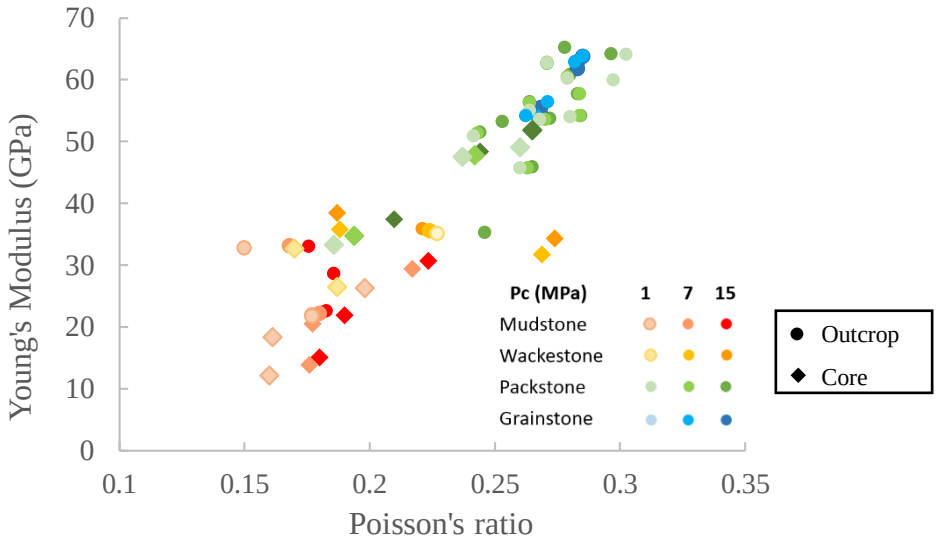

Figure 2.11 Examples of stress-strain behavior and cross plot of Young's modulus and Poisson's ratio. **a.** Stress-strain curves of different carbonate facies under 15 MPa confining pressure. Axial strain (solid line), radio strain (solid line), and volumetric strain (dashed line) of representative carbonate facies are plotted. **b.** Young's modulus and Poisson's ratio of the Eagle Ford Formation samples deformed under 1, 7, and 15 MPa.

For the same carbonate facies, samples show a large variation of Young's modulus and Poisson's ratio, which is partially attributed to the variation of composition and mineralogy of each sample (Fig. 2.11a). Young's modulus and Poisson's ratio of the Eagle Ford sample overall increase with carbonate content (Fig. 2.12a, 2.12d). Young's modulus increases from ~20 GPa to ~60 GPa with an increase in carbonate content from 55% to 95%. Poisson's ratio of the Eagle Ford Formation, in general, increases from ~0.18 to ~0.28 with an increase in carbonate content. Due to the scattering of the data, detailed relationship is unknown. Although mudstone facies is the softest in the Eagle Ford Formation samples, carbonate minerals in mudstones are accounted for more than half components in the rock, varying from 53% to 64%. Besides carbonate minerals, quartz mineral is the second major mineral in the Eagle Ford Formation and it is typically considered as a stiff component in a shale (Sone and Zoback, 2013; Rickman, 2008; Rybacki et al., 2016). However, Young's modulus shows a decreasing trend with an increase in quartz minerals. Young's modulus decreases from ~60 GPa for grain-supported facies to ~20 GPa for mud-supported facies, with a variation in quartz content from 5% to 30% (Fig. 2.12b). Poisson's ratio shows a step-like decrease with an increase in quartz minerals in the sample (Fig. 2.12e). The sharp transition coincides with the facies transition from mud-supported texture to grain-supported texture with QPF content of ~ 18%. Yet within mud-supported or grain-supported facies, the Poisson's ratio is insensitive to change in QFP content. It suggests that quartz minerals may not serve as a stiff phase in the Eagle Ford Formation samples as expected. Clay minerals in

shale are typically soft and distributed in a preferred orientation parallel to lamination. Clay minerals identified from XRD in the Eagle Ford Formation samples include kaolinite, muscovite, Illite, and smectite. The content of clay minerals in the Eagle Ford Formation increases with the transition from grain-supported to mud-supported facies. The abundance of clay minerals in packstone/grainstone is less than 10%, yet it is highly variable in mudstones, ranging from 6% to 29%. In general, both Young's modulus and Poisson's ratio of the Eagle Ford Formation samples show a decreasing trend with the increase in clay minerals (Fig. 2.12c, 2.12f). Poisson's ratio of samples is less sensitive to mineralogy compared to Young's modulus. The elastic moduli of the Eagle Ford Formation are highly related to rock composition and mineralogy.

a)

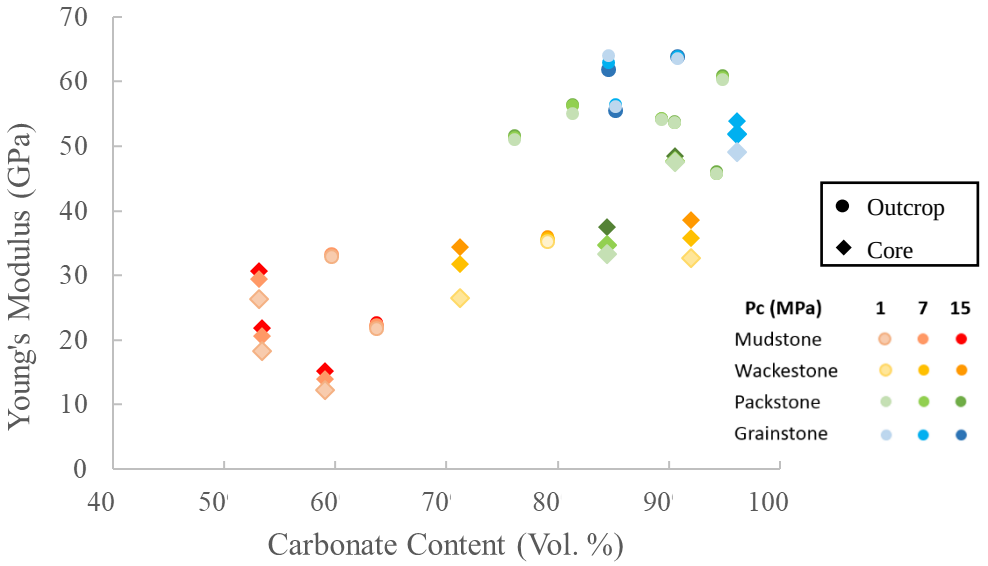

b)

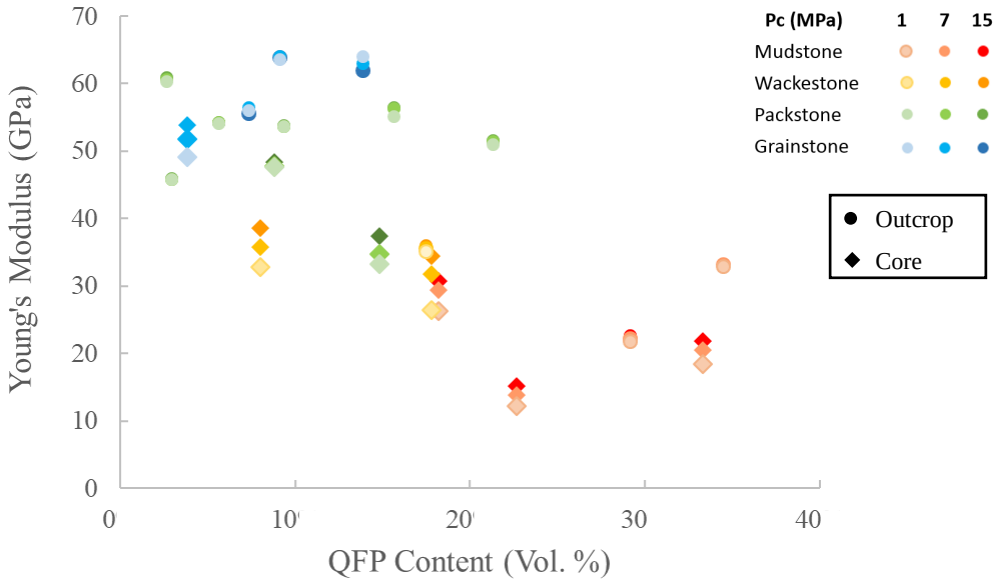

Figure 2.12 Relationship of elastic moduli and composition. Young's modulus (**a-c**) and Poisson's ratio (**d-f**) of the Eagle Ford are plotted against content of carbonate (calcite + dolomite) minerals, QFP (quartz, feldspar, pyrite), and clay minerals. The circle symbols are outcrop samples and the diamond symbols are samples from the reservoir.

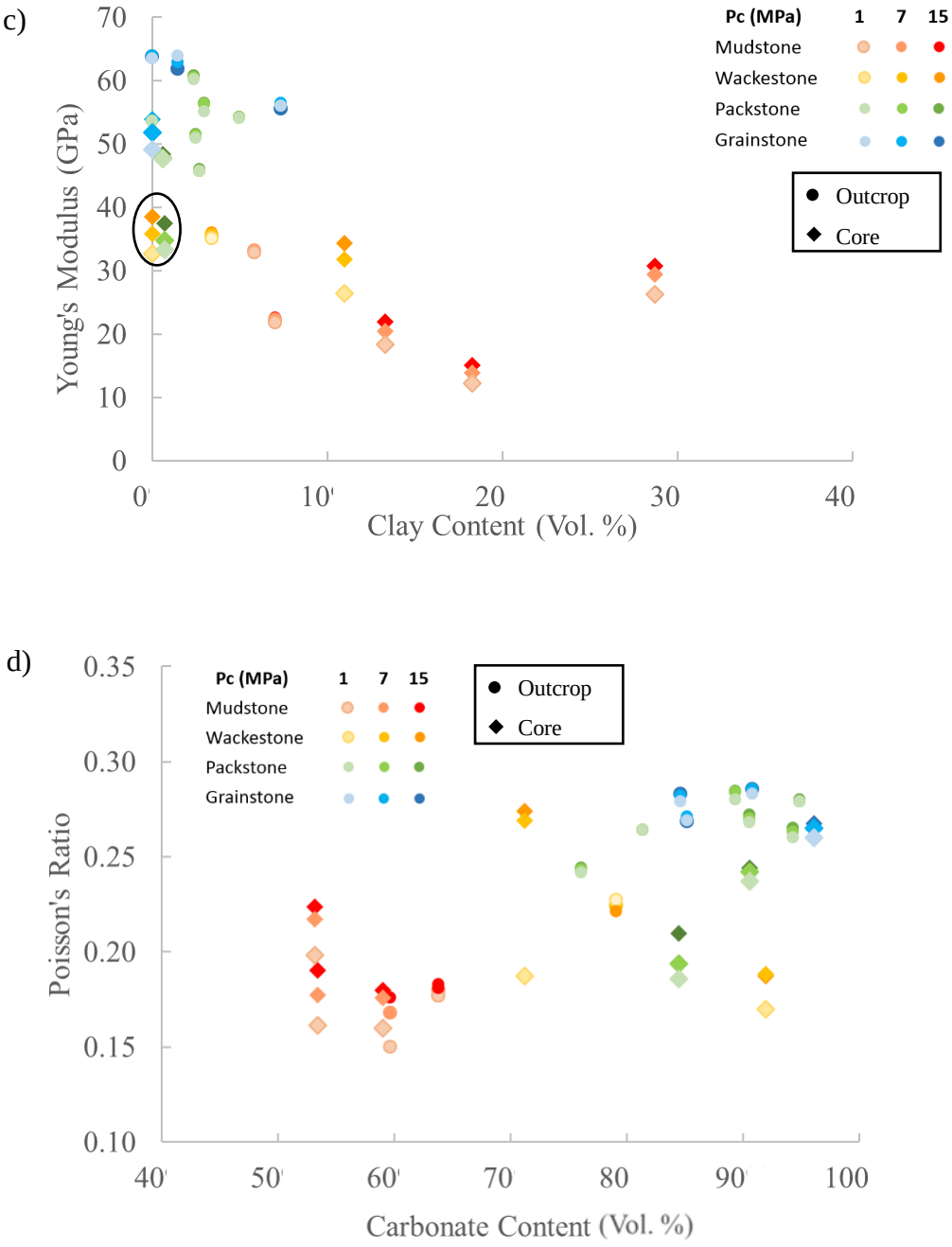

Figure 2.12 Continued

e)

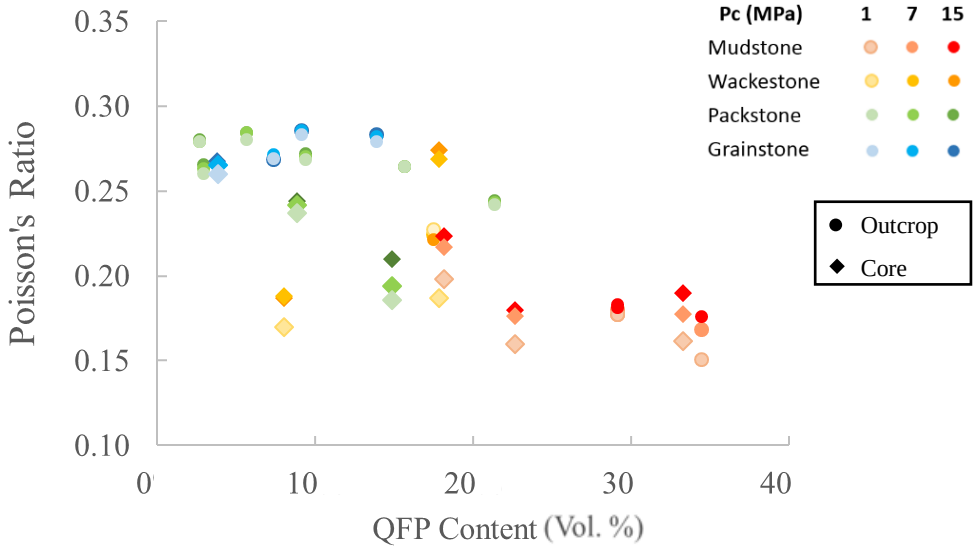

f)

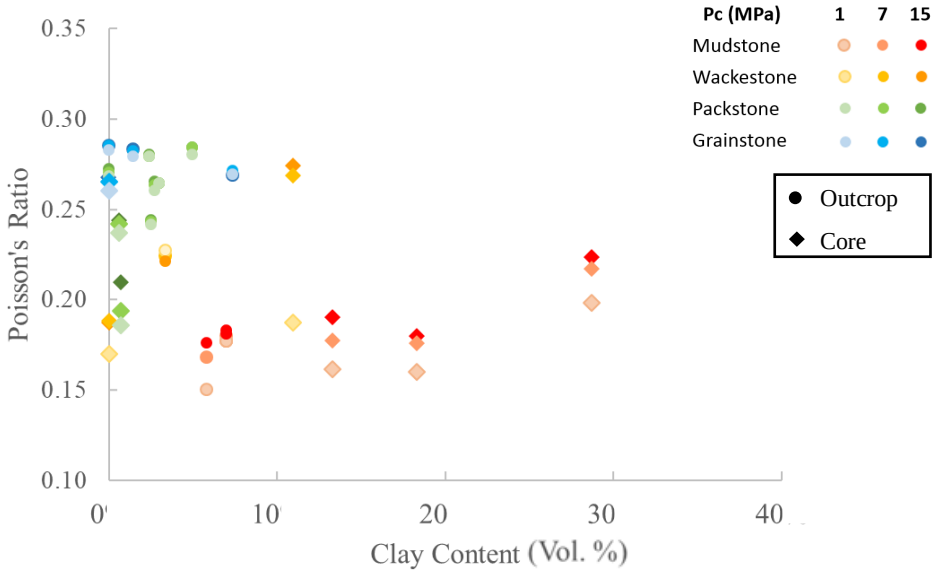

Figure 2.12 Continued

The relationship between elastic moduli and mineralogy suggests rock with similar composition but a different combination of grain distribution could lead to different mechanical properties. Estimated grain fraction of the Eagle Ford formation that characterizes the distribution of large grains and small mud-size particles show a positive relationship. Both Young's modulus and Poisson's ratio of the Eagle Ford Formation show a non-linear positive relationship with the fraction of grains in the samples (Fig. 2.13a, 2.13b). For samples with recrystallized grains such as recrystallized packstone, the grains were counted by estimating the amount of soft dark clay minerals or organic matter. With increasing numbers of grains in a sample, the distribution of grains in the rock changes from isolated, patches of grain clusters, connected grains, to laminae of grains. The grains carry the load and dominate the deformation when they are touching each other and connected. The Young's modulus increases sharply from mudstone to wackestone facies where the overall fraction of grain is low in the sample and the increase rate of Young's modulus slows down for packstone/grainstone facies that has high grain fraction.

a)

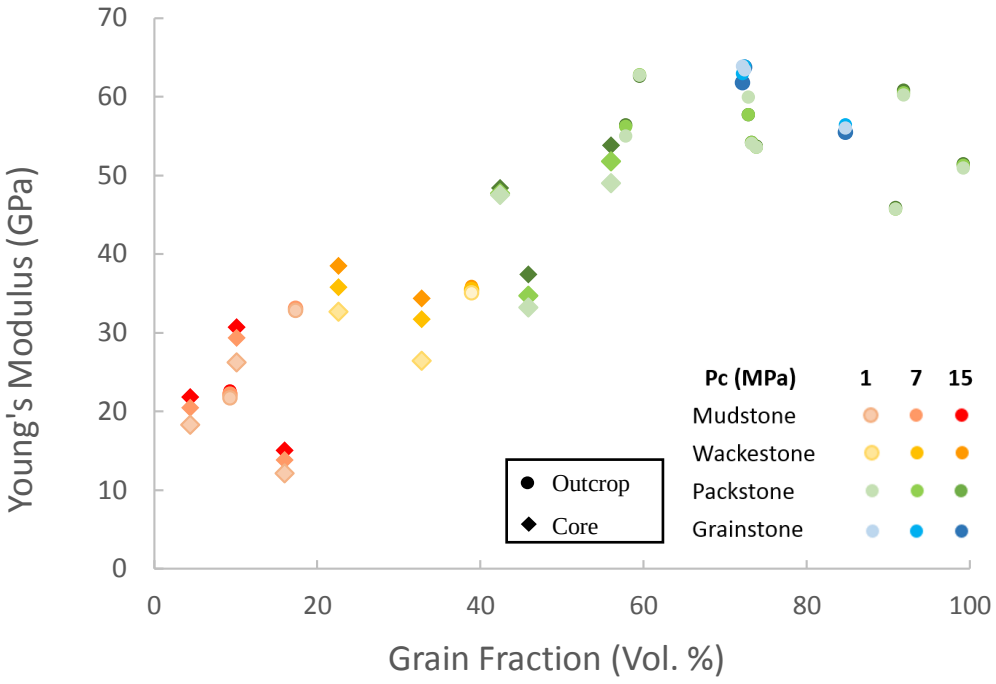

b)

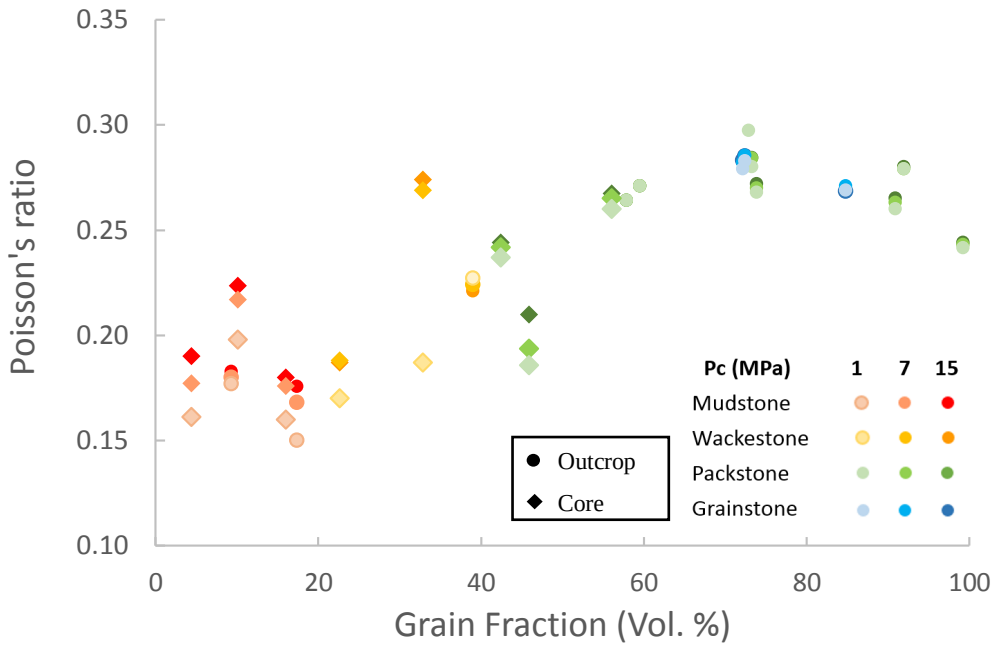

Figure 2.13 Relationship of Young's modulus **(a)** and Poisson's ratio **(b)** of the Eagle Ford as a function of grain fraction.

2.3.3. Pressure Dependency

Previous studies show rock mechanical properties are most sensitive to confining pressure (Table 2.2). In order to investigate the influence of pressure on elastic properties, samples were measured at a series of confining pressures with multiple loading cycles for each pressure step. At 1 MPa confining pressure, Young's modulus at the second cycle is usually found much stiffer than it from the first cycle. It suggests that the first loading cycle involves the closure of pre-existing microcracks in the samples. It also occurs for higher pressure steps for some samples and the elastic moduli of the second cycle are used to explore its relationship with confining pressure. Young's modulus of the Eagle Ford reservoir samples shows an increasing trend with confining pressure (Fig. 2.14a). The correlation can be expressed as a power law function for all rock types. Young's modulus of the rock is generally more sensitive to pressure change when confining pressure is below 15 MPa and the pressure dependency diminishes when confining pressure increases from 15 MPa to 40 MPa. The Young's modulus of the mudstone facies is more sensitive to pressure change compared to other facies and it could increase by 40% from 1 MPa to 40 MPa confining pressure. The pressure dependency decreases from mud-supported to grain-supported facies. The packstone shows the least pressure dependency. The Young's modulus only increases by 4% from 1 MPa to 40 MPa confining pressure (Fig. 2.14b). Compared to core samples, the Eagle Ford Formation samples from the outcrop, on the other hand, are much less sensitive to confining pressure for all carbonate facies. Most outcrop samples increase slightly with

increasing confining pressure. The Young's modulus of the mudstone from outcrop increases by 7% and the packstone/grainstone increases 2%-3% from 1 MPa to 40 MPa confining pressure (Fig. 2.14c, 2.14d). A few samples even show weakening in Young's modulus with pressure. The variation in Young's modulus in are all less than 10% and the pressure dependency is not related to rock types for outcrop samples.

a)

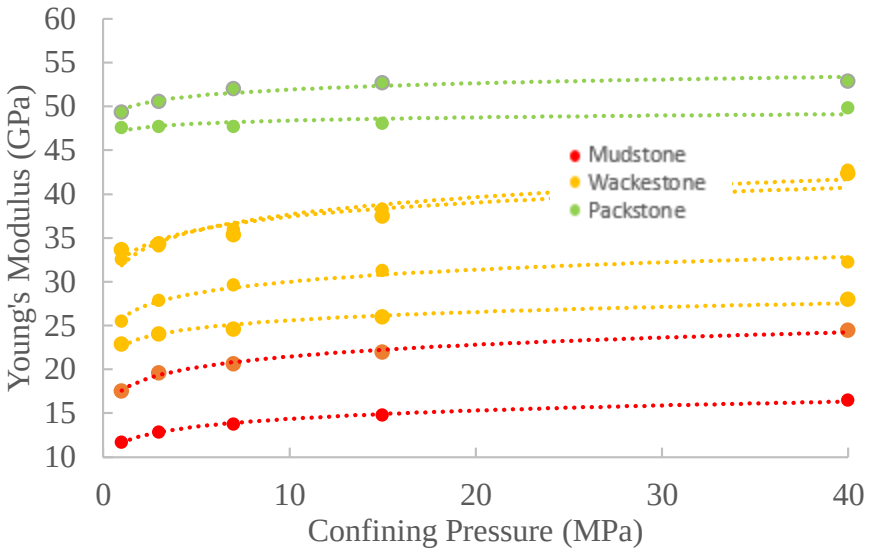

Figure 2.14 Relationship of elastic moduli and confining pressure. **a, c.** Young's modulus as a function of confining pressure for core samples. **b, d.** Normalized Young's modulus ratio of the outcrop samples. The ratio is determined by Young's modulus measured at each confining pressure relative to Young's modulus at 1 MPa confining pressure.

b)

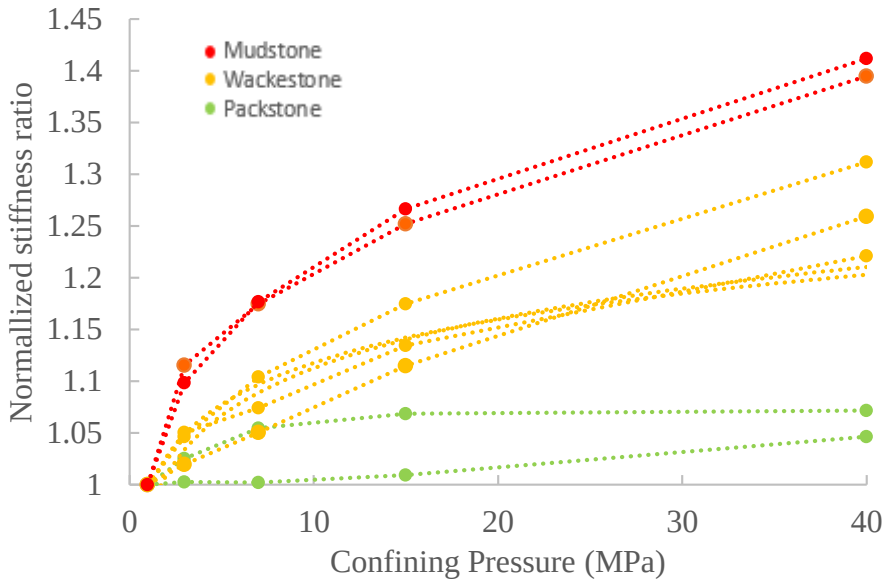

c)

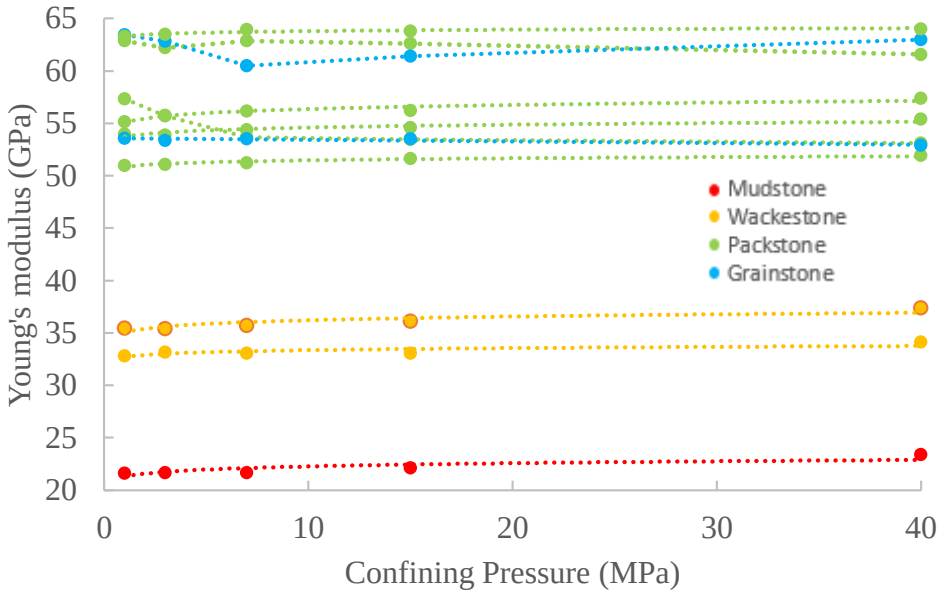

Figure 2.14 Continued

d)

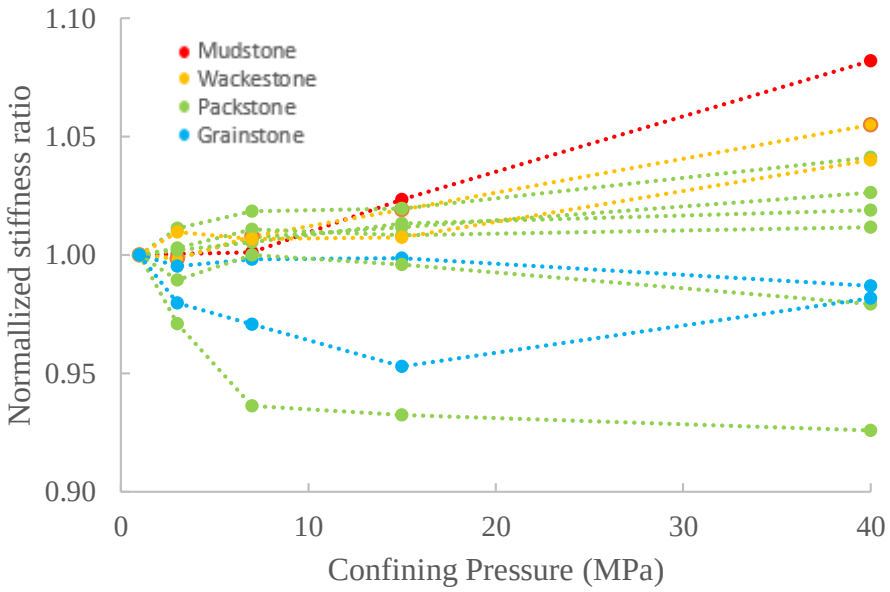

Figure 2.14 Continued

2.3.4. Anisotropy

In addition to elastic moduli measured perpendicular to bedding, Young's modulus and Poisson's ratio parallel to lamination is also measured for selected carbonate rock types. In some samples, Young's modulus and Poisson's ratio measured parallel to bedding are much greater than the properties measured perpendicular to bedding (Fig. 2.15a). For example, Young's modulus of a wavy laminated mudstone is 28 GPa in the direction parallel to its bedding, it is almost 2 times greater than Young's modulus perpendicular to lamination. The difference between elastic properties measured parallel to and perpendicular to lamination, described as elastic mechanical anisotropy, is related to carbonate facies. Mud-supported facies overall shows much

greater mechanical anisotropy than grain-supported facies. The mudstones can display anisotropy in Young's modulus and Poisson's ratio with a directional variation of ~80% and ~50%. Yet most packstones and grainstones show elastic anisotropy with a directional variation up to ~7.5% and ~4% for Young's modulus and Poisson's ratio. The degree of mechanical anisotropic behavior of shale is thought to be related to the soft component in the rock (Ibanez and Kronenberg, 1993; Josh et al., 2012; Sone and Zoback et al., 2013). The relationship between elastic moduli and clay content suggests that the degree of anisotropy is related to clay content (Fig. 2.15a, 2.15b, Fig. 2.16). In general, elastic anisotropy increases with an increase in clay content except for one packstone sample with no clay but connected organic matter which is also a soft phase.

a)

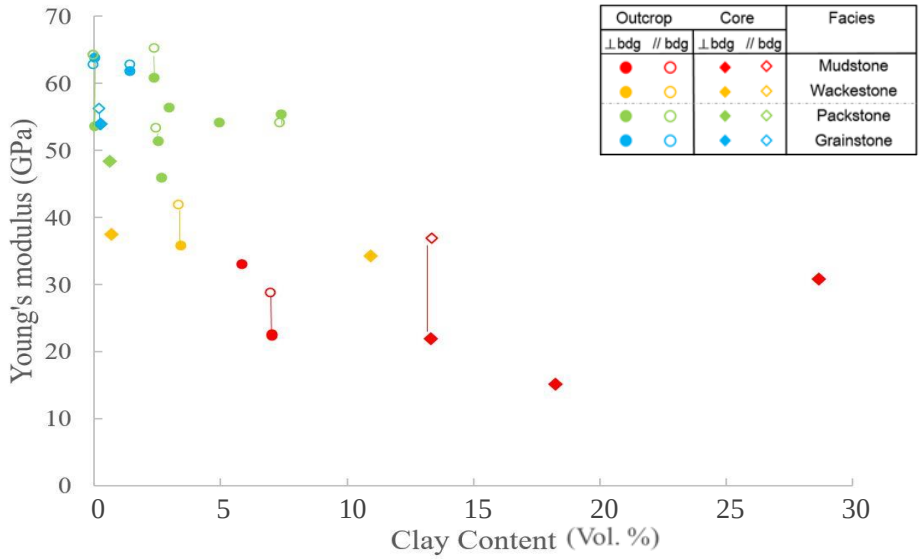

Figure 2.15 Relationship of Young's modulus **(a)** and Poisson's ratio **(b)** of the samples at 15 MPa confining pressure and clay content of the rocks. The open symbols are elastic properties measured parallel to lamination. The solid symbols are elastic properties measured perpendicular to lamination. The circle symbols are outcrop samples and the diamond symbols are samples from the reservoir.

b)

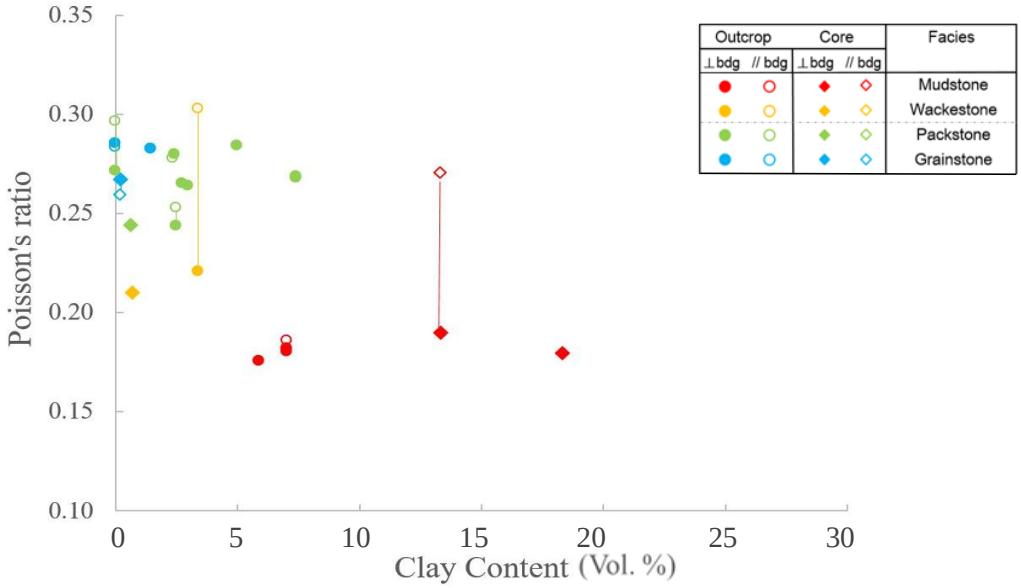

Figure 2.15 Continued

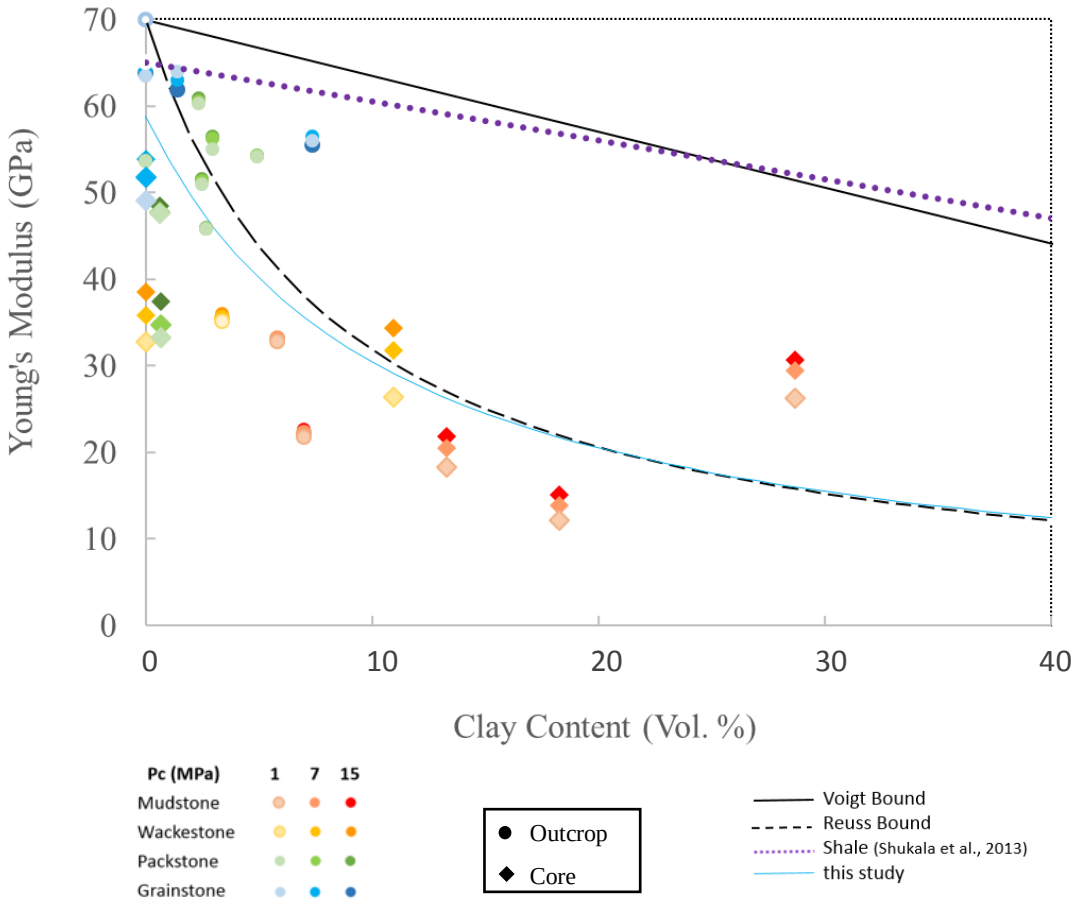

Figure 2.16 Relationship between Young's modulus and clay content. Circled data points are not used for fitting. The solid and dashed black line is theoretical Voigt upper bound and Reuss lower bound for a mixture material. The dotted purple line is the relationship between Young's modulus and clay content derived from different shale formations in the U.S. (Shukla et al., 2013).

2.4. Discussion

Elastic moduli of the Eagle Ford Formation is found related to carbonate fa ies, which is classified based on the mud and grain supported character of the depositional texture. At the sample scale, a rock is sometimes in between two facies. Young's modulus, Poisson's ratio increase from mud-supported facies to grain-supported facies based on the first order estimation as the numbers of grains increases and grains begin to touch each other to form a rigid framework and become stronger. In detail, the variation of elastic moduli and rock properties of a single carbonate facies is large. Young's modulus can vary ~20 GPa for different packstone samples, which could due to a difference in detailed rock composition and texture. Compositional analyses on the Eagle Ford sample is done to divide a rock into strong and weak phases so that it can be related to rock mechanical properties. The strong phase in shale is typically quartz, calcite, feldspar, and calcite. These minerals are considered as the main factor that contributes to the Young's modulus character of the carbonaceous Eagle Ford Formation. The soft phase in the rock is typically clay, mica, TOC, and porosity. Although TOC and porosity are not included in compositional analyses in this study due to various sampling rate, an overall negative trend between soft clay minerals and elastic properties is observed as expected (Fig. 2.12c, 2.12f, Shukla et al., 2013; Sone and Zoback, 2013a). With an increase in clay content from grain-supported to mud-supported carbonate rocks, Young's modulus decreases. The relationship between

Young's modulus and clay content is found between a linear relation and a power law relation. In this study, it can be expressed as a power law function

$$E = \frac{6.3}{X\ clay^{1.04}+0.107} \quad \text{(Eq. 2.1)}$$

Where E is Young's modulus, X_{clay} is the clay content of the sample. The relationship is close to Reuss theoretical bounds which are based on Young's modulus of pure calcite (~69.9 GPa) and pure soft component (5.4 GPa) (Sone and Zoback, 2013a; USGS, 1998). Young's modulus of the carbonaceous Eagle Ford Formation samples reduces by half with a small increase in clay content to 10%. The scattering of Young's modulus is observed for packstone/grainstone facies when the clay content is less than 5% even considering the uncertainty of the measurements. If porosity and clay content included in the mineralogy analyses, a detailed relationship could be seen. It also suggests that clay content has little influence on Young's modulus of these grain-supported facies. Other factors in addition to mineralogy dominate the variation in Young's modulus for grain-supported facies. Since the grain-supported facies is mostly none to little organic matter, TOC would probably have limited effect on variance in Young's modulus of grain-supported facies. Rock spatial distribution of the grains could cause the variance. Another possible factor is rock modification after lithification such as diagenesis. Different degrees of recrystallization has occurred in many samples which changes the distribution of grains in the rock. Two outcrop samples show diagenetic overprint and contain pyritized grains and associated moldic porosity, which could cause a reduction in Young's modulus.

Rock stiff component can be separated into carbonate and quartz, feldspar, pyrite (QFP) content in order to understand the mechanical impact of different phases. The content of carbonate minerals of the Eagle Ford Formation samples shows a positive relationship with Young's modulus and Poisson's ratio (Fig. 2.15a). The elastic moduli are scattered for facies with the least and most carbonate content. A mudstone with carbonates around 60% has Young's modulus of ~ 20GPa, and it is only 1/3 of the Young's modulus compared to a packstone with 20% more carbonate grains. It suggests that besides mineralogy, other factors such as the distribution of carbonate grains could also influence elastic properties. In the grain-supported facies, calcite is commonly present as foraminifera grains that are touching each other and form a rigid framework. Whereas in the mudstones, most carbonates are fine-grained mud-size particles (Fig. 2.7b). The calcite grains (>30 μm) in the mudstones are isolated in the matrix and they are relatively less abundant than dispersed small calcite cement grain. Calcite grains present as small isolated cement grain is very likely to contribute less to the Young's modulus character of a rock compared to calcite grains that have the same volume. Quartz content, on the other hand, shows a negative trend with Young's modulus although quartz is stronger than calcite minerals (Fig. 2.4b). It suggests that the strong quartz minerals may not necessarily contribute to the Young's modulus character of the sample as one would expect. When the quartz content is low in the carbonate rocks around less than 15% (e.g., for grain-supported facies), Young's modulus of the rocks is insensitive to quartz content. When the quartz content increases in mud-supported facies

that contain 17% -33% quartz content, the clay content of these mud-supported facies also increases. The combined mineralogical change causes an overall decrease in Young's modulus. Texturally, quartz minerals in the Eagle Ford Formation samples are present as either equate cements less than 10 μm or large detrital angular grains (Fig. 2.7b). Angular shape detrital quartz grains are rarely observed in the Eagle Ford Formation (Fig. 2.7b). Equant authigenic quartz cement is the most common form that is present throughout the samples. The quartz cements precipitate associated with coccolith foraminifera or mixed with calcite cements or clay minerals in the matrix (Fig. 2.7b, 2.7c). These randomly distributed quartz cements may not contribute to the Young's modulus character of the sample as expected because they are mixed with soft clay minerals and become weaker as a whole.

Similar to Young's modulus, Poisson's ratio shows a decreasing trend with clay content. Scattering of the Poisson's ratio in rocks with low clay content suggests other factors play a more important role in elastic behavior than mineralogy. Poisson's ratio shows a step decrease with rock QFP content in general. The sharp change in Young's modulus coincides with rock carbonate facies transition, indicating that grain spatial distribution strongly impacts Poisson's ratio.

Grain spatial distribution measured by grain fraction shows its relationship with elastic properties. The grain fraction of the Eagle Ford Formation samples shows a power-law relationship with Young's modulus and Poisson's ratio. The relationship is

overall insensitive to confining pressure for tested pressure range and the relationship yields better with a power-law equation of

$$E = 60.4 \cdot X_{grain}^{0.42 \pm 0.03} \quad \text{(Eq. 2.2)}$$

$$R^2 = 0.72$$

$$v = 0.28 \cdot X_{grain}^{0.185 \pm 0.024} \quad \text{(Eq. 2.3)}$$

$$R^2 = 0.68$$

Where E is Young's modulus, v is Poisson's ratio and X_{grain} is the volume of the grains in a sample that is larger than 30 μm in diameter and varies between 0 and 1. The relationship is not sensitive to confining pressure. Young's modulus is more sensitive to grain fraction for mudstone and wackestone where grain fraction is below 40%. Increase of amount of grains in a rock with mud matrix greatly increases Young's modulus. Textural distribution of grains plays a more important role in elastic properties of mud-supported rocks (mudstone/wackestone) than grain-supported rocks (packstone and grainstone).

The compositional and textural observations suggest that clay fraction, carbonate fraction, and grain fraction of samples have strong impacts on elastic properties. In order to evaluate the combined effect of these lithologic properties, Young's modulus as a function of clay fraction, carbonate fraction, and grain fraction is derived. The function keeps the original form of the relationship between Young's modulus and each 3 lithologic property as following:

$$E = x_1 f(x_{clay}) + x_2 f(x_{carbonate}) + x_3 f(x_{grain})$$

$$f(x_{clay}) = \frac{c}{X\,clay^{a}+b}$$

$$f(x_{carbonate}) = d \cdot x_{carbonate}^{\,e}$$

$$f(x_{grain}) = f \cdot x_{grain}^{\,g}$$

where *x1*, *x2*, and *x3* are the weighting parameters of each lithologic property. *a*, *b*, *c*, *d*, *e*, *f*, and *g* are parameters between Young's modulus and individual lithologic property. Using the simplex search methods (Lagarias et al., 1998), the best fit function is found for Young's modulus as a function of clay content, carbonate content, and grain fraction as follows:

$$E = 0.0703 \cdot \frac{4.83}{X\,clay^{1.32}+0.09} + 0.2015 \cdot (60.7\, x_{carbonate}^{\,1.47}) + 0.7040 \cdot (59.9\, x_{grain}^{\,0.38})$$

The predicted Young's modulus from the function and measured Young's modulus (at 15 MPa) show good agreement (Fig. 2.18, Table 4.2).

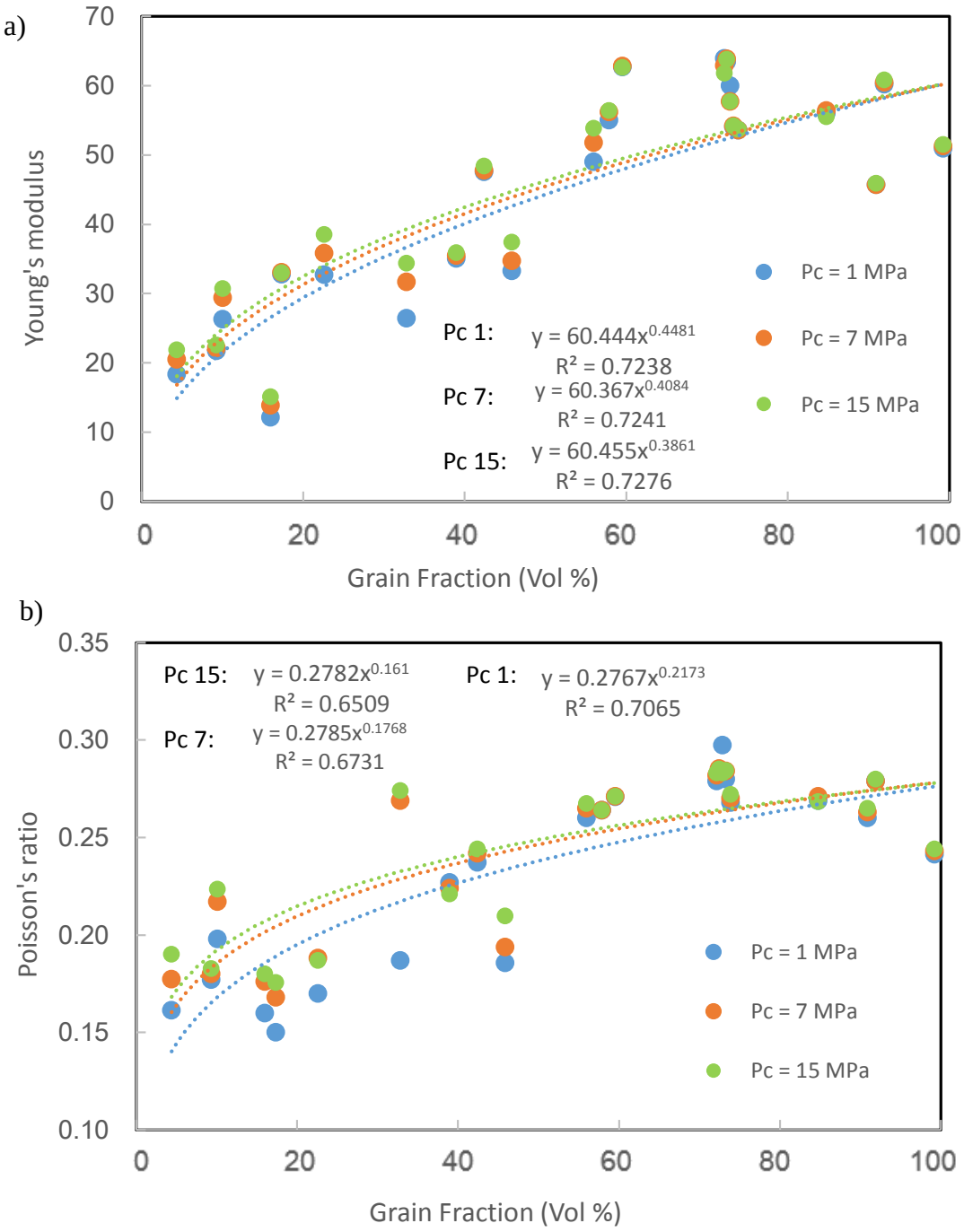

Figure 2.17 Correlation of elastic moduli and grain fraction. Young's modulus (**a**) and Poisson's ratio (**b**) as a function of grain fraction of the sample under 1 MPa, 7 MPa, and 15 MPa confining pressure.

Table 2.4 Summary of measured and predicted Young's modulus based on the relationship with clay fraction, carbonate fraction, and grain fraction.

Name	Facies	E (GPa)	X clay (vol%)	X carbonate (vol%)	X grain (vol%)	predicted E (GPa)
H1B1-2	mudstone	22.6	7.0	63.8	9.3	26.4
AC_B70	mudstone	33.0	5.8	59.7	17.3	30.5
AC_B1-27	wackestone	35.9	3.4	79.1	39.0	41.6
AC_B4-83	packstone	54.2	4.9	89.4	73.3	51.0
AC_D-139	packstone	45.9	2.7	94.3	90.9	55.3
AC_B-60	packstone	56.4	3.0	81.4	56.9	46.5
AC_E2	packstone	60.8	2.4	94.9	91.9	55.6
AC_C98	packstone	51.5	2.5	76.1	99.2	53.7
AC_B-35	packstone	53.7	0.0	90.6	73.9	51.9
AC_C-110	grainstone	61.8	1.4	84.6	72.2	50.5
AC_B-50	grainstone	63.8	0.0	90.8	72.4	51.7
AC_A-1	grainstone	55.5	7.4	85.2	84.8	52.1
SC473	mudstone	21.9	13.3	53.4	4.4	20.0
SC387	mudstone	15.1	18.3	59.1	16.0	28.5
SC506	mudstone	30.7	28.7	53.1	10.1	23.9
SC513	wackestone	34.4	11.0	71.2	32.8	37.5
SC427	wackestone	38.5	0.0	92.0	22.6	38.7
SC477	packstone	37.4	0.7	84.5	45.9	44.7
SC430	packstone	48.4	0.6	90.6	42.4	44.8
SC423	packstone	53.8	0.0	96.2	56.0	49.2

The microstructure fabric at the grain scale of the sample also impacts mechanical anisotropic behavior. Strong mechanical anisotropy is observed in some Eagle Ford Formation samples that measured parallel and perpendicular to its lamination, particularly in mudstones/wackestones facies. Foraminiferal packstone/grainstone and recrystallized packstone/grainstone are composed of uniformly distributed sphere foraminiferal grains with similar sizes and equant grains that with varying grain sizes, respectively. The facies exhibits homogeneous texture with massive structures at the sample scale and does not show directional variance in elastic moduli. Only one packstone sample with laminations and connected organic matter shows a stronger anisotropy in Young's modulus. It shows greater Young's modulus parallel to lamination than perpendicular lamination with a ratio of ~1.2 and it has similar anisotropy to a mud-supported sample with a few laminated foraminiferal rich beds (Fig. 2.17a). Mudstones with higher clay content and TOC content over 20 vol% show a much larger directional variation of a ratio up to 2.5 for Young's modulus measure parallel to versus perpendicular to beddings. Even though no obvious laminae is observed in this facies, both organic matter and clay minerals present in the sample typically have a very low aspect ratio in shape and thus lead to highly heterogeneous fabric and create weak plans along the bedding direction. One of the sample with diagenetic pyrite even shows greater Young's modulus perpendicular to lamination which could result from sampling variation. Overall, heterogeneity in texture leads to a variety of mechanical anisotropic behavior of the Eagle Ford. The amount of clay and TOC in a rock plays a more

important role in anisotropy compared to the occurrence of laminations in the rock. The degree of elastic anisotropy is positively correlated with clay content (Fig. 2.18, Sone and Zoback, 2013a; Rutter et al., 2019). Diagenesis processes such as recrystallization or burrowing could also alter the fabric of the rock and has an impact on directional mechanical properties.

a)

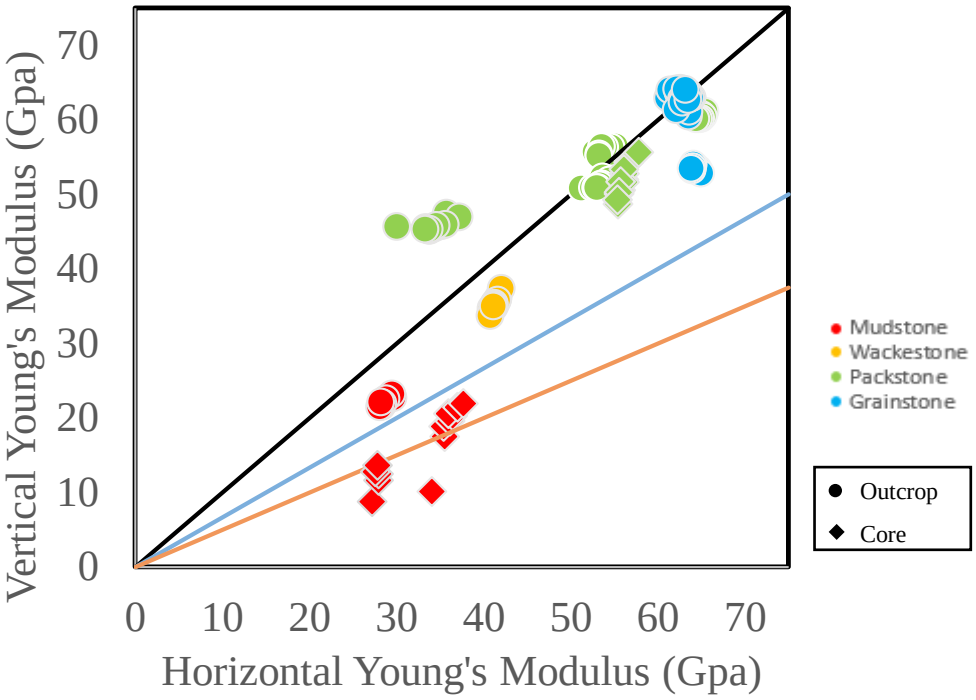

Figure 2.18 Elastic anisotropy and its relation with clay content. **(a)** Young's modulus measured parallel to laminations versus elastic moduli measured perpendicular to laminations illustrates the mechanical anisotropic response of the Eagle Ford Formation sample. The 1:1 ratio line corresponds to the isotropic mechanical response. **(b)** Elastic anisotropy of the samples as a function of clay content.

b)

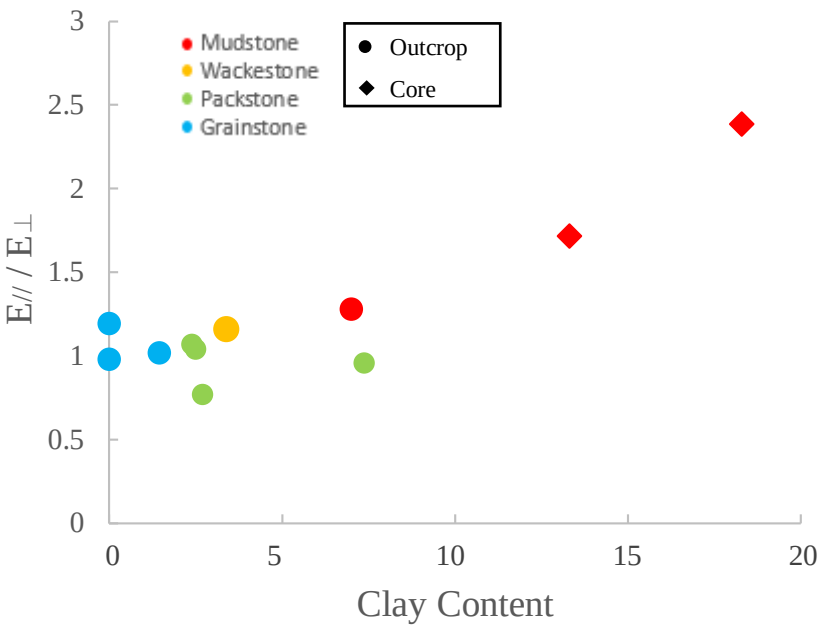

Figure 2.18 Continued

Besides mineralogy and rock texture, pressure has shown an evident effect on Young's modulus of the Eagle Ford Formation samples. Young's modulus stiffening of the second cycles relative to the first loading cycle is commonly seen in core samples at the lower confining pressure steps. It may correspond to the closure of microcracks as a result of depressurization. Samples from the reservoir core show a monotonic stiffening trend against pressure, as suggested by pore closure with increasing confining pressure. The modulus stiffening behavior is also related to carbonate rock types. The modulus stiffening of the mudstone facies is the greatest and is best expressed as a power law function. The packstone shows the least stiffening of Young's modulus with respect to pressure and the relationship can be described as a power law or a linear function. An exponential increase in Young's modulus with pressure indicates crack-like pores in the sample, yet a linear relationship between Young's modulus and confining pressure suggests a response similar to non-porous isotropic material (Ong, et al., 2016). The outcrop samples do not show a monotonic relationship with confining pressure. Most outcrop samples show modulus stiffening with pressure as observed in reservoir core samples. A few packstone/grainstone samples show a little variation or even weakening in Young's modulus with an increase in confining pressure. Samples that show modulus weakening all exhibit partial recrystallization/micritization. Some permanent deformation may occur with elevated pressure and causes a reduction in Young's modulus. It could also result from the measurement uncertainty. Overall, the pressure dependence of Young's Modulus of the outcrop sample is up to 10%, much smaller than

the same facies from the core which shows up to 40% variation. If the reservoir rock has more porosity than the outcrop rocks, the reservoir rocks would exhibit larger pressure dependency. The pressure dependency of lithology should also be expected in the outcrop samples as seen in the reservoir rocks, yet it is not observed. If the outcrop and core samples have a similar range of porosity, the discrepancy mainly reflects the formation of cracks/microcracks in the reservoir rocks as a result of depressurization. This also explains the lower rock strength determined in the core samples for the same carbonate facies, especially packstone. For reservoir rocks, the pressure dependency across facies may reflect.

2.5. Conclusions

The carbonaceous Eagle Ford Formation shows a wide range in Young's modulus and Poisson's ratio for different facies with carbonate content varying from 53% to 99%. It is found that sample elastic moduli are a function of lithology, mineralogy, texture, sample orientation, and pressure. From mud-supported to grain-supported carbonate facies, elastic moduli increase gradually. Compared to a mudstone, Young's modulus and Poisson's ratio of a grainstone could reach up to ~4 times and ~1.5 times greater, respectively. The mineralogy analyses of the samples show both Young's modulus and Poisson's ratio are positively correlated with carbonate content. Quartz minerals in the sample are typically considered as a stiff phase, however, quartz minerals in the Eagle Ford Formation samples present as microcrystalline cement

associated with clay minerals, and thus do not contribute to the Young's modulus character of rocks as expected; it is negatively correlated to elastic moduli. A power-law relationship is found between Young's modulus and clay content and the relationship has shown a good agreement with theoretical Reuss bound. For rocks with little clay (e.g., grain-supported facies), the clay content plays a more important role in Young's modulus compared to a clay-rich mudstone. The Young's modulus could reduce by half with a 10% increase in clay content. In addition to mineralogy, rock texture such as grain density distribution also plays a role in elastic properties. Grain fraction of the rocks show a power law relationship with elastic moduli. An increase in the number of grains in a mud-matrix carbonate rock has a greater effect on an increase in Young's modulus compared to a grain-supported facies. The relationship between rock texture and elastic moduli is insensitive to pressure. Both mineralogy and rock texture affect rock anisotropic elastic behavior. The clay content of the Eagle Ford Formation shows a positive correlation with rock anisotropic behavior expressed as Young's modulus deformed parallel to bedding versus perpendicular to bedding. With an increasing degree of lamination, the degree of anisotropy also increases.

2.6. References

Altowairqi, Y., Rezaee, R., Evans, B., and Urosevic, M., 2015. Shale elastic property relationships as a function of total organic carbon content using synthetic samples. Journal of Petroleum Science and Engineering, 133, 392-400.

Bourg, I. C., 2015. Sealing shales versus brittle shales: a sharp threshold in the material properties and energy technology uses of fine-grained sedimentary rocks. Environmental Science and Technology Letters, 2(10), 255-259.

Campbell, C. V., 1967. Lamina, laminaset, bed and bedset. Sedimentology, 8(1), 7-26.

Donovan, A. D., and T. S. Staerker, 2010. Sequence stratigraphy of the Eagle Ford (Boquillas) Formation in the subsurface of South Texas and outcrops of West Texas: GCAGS Journal, v. 60, p. 861-899.

Donovan, A. D., Staerker, T. S., Pramudito, A., Li, W., Corbett, M. J., Lowery, C. M., Romero, AA.M., and Gardner, R. D., 2012. The Eagle Ford outcrops of West Texas: A laboratory for understanding heterogeneities within unconventional mudstone reservoirs, GCAGS Journal, v. 1, p. 162-185.

Donovan, A.D., Staerker T.S., Gardner R., Pope M., Pramudito A., and Wehner M., 2016. Findings from the Eagle Ford outcrops of west Texas and implications to the subsurface of south Texas: in J. A. Breyer, ed., The Eagle Ford Shale: A renaissance in U.S. oil production: AAPG Memoir 110, p. 301–336.

Dunham, R. J., 1962. Classification of carbonate rocks according to depositional texture, in W. E. Ham, ed., Classification of carbonate rocks—A symposium: American Association of Petroleum Geologists Memoir 1, p. 108–121.

Gardner, R.D., Pope, M.C., Wehner, M.P., and Donovan, A., 2013. Comparative Stratigraphy of the Eagle Ford Group Strata in Lozier Canyon and Antonio Creek, Terrell County, Texas. GCAGS Journal, v. 2, p. 42–52.

Gu, H., and Siebrits, E., 2006. Effect of formation modulus contrast on hydraulic fracture height containment. In International Oil and Gas Conference and Exhibition in China. Society of Petroleum Engineers. 10.2523/103822-MS.

Ibanez, W. D., and Kronenberg, A. K., 1993. Experimental deformation of shale: Mechanical properties and microstructural indicators of mechanisms. In International journal of rock mechanics and mining sciences and geomechanics abstracts. Vol. 30, No. 7, pp. 723-734

Josh, M., Esteban, L., Delle Piane, C., Sarout, J., Dewhurst, D. N., and Clennell, M. B., 2012. Laboratory characterisation of shale properties. Journal of Petroleum Science and Engineering, 88, 107-124.

Ko, L. T., Loucks, R. G., Zhang, T., Ruppel, S. C., and Shao, D., 2016. Pore and pore network evolution of Upper Cretaceous Boquillas (Eagle Ford–equivalent) mudrocks: Results from gold tube pyrolysis experiments. AAPG Bulletin, 100(11), 1693-1722.

Kwon, O., Kronenberg, A. K., Gangi, A. F., and Johnson, B., 2001. Permeability of Wilcox shale and its effective pressure law. Journal of Geophysical Research: Solid Earth, 106(B9), 19339-19353.

Lagarias, J. C., J. A. Reeds, M. H. Wright, and P. E. Wright, 1998. Convergence Properties of the Nelder-Mead Simplex Method in Low Dimensions. SIAM Journal of Optimization. Vol. 9, pp. 112–147.

Li, Q., Xing, H., Liu, J., and Liu, X. 2015. A review on hydraulic fracturing of unconventional reservoir. Petroleum, 1(1), 8-15.

Li, H., Lai, B., and Lin, S., 2016. Shale Mechanical Properties Influence Factors Overview and Experimental Investigation on Water Content Effects. Journal of Sustainable Energy Engineering, 3(4), 275-298.

Ma, Xiaodong, and Mark D. Zoback. 2018. Static and Dynamic Response of Bakken Cores to Cyclic Hydrostatic Loading. Rock Mechanics and Rock Engineering 51, no.

6: 1943-1953.

Masri, M., Sibai, M., Shao, J. F., and Mainguy, M., 2014. Experimental investigation of the effect of temperature on the mechanical behavior of Tournemire shale. International Journal of Rock Mechanics and Mining Sciences, 70, 185-191.

Mokhtari, M., Honarpour, M. M., Tutuncu, A. N., and Boitnott, G. N., 2016. Characterization of elastic anisotropy in Eagle Ford Shale: Impact of heterogeneity and measurement scale. SPE Reservoir Evaluation and Engineering, 19(03), 429-439.

Niandou, H., Shao, J. F., Henry, J. P., and Fourmaintraux, D., 1997. Laboratory investigation of the mechanical behaviour of Tournemire shale. International Journal of Rock Mechanics and Mining Sciences, 34(1), 3-16.

Ong, O.N., Schmitt, D.R., Kofman, R.S. and Haug, K., 2016. Static and dynamic pressure sensitivity anisotropy of a calcareous shale, Geophys. Prospect. 64(4), 875–897

Plumb, R. A., 1994. Influence of composition and texture on the failure properties of clastic rocks. Paper SPE 28022, presented at Rock Mechanics in Petroleum Engineering, Delft, the Netherlands. 29-31,

Rickman, R., Mullen, M. J., Petre, J. E., Grieser, W. V., and Kundert, D. 2008. A practical use of shale petrophysics for stimulation design optimization: All shale plays are not clones of the Barnett Shale. In SPE annual technical conference and exhibition. Society of Petroleum Engineers. SPE 115258.

Rutter, Ernest, Julian Mecklenburgh, and Kevin Taylor, 2017. Geomechanical and petrophysical properties of mudrocks: introduction. Geological Society, London, Special Publications 454, no. 1: 1-13.

Rybacki, E., Meier, T., and Dresen, G., 2016. What controls the mechanical properties of shale rocks?–Part II: Brittleness. Journal of Petroleum Science and Engineering, 144, 39-58.

Shukla, Priyavrat, Vikas Kumar, Mark Curtis, Carl H. Sondergeld, and Chandra S. Rai. "Nanoindentation studies on shales, 2013. In 47th US Rock Mechanics Geomechanics Symposium. American Rock Mechanics Association. 2013. 2. 1194-1203.

Suarez-Rivera, R., Green, S. J., McLennan, J., and Bai, M., 2006. Effect of layered heterogeneity on fracture initiation in tight gas shales. In SPE Annual Technical Conference and Exhibition. Society of Petroleum Engineers. 10.2523/103327-MS.

Sone, H. and Zoback, M.D., 2013. Mechanical properties of shale-gas reservoir rocks—Part 1: Static and dynamic elastic properties and anisotropy. Geophysics, 78(5), pp.D381-D392.

Sone, H. and Zoback, M.D., 2013. Mechanical properties of shale-gas reservoir rocks—Part 2: Ductile creep, brittle strength, and their relation to the elastic modulus. Geophysics, 78(5), pp.D393-D402.

Teufel, L. W., Hart, C. M., Sattler, A. R., and Clark, J. A., 1984. Determination of hydraulic fracture azimuth by geophysical, geological, and oriented-core methods at the Multiwell Experiment Site, Rifle, CO. In SPE Annual Technical Conference and Exhibition. Society of Petroleum Engineers. SPE 13226

USGS, 1998, Seismic rock-physics model for carbonates at low effective stress levels, Published Research. 509. http://digitalcommons.unl.edu/usgsstaffpub/509

Wu, Y., Li, X., He, J., and Zheng, B., 2016. Mechanical Properties of Longmaxi Black Organic-Rich Shale Samples from South China under Uniaxial and Triaxial Compression States. Energies, 9(12), 1088.

Zeng, Z., Pike, M., Tice, M. M., Kelly, C., Marcantonio, F., Xu, G., and Maulana, I., 2018. Iron fertilization of primary productivity by volcanic ash in the Late Cretaceous (Cenomanian) Western Interior Seaway. Geology, 46(10), 859-862.

3. TRIAXIAL INELASTIC DEFORMATION AND BRITTLENESS OF THE EAGLE FORD FORMATION AS A FUNCTION OF COMPOSITION AND GRAIN STRUCTURE USING OUTCROP AND CORE SAMPLES

3.1. Introduction

Unconventional shale gas reservoirs are typically highly heterogeneous vertically and laterally in lithology and stratigraphy depending on the source of sediments and depositional environment (Passey et al., 2010). The lithologic variations of shale formations can greatly impact deformation behavior under reservoir stress conditions. The mechanical behavior can be predicted based on mineralogy and texture because the mineral and distribution of minerals of shale are related to the physics that governs rupture. Shales with high quartz and carbonate content tend to deform in a more brittle manner than shales having a greater percentage of clay minerals (Hucka and Das, 1974; Hajiabdolmajid and Kaiser, 2003; Jarvie et al., 2007; Rickman et al., 2008; Tarasov and Potvin, 2013; Wang and Gale, 2009). Landing laterals in brittle zones near strata with high TOC, or in zones with pronounced mechanical layering may promote the formation of new fractures and enhance the opportunity to reactivate existing fractures offering the best potential for connectivity to the reservoir, and with the least tendency for fracture closure and loss of permeability (Maxwell and Cipolla, 2011; Van Der Baan et al., 2013). Bourg (2015) proposed that an increase in clay content in shale can be related to a sudden reduction, up to a factor of 20, in compressive rock strength (Bourg, 2015) and

that the clay mineral content threshold for this reduction is 35%. During large-scale hydraulic fracturing, shale mineralogy plays a critical role during fracture initiation and propagation where a large portion of production is related to induced slow slip on pre-existing fractures (shearing on faults) rather than creating new tensile fractures (Das and Zoback, 2011; Stanek and Eisner, 2013). Laboratory studies have shown that the slip behavior of pre-existing fractures in shales can be correlated with compositional variations, specifically the TOC content and the clay mineral content (Kohli and Zoback, 2013).

In this study, samples of the carbonate-rich Eagle Ford Formation from outcrops in west Texas and from a productive reservoir in south Texas provide a unique opportunity to investigate the fracture strength and behavior under stress states similar to hydraulic fracturing conditions. The reservoir rocks were buried to a maximum depth of ~ 3.8 km, 1 km greater than the outcrop sections, during a period of fast sedimentation, and thus have high pore pressure gradient in-situ. Both outcrop and reservoir samples are highly variable in lithology at scales from cm to tens of meters. Representative samples were based on detailed lithofacies characterization to cover the broad spectrum of mineralogical variation in the formation. The mineralogy, texture, and elastic properties of the Eagle Ford Formation samples are summarized in Section 2. Yield strength, ultimate strength, frictional sliding strength, ductility (plastic yielding prior to failure), uniaxial compressive strength (UCS), and failure envelopes are determined in this Section. The influence of mineralogy, texture, and pressure on failure behavior are

discussed. In addition, several brittleness indices that are commonly used in the petroleum industry are quantified to better understand the brittle or ductile character of rupture. There are many ways to calculate and evaluate brittleness indices. Based on the laboratory data of triaxial experiments, brittleness indices of the Eagle Ford Formation samples are determined to provide insights into application in hydraulic fracture stimulation of the formation. The relationship between elastic properties and inelastic properties are investigated.

3.2. Methodology

3.2.1. Sample Selection, Lithology, and Mineralogy

The core and outcrop samples described in Section 2 include the range of textures and representative carbonate facies of Dunham's classification (1962). To explore the inelastic behavior of the Eagle Ford Formation suite, a subset of the samples investigated in the elastic property tests were chosen. The sample subset was selected on the basis of the elastic properties, carbonate facies classification, and texture. Specifically, samples chosen include those from the different carbonate facies (i.e., mudstone, wackestone, packstone, grainstone) but with distinct elastic behavior, and samples with similar Young's modulus but different textures (e.g., homogeneous texture vs. laminated). It is noted that reservoir samples often display more decompaction related imperfections, such as partings, that result from the extraction of the core from the subsurface. When these partings interfered with obtaining intact sub-core samples, or we had limited access to specific carbonate facies in the Swenson core, outcrop samples

with similar textures were selected. For each facies selected, several sub-cores were extracts adjacent to and across the linear strain-gauged horizons targeted for the elastic property testing. As such, the inelastic behavior determined can be compared directly with elastic behavior and with the previously described detailed textural characterization.

The compositions of the samples for described herein was also, provided by X-ray diffraction analyses are given in Table 3.1. These samples contain 0-13 vol% clay, 3 % to 29 vol% QFP minerals (quartz, feldspar, and pyrite), and 53%-96 vol% carbonate minerals. Total organic content was measured through pyrolysis tests on nearby samples of same/similar facies no more than 0.3 m away. Overall, the TOC content of the core and outcrop Eagle Ford Formation samples of this study varies from 0.1 wt% to 5.8 wt%. Since the uncertainty of the TOC estimate for each sample is not systematic, TOC is not included in the compositional analyses. Without considering TOC, the Eagle Ford Formation samples are composed of more than 70 vol% by volume strong phases including carbonate, quartz, feldspar, and pyrite minerals (Fig. 3.1).

The lithology, mineralogy, and texture of the core and outcrop samples were described (reference a table here). In order to quantify the relationship between grain fraction and inelastic behavior, a semi-quantitative estimate of the grain fraction was determined using the mosaic micrograph for each thin section (described in the methods of Section 2), focusing on the equivalent horizon for mechanical property measurements using ImageJ ®.

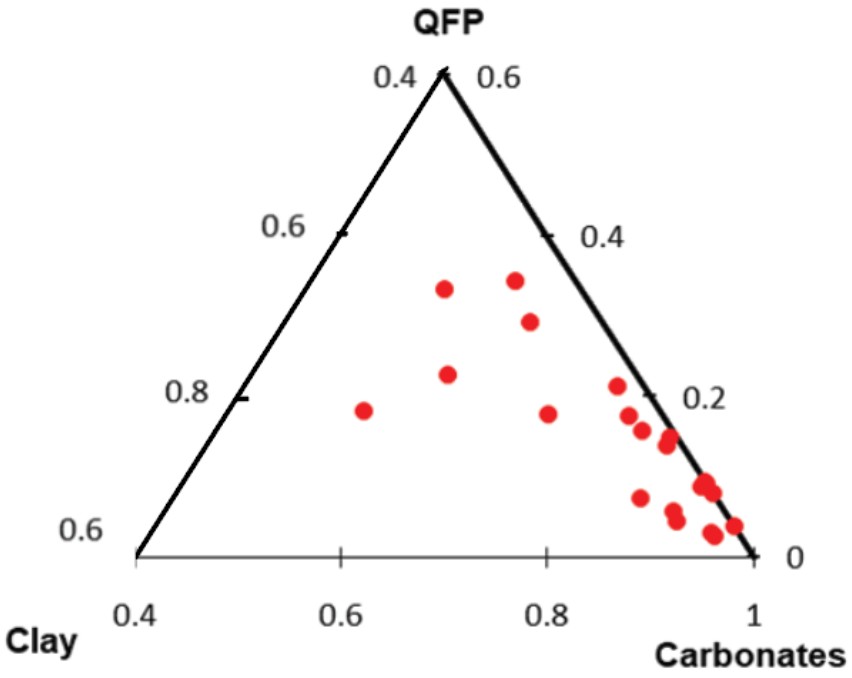

Figure 3.1 Bulk mineralogy of the Eagle Ford Formation sample from outcrop and core measured by X-ray diffraction

Table 3.1 Summary of Eagle Ford samples from outcrop and core for rock strength tests and their bulk mineralogy.

Location[a]	Name	facies	Calcite	Quartz	Kaolinite	pyrite	muscovite	dolomite	illite	albite	smectite
H1	H1B1-2	mudstone	63.8%	28.1%	7.0%	1.1%	0%	0%	0%	0%	0%
AC	B1-27	wackestone	79.1%	17.0%	3.4%	0.5%	0%	0%	0%	0%	0%
AC	B4-83	packstone	89.4%	5.3%	4.9%	0.4%	0%	0%	0%	0%	0%
AC	D-139	packstone	94.3%	3.0%	1.4%	0%	1.3%	0%	0%	0%	0%
AC	E2	packstone	94.9%	2.7%	2.4%	0%	0%	0%	0%	0%	0%
AC	C98	packstone	74.7%	21.2%	2.5%	0.2%	0%	1.5%	0%	0%	0%
AC	B-35	packstone	90.6%	9.4%	0%	0%	0%	0%	0%	0%	0%
AC	C-110	grainstone	84.2%	13.6%	1.4%	0.3%	0%	0.4%	0%	0%	0%
AC	B-50	grainstone	90.8%	9.2%	0%	0%	0%	0%	0%	0%	0%
AC	A-1	grainstone	74.9%	7.4%	7.4%	0%	0%	10.3%	0%	0%	0%
SC	SC473	mudstone	53.4%	30.9%	6.2%	2.4%	7.1%	0%	0%	0%	0%
SC	SC513	wackestone	71.2%	16.3%	11.0%	1.5%	0%	0%	0%	0%	0%
SC	SC427	wackestone	92.0%	7.7%	0%	0.4%	0%	0%	0%	0%	0%
SC	SC430	packstone	90.6%	8.8%	0.6%	0%	0%	0%	0%	0%	0%
SC	SC423	packstone	96.2%	3.2%	0%	0.6%	0%	0%	0%	0%	0%

a. H1 refers to U.S. Highway 90 road-cut samples taken just north of Del Rio, TX
AC refers to Antonio Creek outcrop samples; SC refers to Swenson Core samples

3.2.2. Determination of Inelastic Mechanical Properties

The triaxial compression tests to determine the inelastic properties of the Eagle Ford Formation samples focus on low confining pressures to quantify failure criteria at low mean stress conditions that are representative of conditions for hydraulic fracturing. The experiments were conducted using the same modified variable strain-rate triaxial apparatus (MVSR) employed for the elastic tests (see Section 2). This apparatus is particularly well suited for testing fine-grained rocks. All samples were deformed at room-humidity, room temperature, and at a constant strain rate of 10^{-5} s^{-1}. Preliminary tests demonstrated that the Eagle Ford Formation samples are very strong; therefore a smaller sample size was necessary for the inelastic tests to avoid exceeding the load limit of the MVSR (Fig. 3.2).

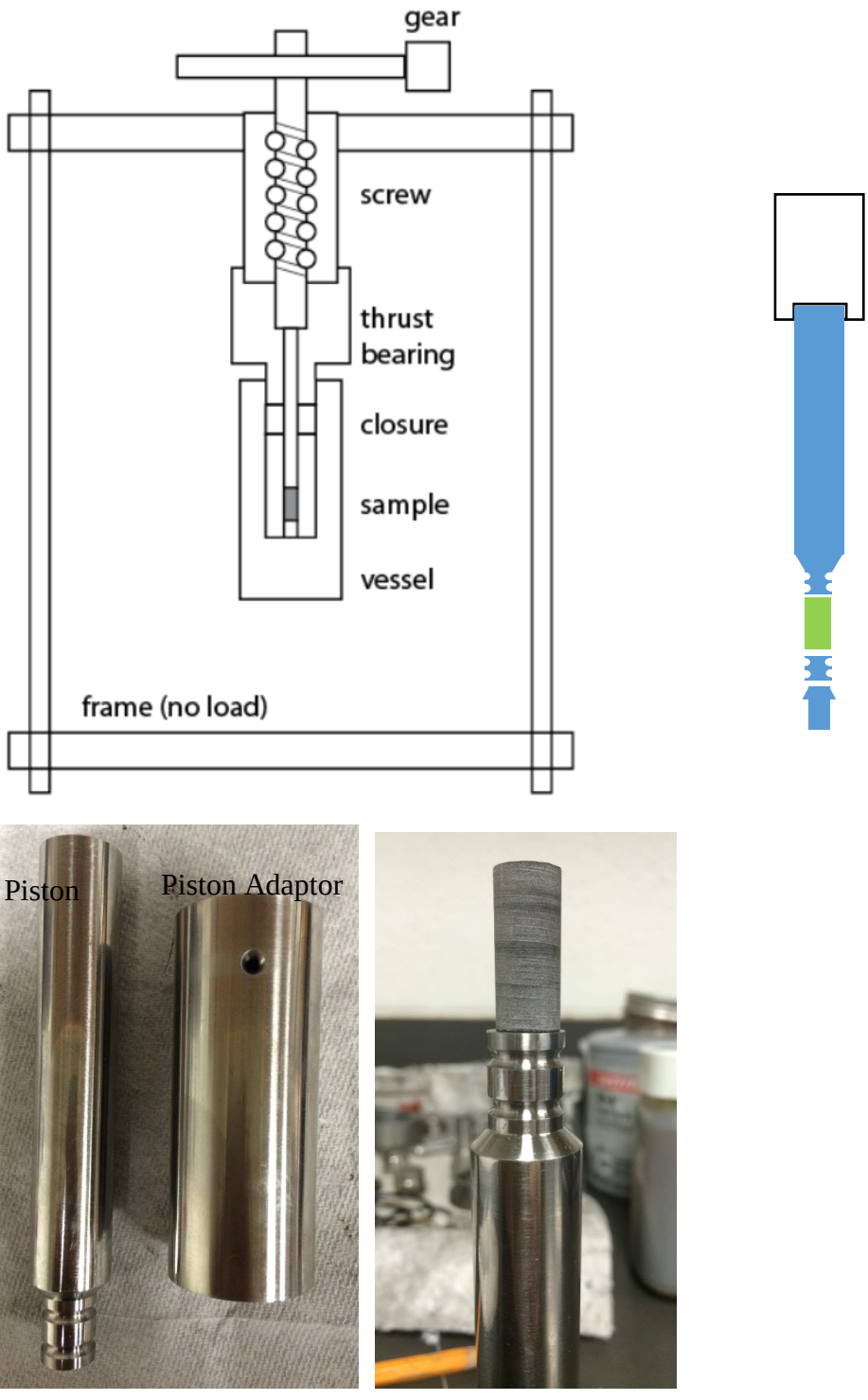

Figure 3.2 Loading system for triaxial compression tests and sample assembly setup.

The cylindrical samples are 12 mm in diameter, and have a length-to-diameter ratio of ~2.25. The smaller diameter samples also ensured that multiple similar sub-core samples for each representative carbonate facies would be available for the series of triaxial compression tests, which helped because of the limited volume of the subsurface core material available to us. A top piston adaptor was located between the load cell of the apparatus and a smaller piston, compatible with the sample diameter (Fig. 3.2). A heat-shrink polyolefin jacket was used to seal the sample from the confining fluid. Force was measured internal to the pressure vessel and mechanical data was measured at 10 Hz and recorded digitally at 1 Hz. The strain was measured externally with a displacement transducer (LVDT); external strain gauges were not glued to the outside of the sample during this sequence of tests. A correction for elastic distortion of the loading system was applied. The correction for elastic distortion was determined using the small piston with a stainless steel sample that was 12.7 mm in diameter. The elastic distortion is reflected by the difference of axial displacement of the sample and a reference curve calculated using the known Young's modulus of the steel sample. The correction was performed up to the full load capacity of the apparatus and under confining pressures up to 20 MPa.

The sub-cores were loaded directly to failure at confining pressures of 1, 7, and 15 MPa, and after macroscopic fracture, the sample was deformed further to determine the

frictional sliding strength. A typical triaxial stress-strain curve of the Eagle Ford Formation shows three regimes: elastic deformation until yield strength, subsequent hardening of the rock until failure point, and post-failure stress drop with frictional sliding on the fracture plane (Fig. 3.3). From the stress-strain curve, Young's modulus,-elastic strain, yield strength, ultimate strength, frictional sliding strength, and ductile strain can be determined. Young's modulus is determined by fitting a line to the linear portion of the stress-strain curve. The yield stress, defined as the onset of irrecoverable plastic deformation, is determined at the point where the curve deviates from the best-fit line to the elastic portion of the curve. Herein, plastic strain at any part of the curve is defined relative to the best fit line for the elastic portion, assuming that the elastic modulus is constant. The ultimate strength is the greatest differential stress achieved prior to fracture. Ductility, defined as the plastic strain prior to failure, is determined from the ultimate strength. Elastic energy that represents the energy stored in the rock before failure can be determined from the area under the stress-strain curve (Fig. 3.3). The plastic energy is related to irreversible plastic deformation of the rock and the sum of elastic and plastic energy is the total energy generated due to the work done by the external load. After macroscopic failure, associated with a large stress drop, frictional sliding on a distinct failure surface occurs. The frictional sliding strength is determined

from an average value of the steady-state sliding portion of the stress-strain curve where the stress level is almost constant with continuous deformation.

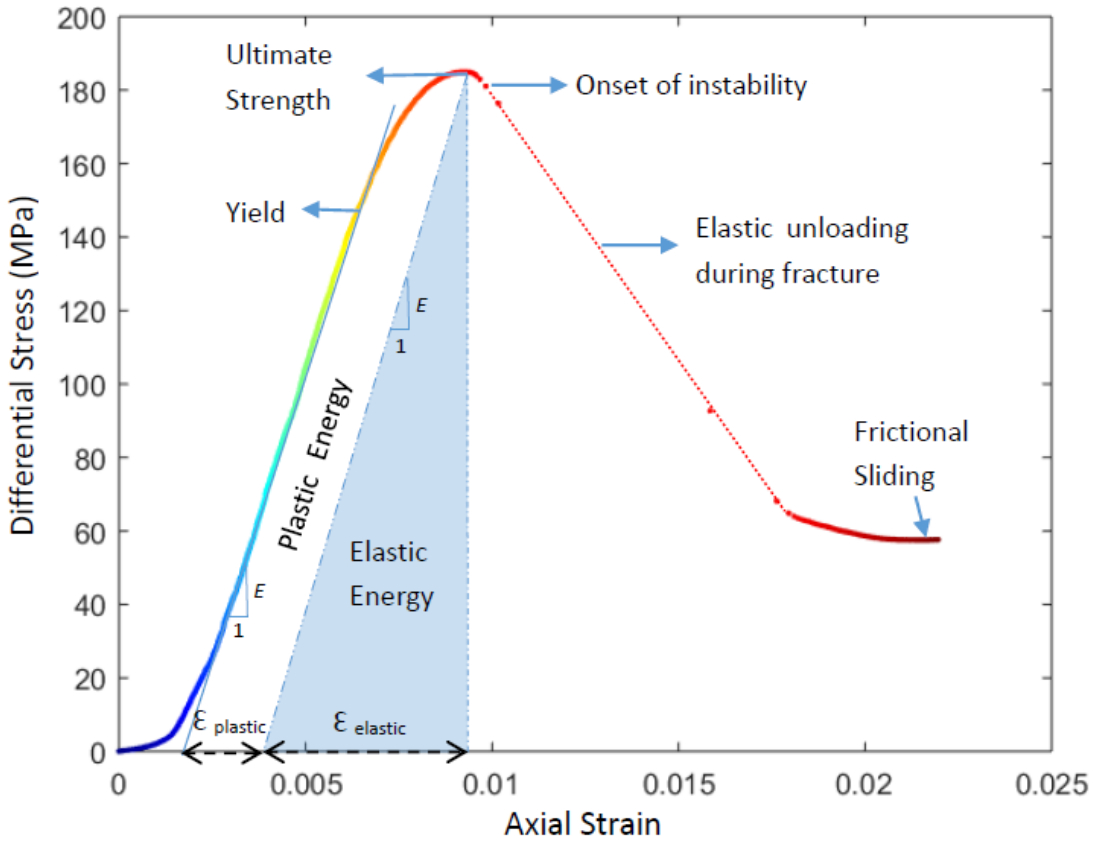

Figure 3.3 Example of stress-strain curve illustrating mechanical response descriptors. The descriptors include yield point, ultimate strength, frictional sliding strength, elastic strain, and plastic strain.

3.3. Results

3.3.1. Mechanical Behavior

All samples at all confining pressures tested show a classic mechanical response for brittle failure (Fig. 3.4a). Overall, mechanical properties vary systematically with lithofacies classification, with the lowest ultimate strength and Young's modulus in the mudstones and greatest ultimate strength and highest moduli in the grainstones. There is, however, sample-to-sample variation (Table 3.2). Under 15 MPa confining pressure, the grainstone facies yields at ~ 230 MPa and fails at ~300 MPa, which is nearly 3 and 2 times stronger than the organic-rich mudstones. The grain-supported facies from the Swenson core displays a much lower ultimate strength when compared to outcrop samples with similar mineralogy; this same observation is not observed for the mud-supported facies. The frictional sliding strength of the grainstone facies is up to ~ 1.6 times stronger than that of the mudstone facies. With an increase in grain fraction to mud fraction, from mud-supported to grain-supported facies, plastic yielding and ductile strain prior to fracture (ductility) and percent strain at ultimate failure decreases. Ductility of the organic-rich mudstones varies from 0.2 to 0.7%, which is 2-4 times greater than the ductility of the packstones and grainstone (Fig. 3.4c).

a)

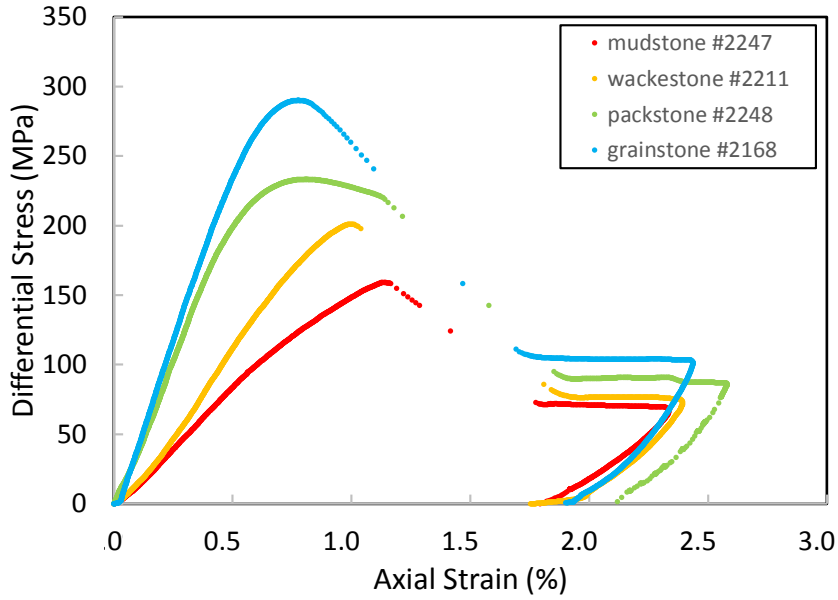

b)

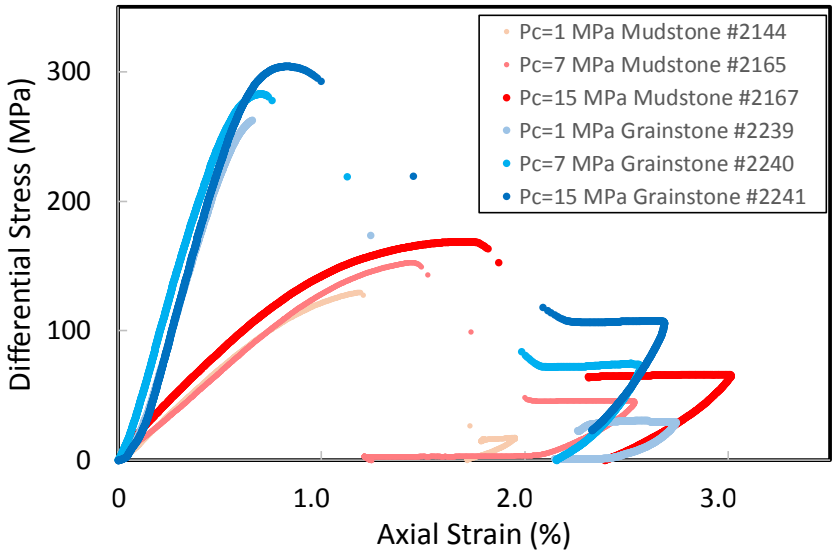

Figure 3.4 Stress-strain behavior and ductility of different carbonate facies. **a.** Model response of representative samples from the four lithofacies of the Eagle Ford Formation. The thin dashed line represents unstable fracture development. **b.** Mechanical behavior of representative mudstone and grainstone samples at 1, 7, and 15 Mpa confining pressures. The thin dashed line indicates unstable fracture development. **c.** Ultimate strength (fracture strength) as a function of carbonate facies under 1 MPa, 7 MPa, and 15 MPa confining pressures. **d.** Ductility of each sample as a function of carbonate facies.

c)

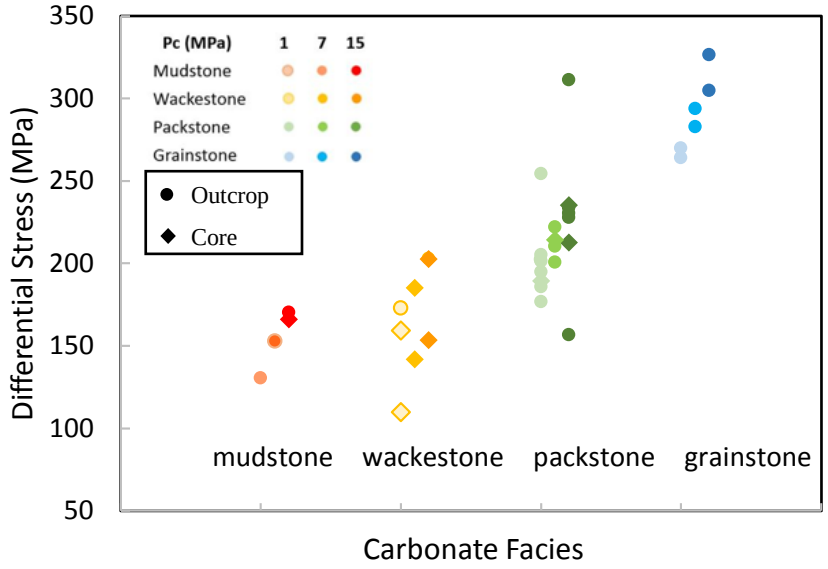

d)

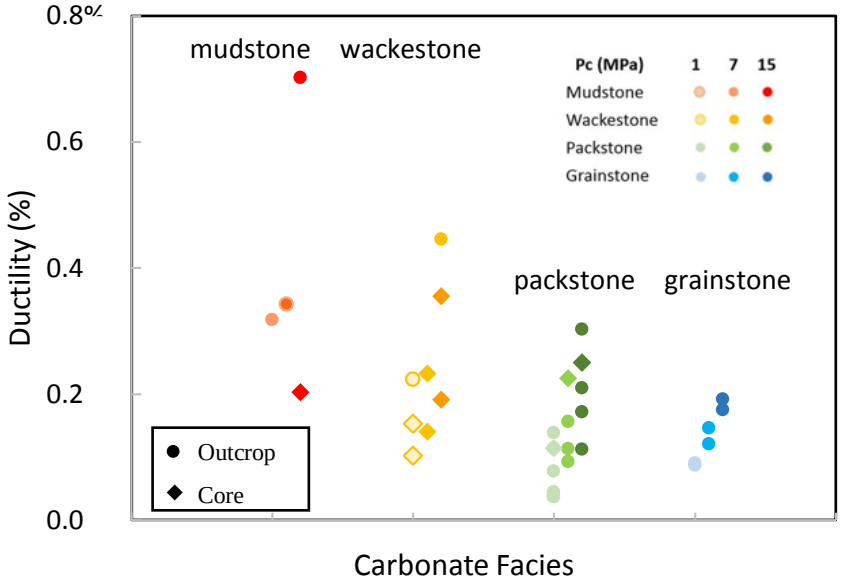

Figure 3.4 Continued

Table 3.2 Inelastic mechanical properties of samples of the Eagle Ford Formation determined in triaxial compression at three confining pressures.

Sample	Rock Type	Pc = 1 MPa				Pc = 7 MPa				Pc = 15 MPa							
		yield strength	ultimate strength	residual strength	ductility (%)	yield strength	ultimate strength	residual strength	ductility (%)	yield strength	ultimate strength	residual strength	ductility (%)	Angle of internal friction	Coefficient of internal friction	Cohesion	UCS
outcrop		MPa	MPa	MPa		MPa	MPa	MPa		MPa	MPa	MPa		degrees		MPa	MPa
H1B1-2	mudstone	78	131	17	0.32	92	153	46	0.33	81	171	67	0.70	36	0.73	34	130
AC_B1-27	wackestone	97	173	22	0.22	97	188	56	0.19	208	203	78	0.45	31	0.60	49	170
AC_B4-83	packstone	156	195	21	0.08	128	193	51	0.16	167	230	81	0.21	34	0.67	52	193
AC_D-139	packstone	135	177	24	0.05	157	201	76	0.11	143	234	107	0.17	41	0.87	41	173
AC_E2	packstone	177	205	25	0.04	177	222	55	0.09	179	228	78	0.11	38	0.78	51	202
AC_C98	packstone	192	255	5	0.14					232	311	93	0.30	41	0.87	59	251
AC_C-110	packstone	164	270	25	0.09	158	294	62	0.12	173	290	105	0.17	33	0.65	50	183
BAC_-50	grainstone	229	264	32	0.09	243	283	72	0.15	227	305	108	0.19	42	0.90	57	266
AC_B-35	grainstone	208	186	29	0.04	225	201	71	0.16	232	219	86	0.19	37	0.75	67	261
AC_A1	grainstone	120	130	19	0.04	116	141	44	0.11	98	157	77	0.19	33	0.65	30	128
core																	
SC_473	mudstone									101	166	76	0.20				
SC_513	wackestone	143	159	17	0.1	140	160	47	0.14	161	203	78	0.19	37	0.75	40	164
SC_427	wackestone	96	110	16	0.15	101	142	48	0.23	97	154	63	0.36	37	0.74	30	105
SC_430	packstone	159	190	17	0.11	160	185	58	0.16	178	213	83	0.25	28	0.53	57	199
SC_423	packstone	145	202	26	0.11	149	214	62	0.23	165	235	92	0.25	32	0.62	55	185

Ductility is presented as plastic strain prior to ultimate strength.
Sample AC_B1-27 is half mud-size fraction and half packstone. Sample AC_C98 is fine-grained packstone; Sample B35 is recrystallized coarse-grained grainstone.

The Young's moduli reported here also are derived from the slope of the linear portion of the stress-strain curve, and are compared with the Young's moduli determined from the elastic properties tests that used the larger samples and the linear and rosette strain gauges (Table 3.3, Fig. 3.5). Overall, the estimated Young's moduli from the inelastic tests are consistently less than the Young's moduli directly measured by the strain gauges, with an average of ~20% difference. The largest discrepancy between the two sets of tests is noted in the organic-rich mudstone facies where the Young's modulus calculated from the inelastic tests is up to 35% less than the direct measurement derived from the linear and rosette strain gauge data. Yet for the packstone and grainstone facies, the difference is less than 10%. It is important to note that the Young's moduli determined using the strain gauges were performed on larger samples (19 mm diameter with length to diameter ratios of ~2.25:1) under multiple confining pressure steps, and the ends of these samples were lubricated. The Young's moduli calculated from the inelastic tests at different confining pressures were performed on three separate smaller samples for each facies and the ends of samples were not lubricated. It is possible that the smaller sample size may have been more disturbed during coring and preparation of the samples ends, even though all sample ends appeared intact and parallel prior to the deformation tests. This is particularly true for the weak mudstone facies samples. The distribution of minerals and concentration of grains could also be a bit different, even though the subcores were taken at adjacent locations from the same blocks. This latter factor could impact the experimental data more for the laminated samples and the

heterogeneous organic-rich samples. In addition, the Young's moduli measured in elastic property tests records the response of the sample centers, where deformation typically concentrates in triaxial compression tests, whereas Young's moduli in the inelastic tests represent the response of the entire sample. These differences may explain the variations in Young's moduli noted in the two different sets of tests.

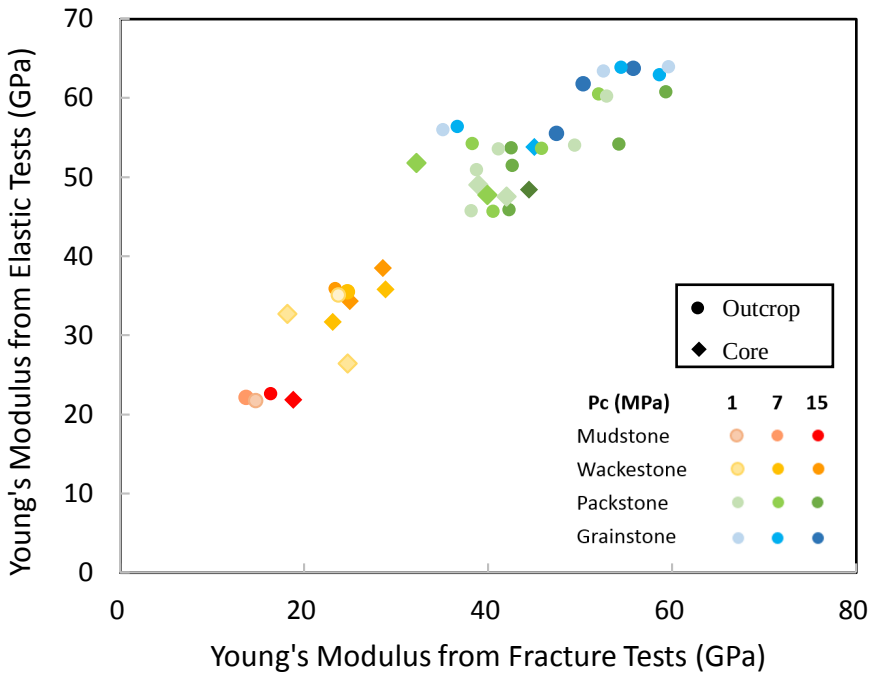

Figure 3.5 Comparison of two Young's modulus measurements. Young's modulus determined from fracture tests on small samples are plotted against Young's modulus determined from elastic tests on strain gauged, larger samples.

Table 3.3 Elastic properties and grain fraction of triaxial fracture test samples.

Sample	rock type	Grain Fraction	Pc = 1 MPa			Pc = 7 MPa			Pc = 15 MPa		
			E	*E (SG)*	v (SG)	*E*	*E (SG)*	v (SG)	*E*	*E (SG)*	v (SG)
Outcrop		Vol%	GPa	GPa		GPa	GPa		GPa	GPa	
H1B1-2	mudstone	16.8	14.8	21.7	0.18	13.7	22.2	0.18	16.4	22.6	0.18
AC_B1-27	wackestone	38.9	23.8	35.1	0.23	24.7	35.5	0.22	23.4	35.9	0.22
AC_B4-83	packstone	72.4	49.5	54.0	0.28	38.3	54.2	0.28	54.3	54.2	0.28
AC_D-139	packstone	89.1	38.2	45.7	0.26	40.6	45.7	0.26	42.3	45.9	0.27
AC_E2	packstone	91.5	52.9	60.2	0.28	52.0	60.5	0.28	59.3	60.8	0.28
AC_C98	packstone	99.2	38.8	50.9	0.24		51.3	0.24	42.6	51.5	0.24
AC_B-35	packstone	71.7	41.1	53.6	0.27	45.8	53.6	0.27	42.5	53.7	0.27
AC_C-110	grainstone	66.1	59.6	63.9	0.28	58.6	62.9	0.28	50.3	61.8	0.28
AC_B-50	grainstone	53.1	52.6	63.4	0.28	54.5	63.9	0.29	55.8	63.8	0.29
AC_A-1	grainstone	97.8	35.1	56.0	0.27	36.7	56.4	0.27	47.4	55.5	0.27
Core											
SC473	mudstone	5.1	n/a	18.3	0.16	n/a	20.5	0.18	18.8	21.9	0.19
SC513	wackestone	32.4	24.7	26.4	0.19	23.1	31.7	0.27	25.0	34.4	0.27
SC427	wackestone	22.0	18.2	32.7	0.17	28.8	35.8	0.19	28.6	38.5	0.19
SC430	packstone	40.9	42.0	47.6	0.24	39.9	47.8	0.24	44.5	48.4	0.24
SC423	packstone	54.0	38.9	49.0	0.26	32.2	51.8	0.27	45.0	53.8	0.27

E: Young's modulus obtained from stress-strain relation for fracture tests
E (SG): Young's modulus measured using strain gauges on elastic property tests
v (SG): Poisson's ratio measured using strain gauges on elastic property tests

The ultimate strength increases with confining pressure and this increase is facies dependent. The ultimate strength of a grainstone facies increases by 15% from 1 MPa to 15 MPa. By contrast, the ultimate strength of samples from the mudstone facies increases by up to 30%. A few samples show a slight decrease in ultimate strength from 1 MPa to 7 MPa confining pressure (Table 3.2). This later observation most likely is due to small textural difference among samples taken from the same horizon. Under confining pressures from 1 MPa to 15 MPa, the pressure dependency of ultimate strength can be fit using a linear relation for most samples, increasing about 1.71 to 2.9 MPa per 1 MPa increase of confining pressure at room temperature. The unconfined compressive strength of each sample is estimated from the relation between ultimate strength and confining pressure (Table 3.2).

The frictional sliding strength of the Eagle Ford Formation shows a stronger dependence on confining pressure when compared to the ultimate strength data (Fig. 3.6a). For instance, the frictional sliding strength of the mudstone and packstone facies increases up to a factor of 3.8 and 3.4, respectively, with a change in confining pressure from 1 to 15 MPa. Under reservoir conditions (~15 MPa), frictional sliding strength for all carbonate facies varies from 63 MPa to 108 MPa. The frictional sliding strength increases non-linearly with confining pressure, as the dependence on pressure decreases at the higher confining pressures (Fig. 3.6b). Although the mud-supported facies has lower ultimate and frictional sliding strengths than the grain-supported facies, the pressure dependence of these strengths is independent of the carbonate facies. Overall,

the ductility increases with confining pressure for all of the carbonate facies, (Fig. 3.6c). The mudstone facies displays the greatest degree of ductility when compared to the grainstone facies. The pressure dependency of ductility is related to carbonate facies. The mud-supported facies is much more sensitive to changes in confining pressure when compared to grain-supported facies. From 1 MPa to 15 MPa, the ductility of mud-supported facies increases by about 0.2% to 0.4%, yet the ductility of packstone and grainstone facies only increases by about 0.05% to 0.1%.

a)

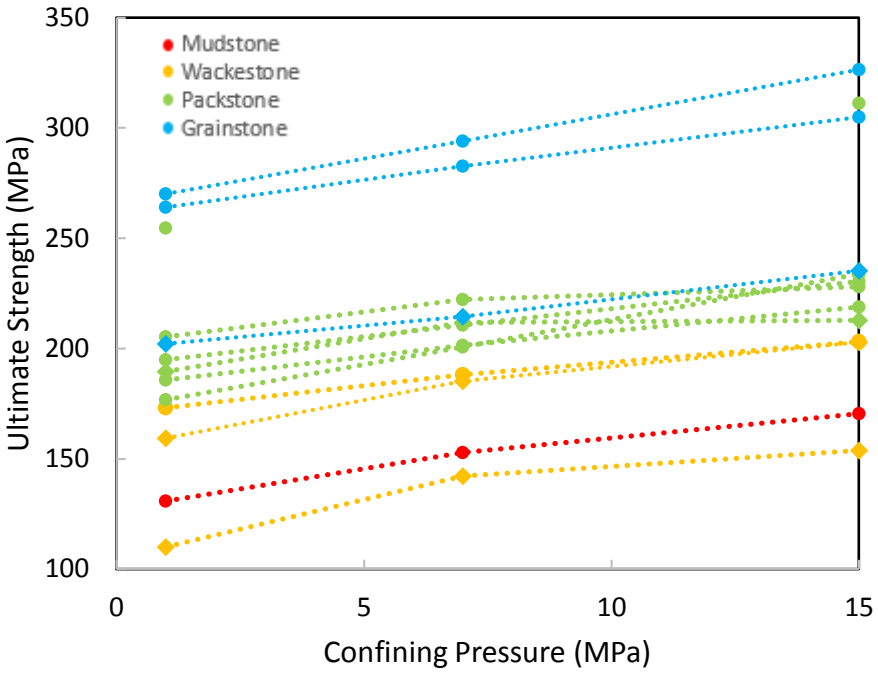

b)

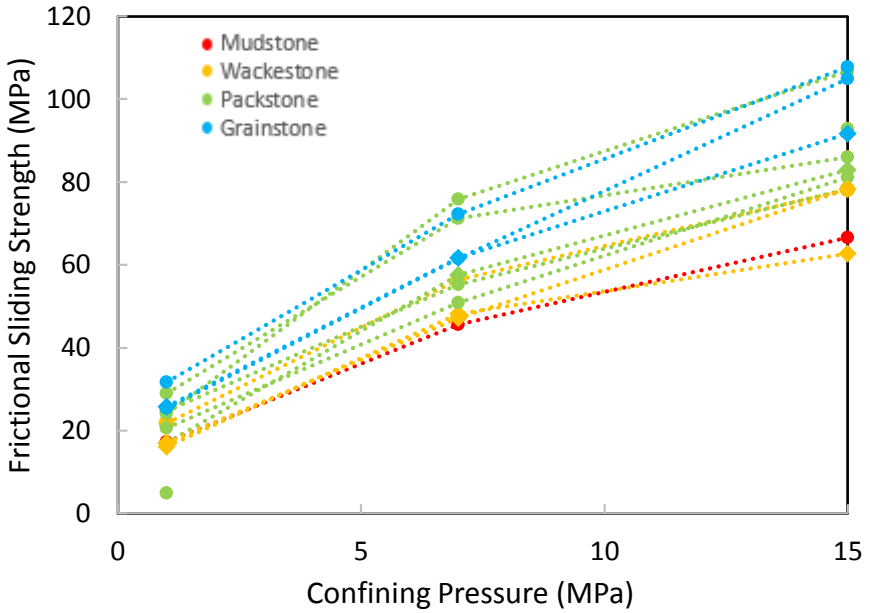

Figure 3.6 Ultimate strength **(a)**, frictional sliding strength **(b)**, and ductility **(c)** as a function of confining pressure.

c)

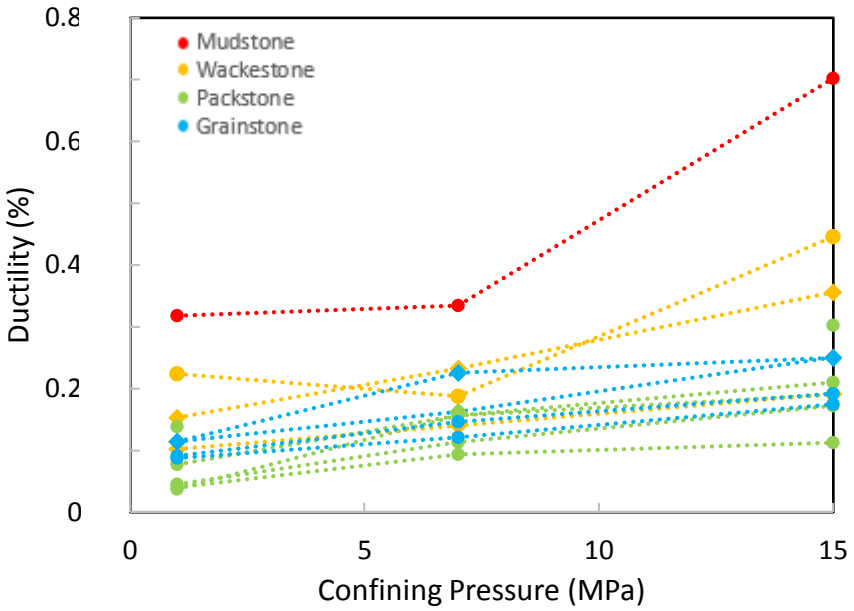

Figure 3.6 Continued

3.3.2. Macroscopic mode of failure and frictional sliding

Under low-pressure conditions, all carbonate facies failed by the formation of a discrete throughgoing macroscopic fault with associated smaller localized fractures at less than ~2 % strain. These fractures are oriented parallel to subparallel to the main fracture surface. The angle of the failure plane to the loading direction is similar for all carbonate facies at a specific confining pressure (Fig. 3.7).

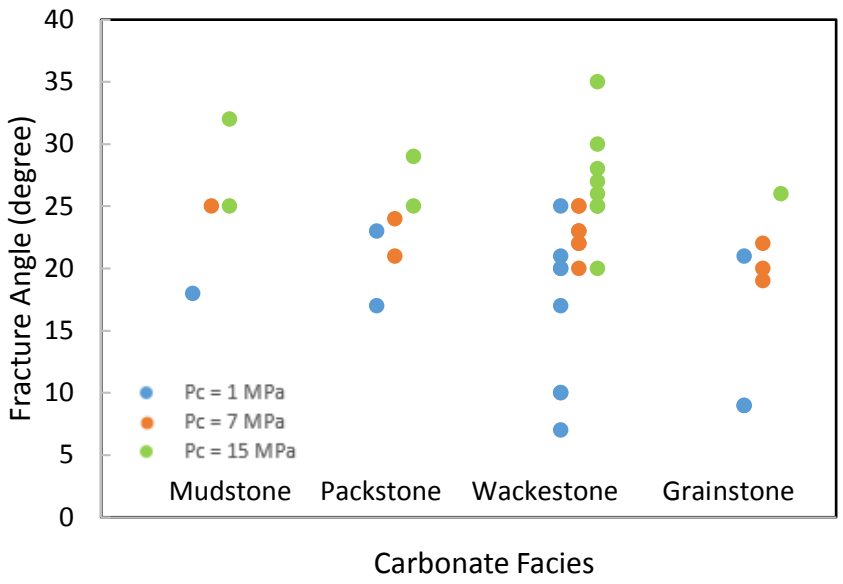

Figure 3.7 The angle of internal friction determined from the failure envelope as a function of carbonate facies.

The failure mode for this suite of samples is independent of carbonate facies but strongly dependent on confining pressure (Fig. 3.8). At 1 MPa, the samples tend to develop Mode I fractures parallel to the loading direction, shear fractures at a low angle to the loading direction, or both types of fractures in the samples. Typically, fractures are most abundant in the samples deformed under a 1 MPa confining pressure. With increasing confining pressure, the angle of the fracture plane, relative to loading direction, increases and some samples develop a conjugate shear fracture. Smaller faults associated with the thoroughgoing shears are observed in some samples. The dominant deformation in all samples is brittle fracture and frictional sliding along a throughgoing fault. The failure criteria of the samples, determined from the different confining pressure experiments. At low confining pressures, a linear coulomb failure criteria can

be applied to all facies. The coefficient of internal friction and the angle of internal friction do not change with confining pressure. The mean angle of internal friction is ~37 °and is independent of carbonate facies (Table 3.3). Cohesion also is obtained from the failure criteria. Overall, the cohesion increases from ~ 35 MPa, for mud-supported facies, to ~65 MPa for the grain-supported facies.

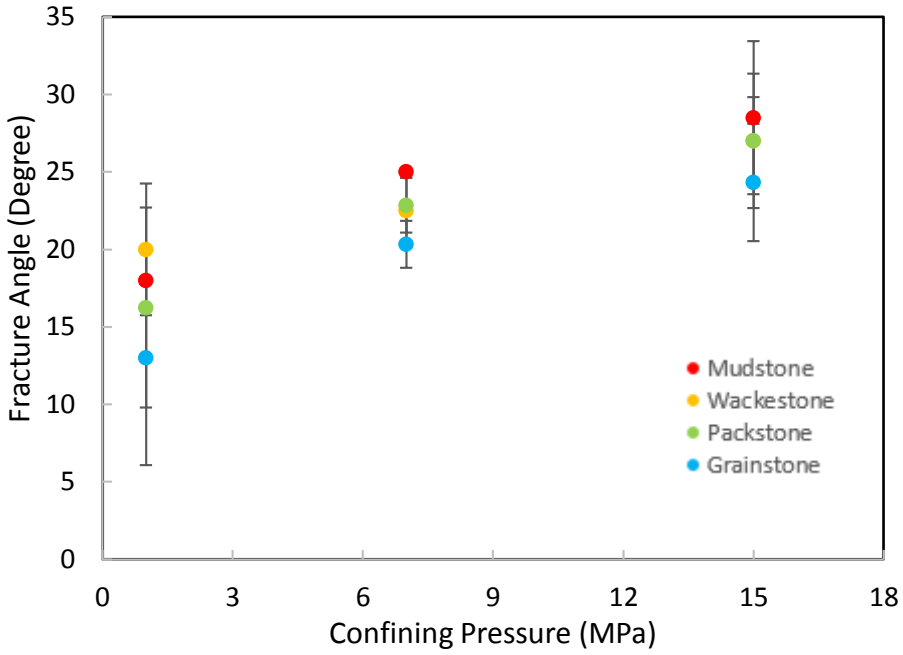

Figure 3.8 The angle of internal friction determined from the failure envelope as a function of confining pressure.

3.3.3. Brittleness Indices

Brittleness indices are widely used in industry as an indicator of failure behavior during hydraulic stimulation or to assess the quality of completion (e.g., Bishop, 1967; Hucak and Das, 1974; Hajiabdolmajid and Kaiser et al., 2003; Jarvie et al., 2007; Rickman et al., 2008; Wang and Gale, 2009). The mechanical properties derived from laboratory triaxial tests can be utilized to quantify brittleness and be used to describe failure characteristics of in situ shales. On the basis of the mechanical data, the stress, strain, and energy prior to and after failure are used in a number of brittleness indices to help characterize the degree of the brittleness of a rock.

Brittleness indices BI_{yield}, BI_{energy}, and $BI_{\text{post-failure}}$ are laboratory-based brittleness indices which rely on triaxial rock deformation tests on rock samples. The brittleness index, BI_{yield} (Eq. 3.1), is defined as the ratio of the elastic strain to the total strain (i.e., elastic plus plastic strain) prior to the failure of the rock (Hucka and Das, 1974; Andreev, 1995). Similar to BI_{yield}, the brittleness index that is based on energy, BI_{energy}, uses the ratio of reversible elastic energy to the total energy that the rock consumes before failure (Eq. 3.2) (Baron, 1962). By using the yield strength and ultimate strength of each experiment, and the elastic energy and the inelastic strain/energy one can determine BI_{energy}. When the ratio of BI is close to 1, elastic deformation is dominant and the rock is relatively brittle. When the ratio is approaching 0, the rock is dominated by plastic deformation and thus is more ductile.

$$BI_{yield} = \frac{\varepsilon_{elastic}}{\varepsilon_{elastic} + \varepsilon_{plastic}} \qquad \text{(Eq. 3.1)}$$

$$BI_{energy} = \frac{W_{elastic}}{W_{elastic} + W_{plastic}} \quad \text{(Eq. 3.2)}$$

$$BI_{post-failure} = \frac{\tau_{ultimate\ strength} - \tau_{frictional\ strength}}{\tau_{ultimate\ strength}} \quad \text{(Eq. 3.3)}$$

where $\mathcal{E}_{\text{elastic}}$ and W_{elastic} describe the elastic strain and elastic energy, respectively, that the sample absorbs during deformation, and $\mathcal{E}_{\text{plastic}}$ and W_{plastic} are a plastic strain and plastic energy, respectively, prior to failure. $\tau_{\text{ultimate strength}}$ and $\tau_{\text{frictional strength}}$ correspond to the ultimate strength (peak differential stress) and frictional sliding strength, respectively, of the rock at a certain confining pressure condition.

The brittleness index $BI_{\text{post-failure}}$ focuses on the post-failure behavior of the rock and is dependent on the energy release (stress drop) after failure. When the rock fails and loses its integrity, the energy is dissipated by fracture and friction during the failure. The amount of energy release is related to the stress drop, represented as a difference between ultimate strength and frictional sliding strength. $BI_{\text{post-failure}}$ is defined as the ratio of the stress drop to the frictional sliding strength (Eq. 3.3). When a rock dissipates most of its energy after failure, in other words, the stress drop of the rock after failure is close to the peak strength, $BI_{\text{post-failure}}$ is approaching 1 and the rock behaves in a brittle fashion. A $BI_{\text{post-failure}}$ value of 0 suggests that the rock fails in a ductile manner, and that the energy required for failure is released through plastic deformation.

Brittleness indices based on triaxial experiment data are determined using failure characteristics measured under a series of confining pressures (Table 3.4). Therefore,

brittleness indices can display pressure dependent behavior such as a decrease with an increase in confining pressure. Brittleness indices BI_{yield} and BI_{energy} capture pre-failure mechanical characteristics and are calculated based on the elastic deformation relative to the total deformation prior to failure (Fig. 3.4b, 3.4c). Under reservoir conditions (15 MPa), BI_{yield} and BI_{energy} vary from 0.6 to 0.8, and from 0.47 to 0.78, respectively. In general, BI_{yield} and BI_{energy} increase as the facies change from mudstones to grainstones. $BI_{post\text{-}failure}$ captures post-failure characteristics and focuses on the magnitude of the stress drop that is associated with energy dissipation after failure. $BI_{post\text{-}failure}$ varies from 0.51 to 0.7 under 15 MPa. However, $BI_{post\text{-}failure}$ does not show an obvious relation with carbonate facies type.

Table 3.4 Summary of triaxial deformation tests-based brittleness indices of the Eagle Ford Formation.

Sample	rock type	Pc = 1 MPa			Pc = 7 MPa			Pc = 15 MPa		
Outcrop		BI_{yield}	$BI_{post\text{-}failure}$	BI_{energy}	BI_{yield}	$BI_{post\text{-}failure}$	BI_{energy}	BI_{yield}	$BI_{post\text{-}failure}$	BI_{energy}
H1B1-2	mudstone	0.74	0.87	0.65	0.71	0.70	0.59	0.60	0.61	0.49
AC_B1-27	wackestone	0.79	0.87	0.65	0.74	0.62	0.60	0.67	0.61	0.52
AC_B4-83	packstone	0.85	0.89	0.73	0.78	0.74	0.66	0.70	0.65	0.51
AC_D-139	packstone	0.91	0.86	0.80	0.72	0.62	0.65	0.76	0.54	0.66
AC_E2	packstone	0.91	0.88	0.75	0.82	0.75	0.70	0.78	0.66	0.65
AC_C98	packstone	0.84	0.98	0.72				0.70	0.70	0.58
AC_B-35	packstone	0.83	0.84	0.84	0.73	0.65	0.51	0.74	0.61	0.58
AC_C-110	grainstone	0.85	0.91	0.71	0.82	0.79	0.64	0.77	0.64	0.67
AC_B-50	grainstone	0.85	0.88	0.73	0.78	0.74	0.63	0.74	0.65	0.60
AC_A-1	grainstone									
Core										
SC473	mudstone								0.55	0.47
SC513	wackestone	0.86	0.89	0.81	0.83	0.70	0.83	0.81	0.61	0.75
SC427	wackestone									
SC430	packstone	0.83	0.87	0.58	0.77	0.71	0.58	0.68	0.61	0.52
SC423	packstone	0.81	0.91	0.68	0.78	0.69	0.65	0.70	0.61	0.62

$$BI_{yield} = \frac{\varepsilon_{elastic}}{\varepsilon_{elastic} + \varepsilon_{plastic}}$$

$$BI_{energy} = \frac{W_{elastic}}{W_{elastic} + W_{plastic}}$$

$$BI_{post-failure} = \frac{\tau_{ultimate\ strength} - \tau_{frictional\ strength}}{\tau_{ultimate\ strength}}$$

3.4. Discussion

3.4.1. Inelastic properties as a function of mineralogy and grain fraction

Inelastic properties are related to carbonate facies. The mechanical response of a section of a shale body that has varying lithology can be predicted based on mineralogy and texture of the rock. It is assumed that the strong or weak phases of a shale contribute to its mechanical properties. Although the TOC and porosity are not included in this study because data were not available for several of the samples. There is an overall decrease in ultimate strength and unconfined compressive strength with clay content (Fig. 3.9). The relationship between ultimate strength and clay mineral content can be expressed as

$$\sigma = \frac{556.7}{1.285 + \left(\frac{X\,clay}{0.01}\right)^{0.345}} + 0.0019 \qquad \text{(Eq. 3.4)}$$

Where σ is ultimate strength and X_{clay} is clay content.

The clay minerals in the Eagle Ford Formation include kaolinite, muscovite, Illite, and smectite (reference the appropriate table with these data here). With an increase in clay content from 0% to ~10%, the strength of a sample decreases by almost 50%. When the clay content exceeds 10%, the rate of decrease in ultimate strength is reduced. It is consistent with observations in other shale formations that the UCS decreases gradually with increasing clay content before the rock reaches a threshold value of ~35% clay content (Bourg, 2015). The variability shown by the data may reflect other factors, such as variations in TOC, porosity, microfabric, and other textural characteristics of samples that are characterized in this study. In addition, most of the

packstone and grainstone samples contain more than 95% strong phases, and the variations in % clay minerals are too small to produce recognizable impacts of mineralogy on elastic and inelastic behavior.

Ductility is characterized by the inelastic strain up to the point of fracture. It often is expected that shales with a greater clay mineral content tend to show greater ductility, particularly if the clay minerals form coatings around the stiffer minerals (e.g., quartz, calcite) (Bourg, 2015; Sone and Zoback, 2013b). The plot of ductility versus carbonate facies for the Eagle Ford Formation (Fig. 3.3d) is consistent with this hypothesis. This plot shows that ductility decreases with decreasing clay mineral content and decreases with increasing carbonate content.

Overall, the ultimate strength clearly decreases with an increase in clay mineral content (Fig. 3.9a) and shows a less dramatic increase with an increase in carbonate content (Fig. 3.9b). The packstones and grainstones in Fig. 3.9b show the greatest variability in ultimate strength, suggesting that other factors (e.g., texture, degree of recrystallization) also have an impact on defining the ultimate strength of the samples. In some cases, this variability is related to the presence of significant recrystallized calcite patches noted when more than 80% of the sample is composed of carbonate minerals. Ultimate strength also decreases with an increase in the QFP content, but again, there is some variability between the samples that are related to specific textural characteristics (Fig. 3.9c).

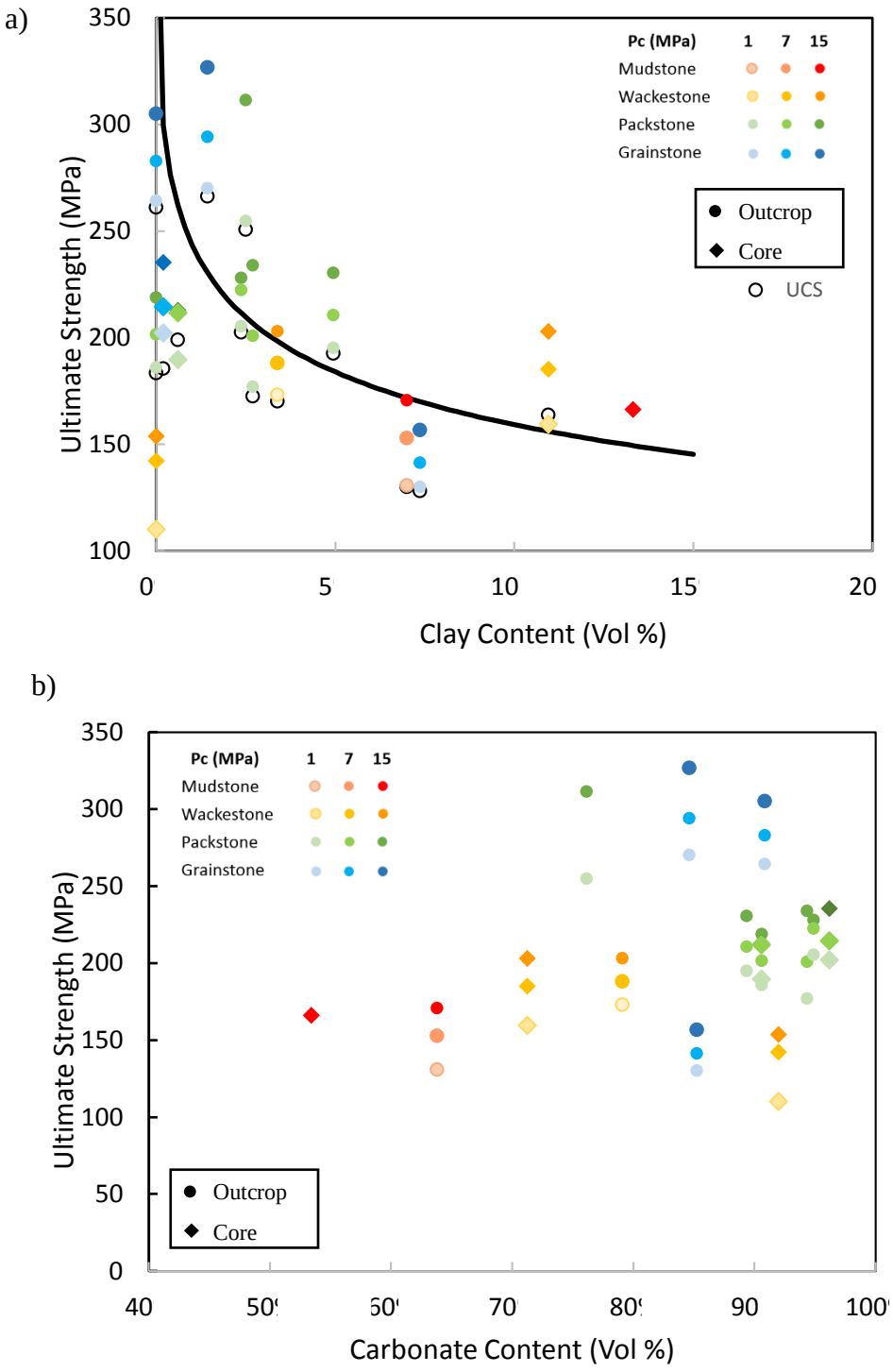

Figure 3.9 The relationship between ultimate strength and (**a**) clay content, **(b)** carbonate content, and **(c)** QFP content.

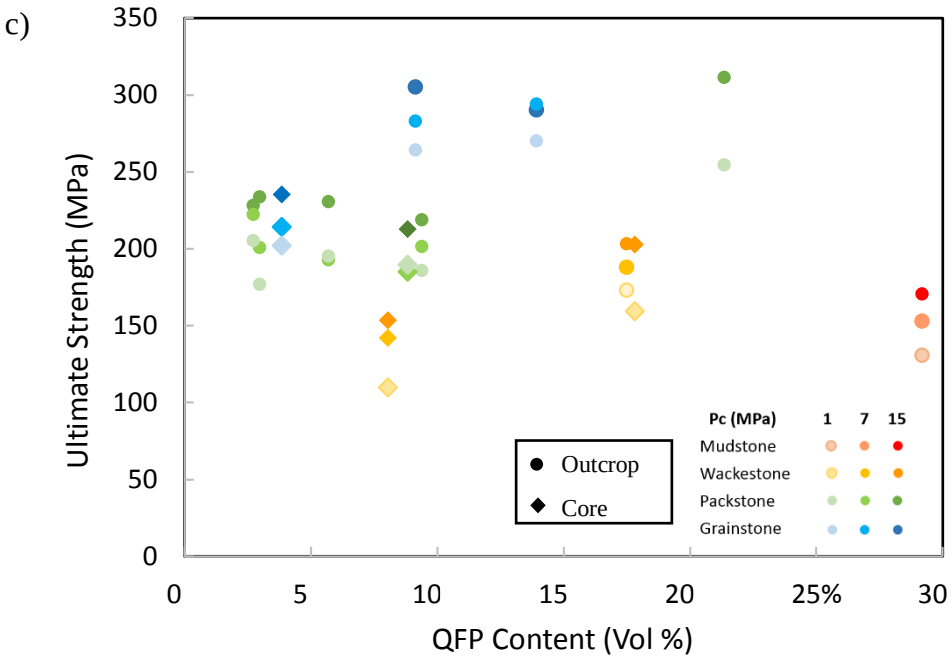

Figure 3.9 Continued

Ultimate strength also is related to the grain fraction of the rock. The ultimate strength increases from ~150 MPa to 300 MPa with as the grain fraction increases from ~7% to ~60% (Fig. 3.10). The ultimate strength shows greater variability above ~65% grain fraction, corresponding to the definition of the grain-supported facies. Above this grain fraction, there is a variation in ultimate strength that also relates to the distribution and size of the carbonate grains and the presence of recrystallized calcite grains and matrix.

These data presented above show that the variation of ultimate strength for the packstone and grainstone facies of the Eagle Ford Formation samples tests also depends on textural characteristics when the carbonate content is in the form of recrystallized patches. Based on the microfabric observations of the samples, the strongest packstone

and grainstone facies samples are recrystallized carbonate rocks with a partially or highly micritized matrix. The presence of micritic cement, reduction in grain size due to recrystallization, and the low porosity result in an increase the ultimate strength. This observation is consistent with the work of others (e.g., Rashed et al., 2014). In contrast, the packstone and grainstones samples that do not share these features, but instead display other significant textural characteristics, such as burrows, pyrite alteration with moldic porosity, and/or laminations of organic matter may have lower Young's moduli and/or ultimate strengths.

Overall, mineralogy and grain fraction have strong influences on Young's modulus and ultimate strength, especially for mud-supported facies. Microstructural features such as the occurrence of diagenetic features, micritized zones, cementation and/or recrystallization, and bioturbation can have a significant impact on the mechanical properties of the grain-supported facies.

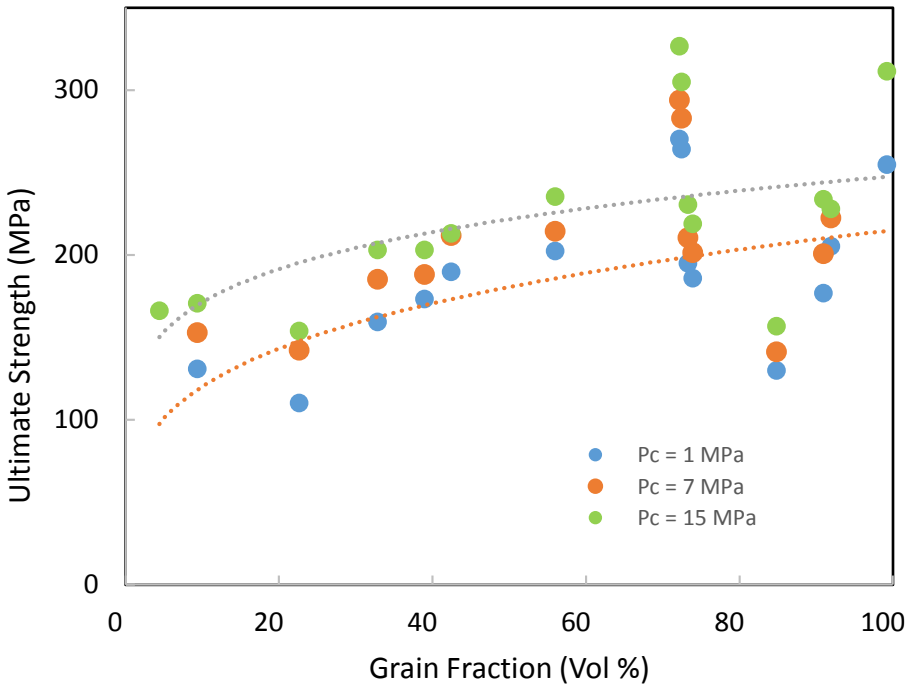

Figure 3.10 Relationship between ultimate strength and grain fraction of the rock.

3.4.2. Brittleness as a Function of Mineralogy and Grain Fraction

Triaxial experiment based brittleness indices BI_{yield}, BI_{energy}, and $BI_{post\text{-}failure}$ are derived from direct measurements of inelastic properties (e.g., Rybacki et al., 2016). $BI_{post\text{-}failure}$ shows no correlation with carbonate facies, BI_{yield} and BI_{energy}, show a very weak relationship to carbonate facies. The ratio of grains to mud-size particles is quantified by grain fraction. Strain-related BI_{yield} shows a positive relationship with a samples grain fraction. The relationship can be fit using linear relationships as

$$BI_{yield} = 0.16 * X_{grain} + 0.73 \qquad \text{For Pc=1 MPa}$$

$$BI_{yield} = 0.17 * X_{grain} + 0.60 \qquad \text{For Pc = 15 MPa,}$$

where BI_{yield} is the brittleness index based on the fraction of elastic strain over the total strain prior to failure, X_{grain} is the grain fraction of the rock estimated from image analysis (Fig. 3.11a).

The energy-related brittleness index, BI_{energy}, also shows an overall increasing trend with an increase in grain fraction of the samples. The scatter in the data makes it difficult to derive a specific correlation. The brittleness index that is based on post failure characteristics, $BI_{post\text{-}failure}$, does not show a significant relation to the grain fraction of the samples (Fig. 3.11b).

In addition to grain fraction, the relationship between brittleness indices and mineralogy also is investigated. $BI_{post\text{-}failure}$ does not show a distinct relationship with clay mineral content, consistent with observations in Yang et al., (2013). Both BI_{yield} and $BI_{energy,}$ however, show a negative relationship with an increase in clay mineral content for each confining pressure tested (Fig. 3.12a, 3.13a). Soft clay minerals interspersed with stiffer minerals could tend to increase a sample's ductility. Clay mineral content, however, is not related to the strain-related brittleness BI_{yield} (Yang et al., 2013). The Eagle Ford Formation samples selected for the experiments herein have clay mineral contents from 0% to nearly 15%. Although shale samples vary from 0 to 40% (Yang et al., 2013), a variation in the lab-based brittleness indices is in general small (e.g., BI_{yield} varies from 0.6 to 0.81 at 15 MPa confining pressure. The relationship between BI_{energy} and clay mineral content is consistent with observations for other black shales (e.g., Rybacki et al., 2016).

Interestingly, BI_{yield} and BI_{energy} increase with an increase in carbonate content, yet decrease with an increase in QFP content (Fig. 3.12b, 3.12c, 3.13b, 3.13c). The relationship between brittleness index and QFP content is opposite to the observations of 4 types of black shales (Rybacki et al., 2016). It may suggest that strong minerals may not necessarily contribute to the Young's modulus character of the sample. Yet, when strong phase QFP content increases in the Eagle Ford Formation and in the black shales reported by Rybacki et al. (2016), another strong phase carbonate content decreases. Ultimate strength also depends on the distribution of the strong phase in the sample. If the strong phase is dispersed and mixed with soft organic matter, clay minerals, or is associated with porosity, the strong phase may not increase the strength of the sample to deformation. Overall, the Eagle Ford Formation samples tested contain 1% to 33% quartz. The mudstones and wackestone facies contain more quartz, varying from 17% to 33% when compared to packstones and grainstones (1%-15%). The quartz is present as either equant recrystallized cement grains that are less than 10 μm, or as large detrital, angular grains dispersed but rarely seen in the sample. Equant authigenic quartz cement is the most common form and is present throughout the samples. Angular shape detrital quartz grains are rarely observed in the Eagle Ford Formation. The quartz cement is associated with the coccolith foraminifera or mixed with the calcite cement and clay minerals in the matrix. These randomly distributed quartz cement grains appear not to contribute to the Young's modulus of the samples because they are dispersed and mixed with soft clay minerals for the most part.

a)

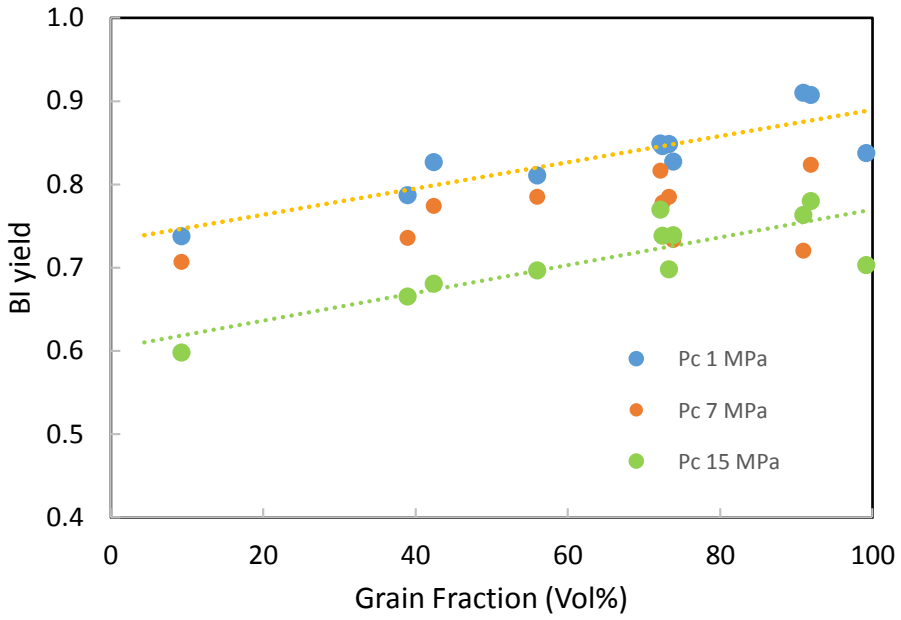

b)

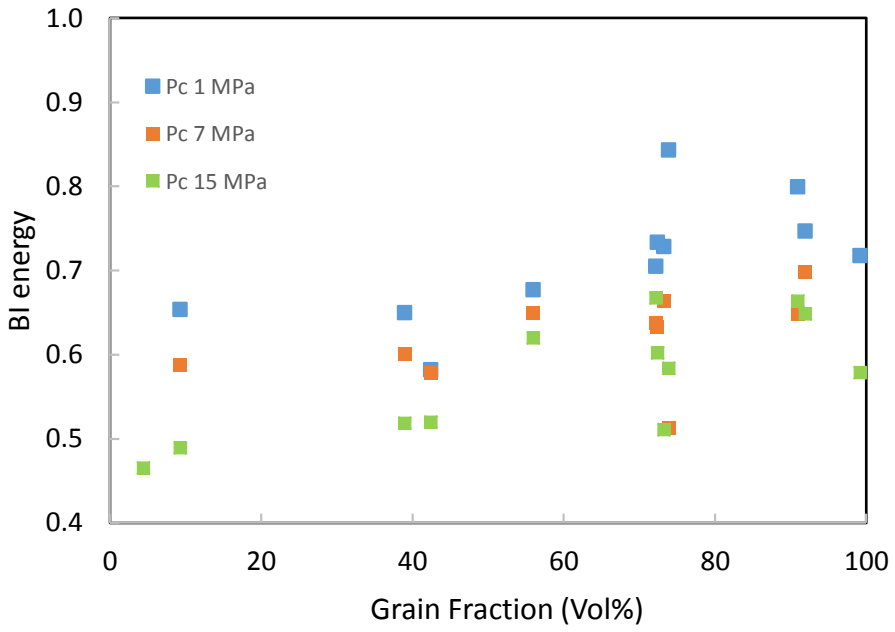

Figure 3.11 Brittleness indices BI_{yield} (a) and BI_{energy} (b) as a function of grain fraction.

a)

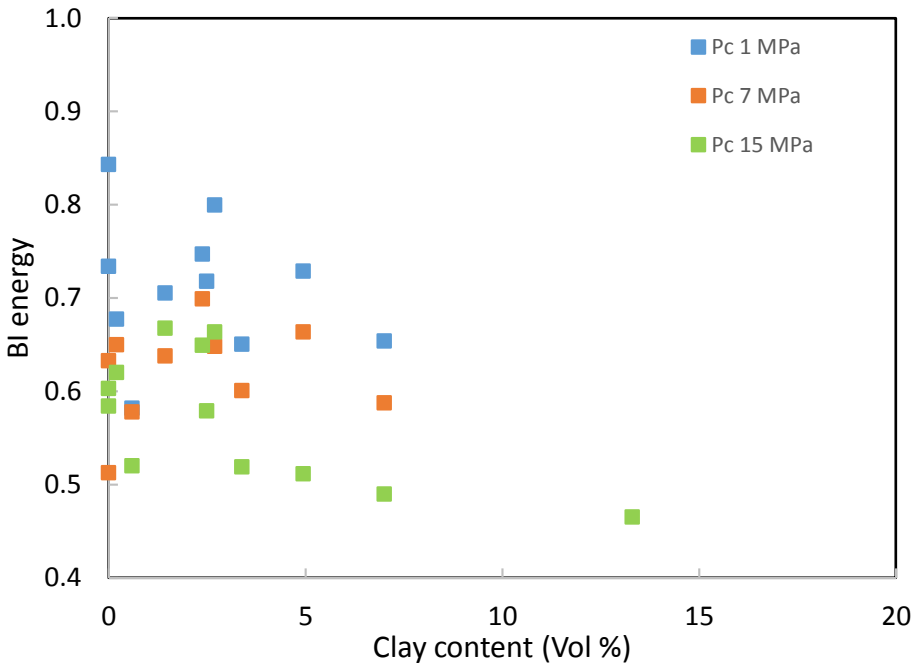

b)

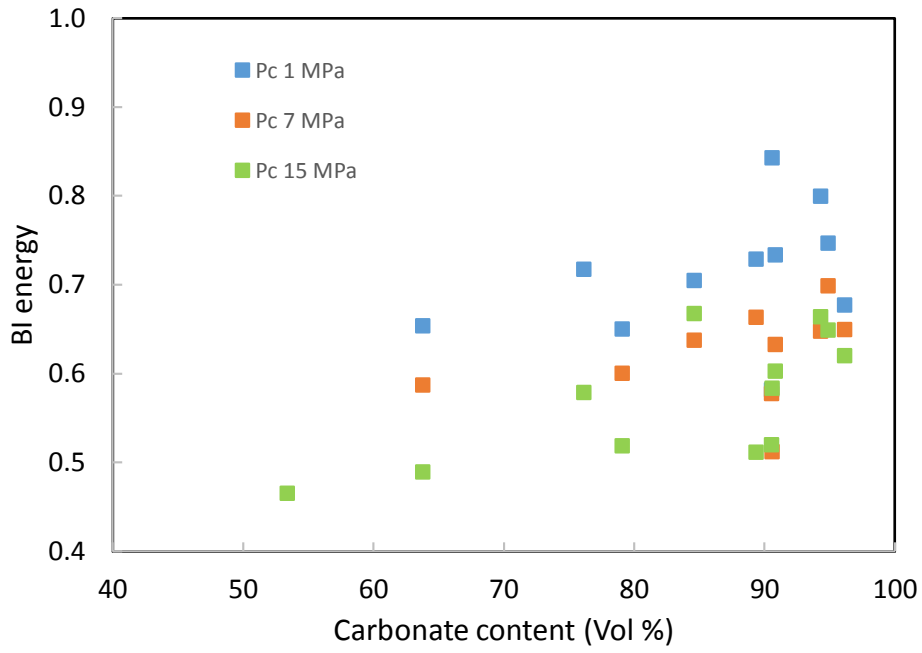

Figure 3.12 Brittleness index *BI* $_{\text{energy}}$ as a function of clay content **(a)**, carbonate content **(b)**, and QFP content **(c)**.

c)

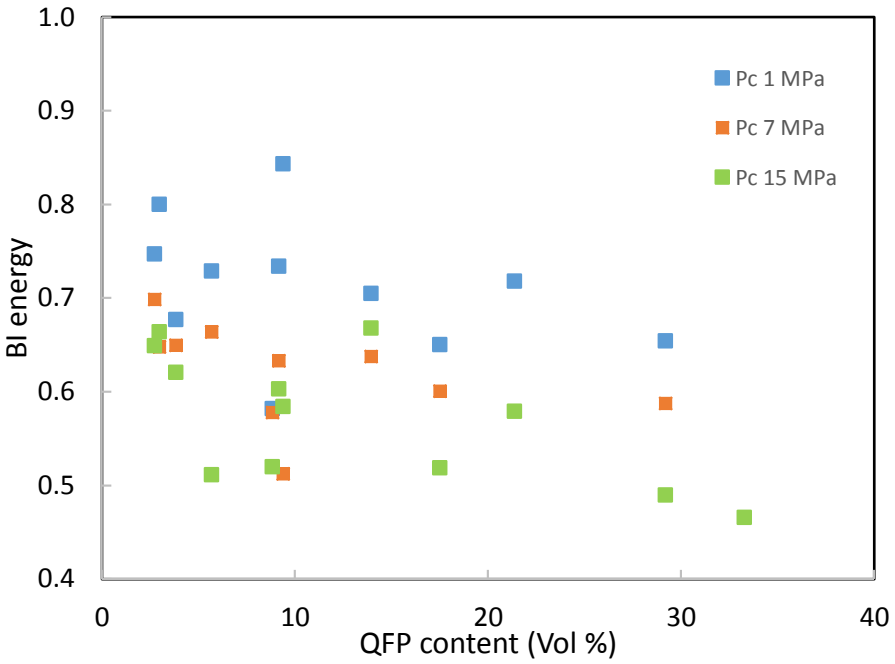

Figure 3.12 Continued

a)

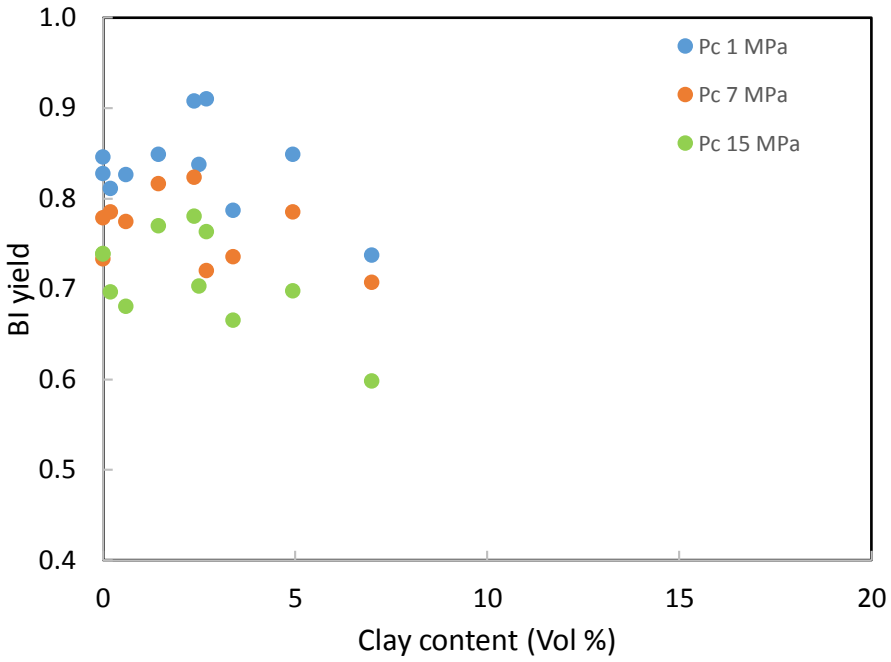

b)

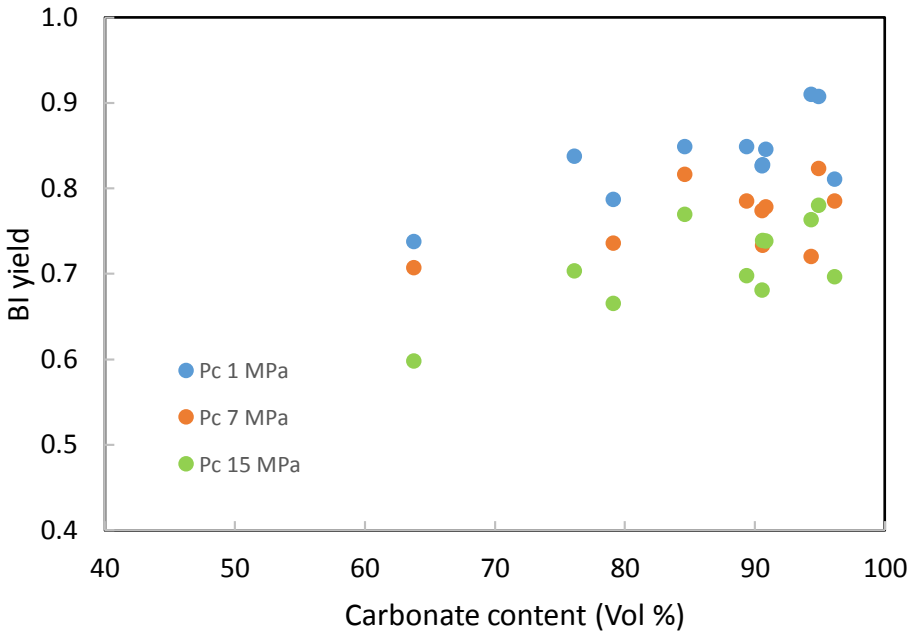

Figure 3.13 Brittleness index BI_{yield} as a function of clay content **(a),** carbonate content **(b),** and QFP content **(c).**

c)

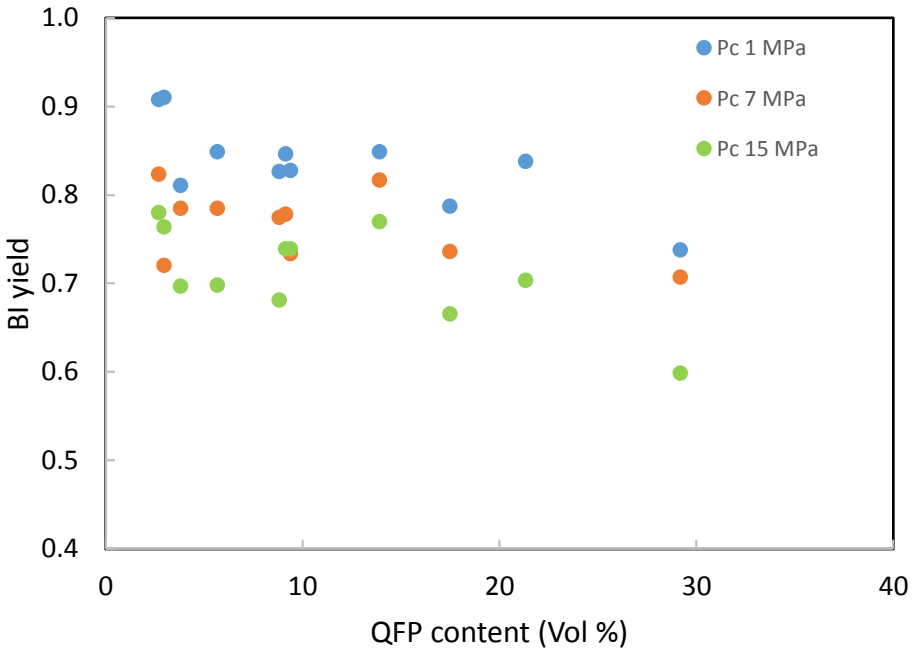

Figure 3.13 Continued

3.4.3. Inferring Inelastic Properties and Brittleness from Elastic Properties

Reliable mechanical properties of shale can be measured in the laboratory through rock mechanics testing. This method provides a more direct approach to predict the initiation and propagation of hydraulic fractures, define failure criteria, identify modes of failure, and characterize the frictional sliding strength. Because of the difficulty in acquiring well-preserved core material from productive subsurface horizons for testing, limited data are available to quantify the mechanical properties of the wide variety of shale rocks. Therefore, many efforts have been made to correlate inelastic properties with elastic properties measured indirectly as the importance of mechanical properties in the course of the exploration and production of an unconventional shale gas reservoir is critical, and routine triaxial experiments are not performed (Chang and Zoback, 2006; Sone and Zoback, 2013b; Rybacki et al., 2016).

Elastic properties can be determined in the laboratory or inferred from the wireline sonic logs. Young's modulus can be important to the initiation of hydraulic. The greater the Young's modulus the longer the hydraulic fractures tend to be (Huang et al., 2018).

In this study, elastic properties and inelastic properties are measured at the same confining pressures, allowing correlation of these two mechanical parameters. The ultimate strength of the Eagle Ford Formation increases with Young's modulus under all tested confining pressures (Fig. 3.14a). The relationship is nearly linear. The mudstone facies has the lowest Young's modulus and ultimate strength around 20 GPa and 150 MPa, respectively, under low confining pressure. The grain-supported facies have higher

ultimate strengths 0 MPa to ~300 MPa and Young's modulus ~ 65 GPa. UCS also shows a positive correlation with Young's modulus (Fig. 3.14b). The trend matches empirical power-law relationships for shale formations (Horsrud, 2001).

Brittleness indices derived from triaxial experiment data can also be related to elastic properties. With an increase in Young's modulus or Poisson's ratio, the strain-related brittleness index BI_{yield} increases (Fig. 3.15a, 3.15b). The relationship is close to a power law function where at low Young's modulus and Poisson's ratio, the increase in BI_{yield} is faster and the rate of increase decreases at higher Young's modulus. A similar relationship is observed between BI_{energy} and Young's modulus (Rybacki et al., 2016). BI_{energy} also has a power law relationship with Young's modulus. With an increase in pressure and temperature, the relationship shifts to lower brittleness values (Fig. 3.15c).

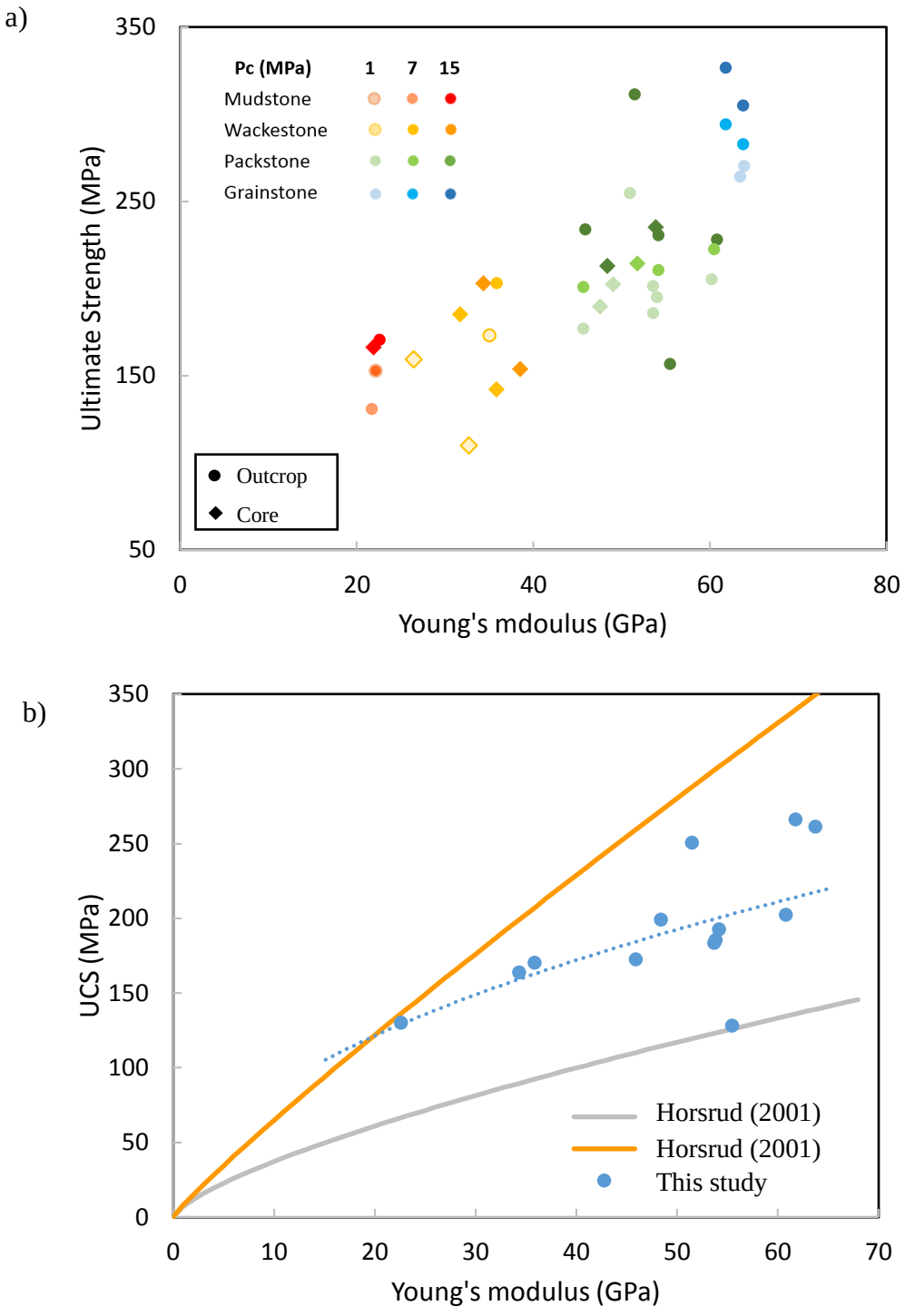

Figure 3.14 The relationship between ultimate strength **(a)** and UCS **(b)** with Young's modulus.

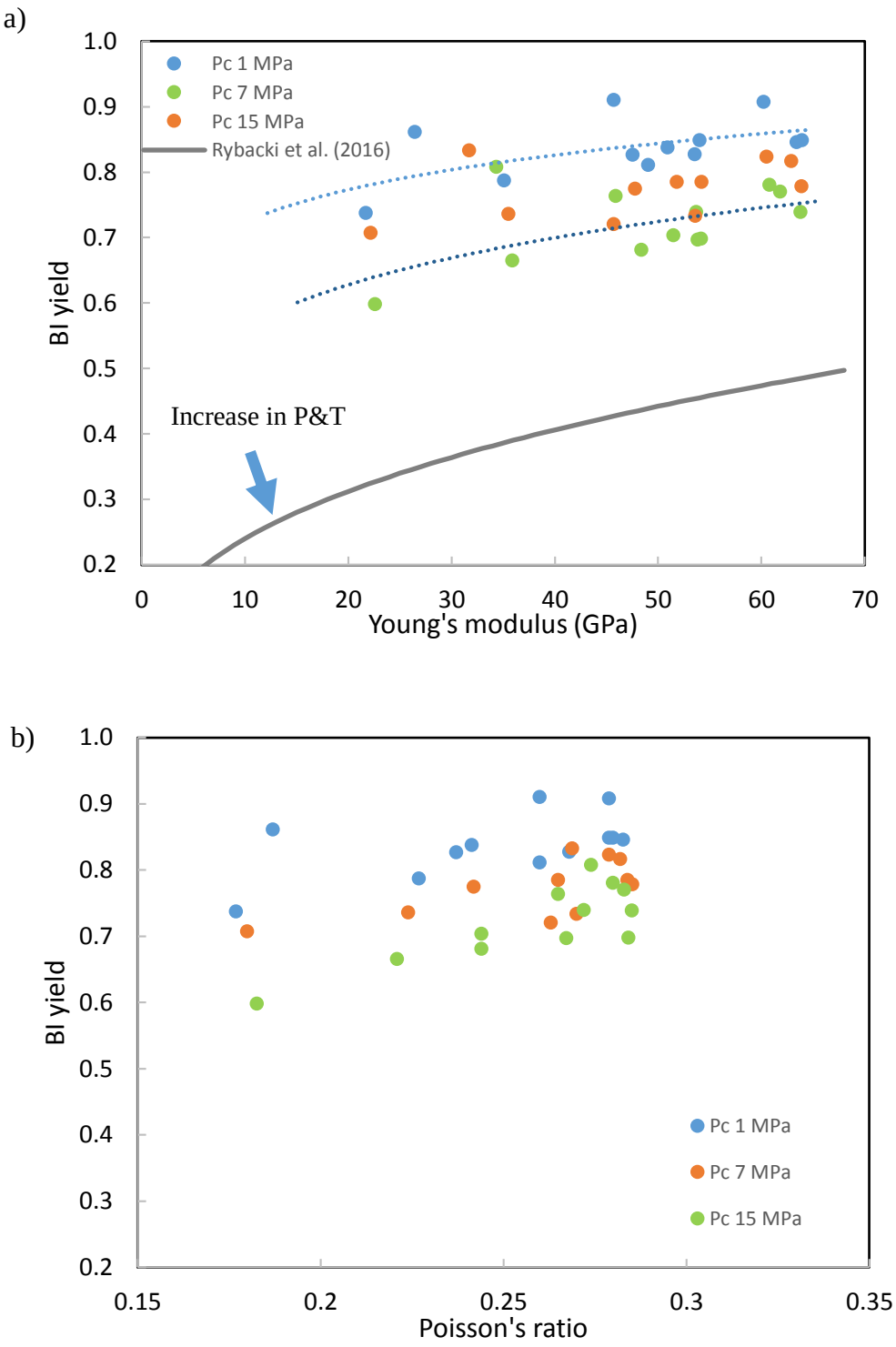

Figure 3.15 The relationship between BI_{yield} and elastic moduli (**a, b**), and between BI_{energy} and Young's modulus (**c**).

c)

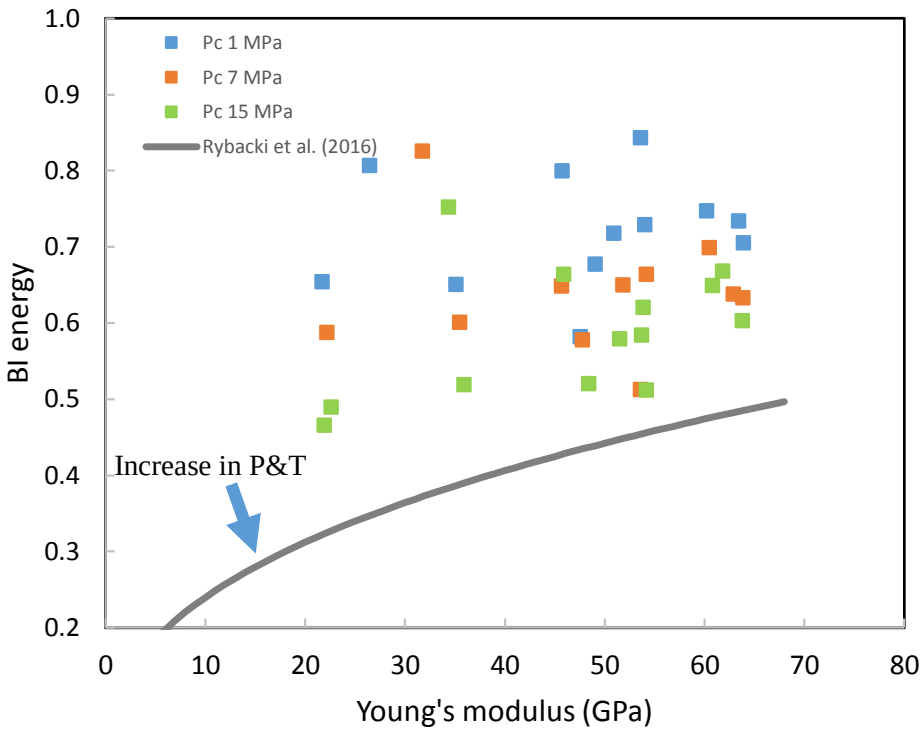

Figure 3.15 Continued

3.5. Conclusions

The mechanical behavior of the calcareous-rich Eagle Ford Formation is investigated to improve our understanding of the mechanical response of a heterogeneous, carbonate-rich shale formation during initiation and propagation of hydraulic fracturing stimulation. Triaxial experiment-related brittleness indices are calculated based on the mechanical properties prior to and after fracturing to provide insights to the prediction of failure behavior. In unconventional exploration and production, elastic properties are standard mechanical properties that are obtained indirectly through wireline log data. Prediction of inelastic properties and brittleness indices from elastic properties is thus important in planning hydraulic fracture treatment

and well-completion in unconventional shale gas formations. The empirical relationships between elastic and inelastic properties are investigated.

Inelastic properties from triaxial compression experiments are related to carbonate facies, mineralogy, texture (including % grain fraction in the samples), and confining pressure. The Eagle Ford Formation samples show a distinct change in ultimate strength under increasing confining pressure conditions. UCS of the Eagle Ford Formation varies from 130 MPa to 260 MPa. The mud-supported carbonate facies have lower yield strengths, lower ultimate strengths, lower frictional sliding strengths, and higher plastic yielding (ductility) when compared to the grain-supported facies. With an increase in confining pressure, yield strength, ultimate strength, frictional sliding strength, and ductility increase. The failure envelop for the Eagle Ford Formation suggests that there is no dependency on the angle of internal friction. Although the ultimate strength is variable in some cases, lab-based brittleness indices BI_{yield}, BI_{energy}, and $BI_{\text{post-failure}}$ only show small variations. Under reservoir conditions, BI_{yield} varies from 0.6 to 0.8, and with an increase in confining pressure, brittleness decreases.

The lithology and carbonate facies designations are related to mineralogy and textural features. Ultimate strength and brittleness indices are greatly impacted by clay mineral content. The ultimate strength could decrease by half with a clay mineral content increase to 10%. BI_{yield} and BI_{energy} decrease with an increase in clay mineral content. Plastic strain prior to fracturing increases as clay mineral content increases. In contrast to clay mineral content, the positive relationship between ultimate strength and carbonate content of the samples are not as distinct in every case, and the ultimate strength

decreases with QFP content. Brittleness indices, BI_{yield}, and BI_{energy} show a positive trend with carbonate content and a negative trend with QFP content. QFP is typically considered a stiff component in rock and often shows a positive relation with brittleness index (Rybacki et al., 2016). Herein, the increase in QFP is associated with a decrease in carbonate content, and an increase in clay mineral content when QFP content increases in the mud-supported facies. Although often thought to be a significant stiff phase, the quartz in the samples in this study herein are dispersed as microcrystalline grains within the clay mineral fraction and microscopic grains of calcite. This textural distinction has a significant impact on the mechanical behavior of the representative samples.

Besides mineralogy, the distribution of minerals in the shale samples also affect the inelastic properties of these samples. Yield strength, ultimate strength, and frictional residual strength show positive relationships with the % grain fraction in the samples. As the amount of foraminifera and skeletal grains increase in the Eagle Ford Formation samples, the ultimate strength increases as more grains are touching each other forming a stronger framework. Brittleness indices BI_{yield} and BI_{energy} also increase with % grain fraction. These relationships can be fitted with a power law or linear relation. Plastic yielding decreases with an increase in % grain fraction and with a decrease in mud size in the samples.

Elastic properties have been correlated to rock inelastic properties. Ultimate strength shows a nearly linear increase with Young's modulus. UCS and brittleness indices of the Eagle Ford Formation samples can be fitted with a power-law relationship with Young's modulus. The relationship agrees with the finding for other shale

formations (Rybacki et al., 2015). Under low confining pressures, the overall high brittleness values suggest the Eagle Ford Formation samples tend to fail in a brittle manner. As the pressure and temperature of deformation increase, the ductility of the rock increases and brittleness indices decreases.

3.6. References

Andreev, G.E., 1995. Brittle failure of rock materials: test results and constitutive models. A.A.Balkema, Rotterdam, p 446.

Baron, L., B. Loguntsov, and E. Pozin, 1962, Determination of the Properties of Rocks: Gosgortekhizdat, Moscow.

Bishop, A. W., 1967. Progressive failure-with special reference to the mechanism causing it. In Proc. Geotech. Conf., Oslo. Vol. 2, pp. 142-150.

Bourg, I. C., 2015. Sealing shales versus brittle shales: a sharp threshold in the material properties and energy technology uses of fine-grained sedimentary rocks. Environmental Science and Technology Letters, 2(10), 255-259.

Chang, C., Zoback, M. D., and Khaksar, A., 2006. Empirical relations between rock strength and physical properties in sedimentary rocks. Journal of Petroleum Science and Engineering, 51(3-4), 223-237.

Das, I., and Zoback, M. D., 2013. Long-period, long-duration seismic events during hydraulic stimulation of shale and tight-gas reservoirs—Part 1: Waveform characteristicsLPLD events: Waveform characteristics. Geophysics, 78(6), KS107-KS118.

Dunham, R. J., 1962. Classification of carbonate rocks according to depositional texture, in W. E. Ham, ed., Classification of carbonate rocks—A symposium: American Association of Petroleum Geologists Memoir 1, p. 108–121.

Hajiabdolmajid, V., and Kaiser, P., 2003. Brittleness of rock and stability assessment in hard rock tunneling. Tunnelling and Underground Space Technology, 18(1), 35-48.

Huang, Z. Q., Zeng, Q. D., Yan, X., and Yao, J., 2018. Hydraulic Fracturing Modeling and Its Extension to Reservoir Simulation Based on Extended Finite-Element Method (XFEM). In Hydraulic Fracture Modeling Gulf Professional Publishing. pp. 111-154.

Hucka, V., and B. Das, 1974, Brittleness determination of rocks by different methods, International Journal of Rock Mechanics and Mining Sciences and Geomechanics Abstracts, 11(10), 389–392.

Horsrud, P., 2001. Estimating mechanical properties of shale from empirical correlations. SPE Drilling and Completion, 16(02), 68-73.

Jarvie, D. M., Hill, R. J., Ruble, T. E., and Pollastro, R. M., 2007. Unconventional shale-gas systems: The Mississippian Barnett Shale of north-central Texas as one model for thermogenic shale-gas assessment. AAPG bulletin, 91(4), 475-499.

Kohli, A. H., and Zoback, M. D., 2013. Frictional properties of shale reservoir rocks. Journal of Geophysical Research: Solid Earth, 118(9), 5109-5125.

Maxwell, S. C., and Cipolla, C. L., 2011. What does microseismicity tell us about hydraulic fracturing? In SPE Annual Technical Conference and Exhibition. Society of Petroleum Engineers. 4. 10.2118/146932-MS.

Passey, Q. R., Bohacs, K., Esch, W. L., Klimentidis, R., and Sinha, S., 2010. From oil-prone source rock to gas-producing shale reservoir-geologic and petrophysical characterization of unconventional shale gas reservoirs. In International oil and gas conference and exhibition in China. Society of Petroleum Engineers. 131350. 10.2118/131350-MS.

Rashed, M. A., Mansour, A. S., Faris, H., and Afify, W., 2014. Factors Affecting the Ultimate Compressive Strength of the Quaternary Calcarenites, North Western Desert, Egypt. World Academy of Science, Engineering and Technology, International Journal of Environmental, Chemical, Ecological, Geological and Geophysical Engineering, 8(2), 117-129.

Rickman, R., Mullen, M. J., Petre, J. E., Grieser, W. V., and Kundert, D. 2008. A practical use of shale petrophysics for stimulation design optimization: All shale plays are not clones of the Barnett Shale. In SPE annual technical conference and exhibition. Society of Petroleum Engineers. SPE 115258.

Rybacki, E., Meier, T., and Dresen, G., 2016. What controls the mechanical properties of shale rocks?–Part II: Brittleness. Journal of Petroleum Science and Engineering, 144, 39-58.

Sone, H. and Zoback, M.D., 2013. Mechanical properties of shale-gas reservoir rocks—Part 2: Ductile creep, brittle strength, and their relation to the elastic modulus. Geophysics, 78(5), pp.D393-D402.

Stanek, F., and Eisner, L., 2013. New model explaining inverted source mechanisms of microseismic events induced by hydraulic fracturing. In SEG Technical Program Expanded Abstracts Society of Exploration Geophysicists. pp. 2201-2205.

Tarasov, B., and Potvin, Y., 2013. Universal criteria for rock brittleness estimation under triaxial compression. International Journal of Rock Mechanics and Mining Sciences, 59, 57-69.

Van Der Baan, M., Eaton, D., and Dusseault, M., 2013. Microseismic monitoring developments in hydraulic fracture stimulation. In Effective and Sustainable Hydraulic Fracturing. Intech, pp. 81–93.

Wang, F.P., and Gale J.F.W., 2009. Screening criteria for shale-gas systems: GCAGS Transactions, v. 59, p. 779-793.

Yang, Y., Sone, H., Hows, A., and Zoback, M. D., 2013. Comparison of brittleness indices in organic-rich shale formations. In 47th US rock mechanics/geomechanics symposium. American Rock Mechanics Association. 2013. 2. 1398-1404.

4. APPLICATION OF LABORATORY ROCK GEOMECHANICAL PROPERTIES IN RESERVOIR EXPLORATION AND PRODUCTION

4.1. Introduction

One of the challenges in the production of unconventional shale gas reservoirs is to identify productive and favorable units for good completion quality and predict the response of reservoir rock to hydraulic fracturing. The mechanical response of rock depends on in-situ conditions, mechanical properties of the rock, and engineering operational design variables. Although geomechanical models of shale gas reservoirs may employ simplified assumptions of several units with different elastic properties and brittleness, the mechanical properties and response to engineering operations can be highly variable and direction-dependent over a range of scale as a result of lithostratigraphic layering. The Eagle Ford Formation, a carbonate-rich shale, is an example of an unconventional reservoir rock that displays a large variation in mechanical properties, and thus a variable deformation response to hydraulic fracturing programs.

The Eagle Ford Formation includes units with high carbonate content (>70%), and granular or crystallized textures, that display high Young's modulus, low Poisson's ratio, high compressive to tensile strength ratio, high angle of internal friction, and a strong tendency to fail by localized fracture under stress (Hucka and Das, 1974; Hajiabdolmajid and Kaiser, 2003; Jarvie et al., 2007; Tarasov and Potvin, 2013). In contrast, other units of the Eagle Ford Formation contain a significant fraction of fine-

grained components including phyllosilicates and organic materials and typically have lower Young's modulus, a lower ratio of compressive to tensile strength (Rickman et al., 2008; Zhang et al., 2016), and greater relative ductility (more permanent deformation prior to fracture) which tends to inhibit the propagation of hydrofracture. Lithologic layering in the Eagle Ford carbonate shales can manifest at a millimeter to meter scales. Accordingly, placement of deviated boreholes (laterals) in the less ductile zones but near strata with high TOC, or in zones with pronounced mechanical layering, are strategies to enhance fracture development as well as to activate the producing horizons. Lithologic layering may promote the formation of new, complex fracture networks and enhance the opportunity to reactivate existing fractures with the best potential for connectivity to the reservoir, and with the least tendency for fracture closure and loss of permeability (Maxwell and Cipolla, 2011; Van Der Baan et al., 2013). Whereas fractures developed only in relatively ductile layers are usually smaller and less conductive and tend to heal faster (Holt et al., 2011; Yao et al., 2012; Baroni et al., 2015). Therefore, characterization of the mechanical properties and deformation response of the component lithologic units at reservoir conditions, as well as the lithostratigraphic sequencing in the reservoir, is necessary to inform geomechanical analyses.

For drilling and well completion operations in the petroleum industry, predicting the mechanical response of reservoir rock to hydraulic fracturing has relied heavily on "brittleness," which is represented by various brittleness indices indicative of the development, extent, and complexity of fracturing during hydraulic stimulation (Teufel and Clark, 1984; Gu et al., 2006). Brittleness, much like the concept of relative ductility,

characterizes the macroscopic mode of failure for rock undergoing permanent deformation that culminates in fracture. In a triaxial deformation experiment, relative ductility is quantified as the amount of permanent axial strain prior to fracture, and is often measured at the ultimate strength (e.g., Handin and Hager, 1957; Griggs and Handin, 1960). It is well understood that the brittleness and ductility depend both on lithology and conditions of deformation (e.g., pressure, temperature and strain rate), and are somewhat correlative to mechanical properties such as Young's modulus (e.g., Heard, 1960; Rybacki et al., 2016).

Characterization of the bulk mechanical behavior of a composite lithostratigraphic unit at the reservoir scale may be facilitated by integrating experimental rock deformation that provides direct measurements of rock mechanical properties such as elastic moduli, fracture strength, and relative ductility for representative lithologic units, with detailed descriptions of the lithostratigraphy that include quantification of composition, mineralogy, texture and strata thicknesses. A result of such integration is a mechanical stratigraphic model that describes bulk mechanical properties and deformation behavior (e.g., relative ductility) quantitatively as a function of position and stratigraphic interval thickness. The model may be represented as plots of individual mechanical properties as a function of position analogous to geophysical logs. Moreover, the mechanical stratigraphic model based on direct measurements of mechanical properties may be compared both qualitatively and quantitatively to other determinations of geomechanical properties from direct and indirect measurement made by geophysical logging and core from wells.

Given increases in computational power and sophistication of multiphysics numerical modeling capabilities, a detailed characterization of the mechanical properties and direction-dependent deformation response of the lithologies comprising unconventional reservoirs would increase our predictive capability of geomechanical reservoir models. To date, most experimental rock-mechanics studies of unconventional reservoir rocks have investigated the range of behavior between different reservoirs with contrasting lithology rather than the variation in properties and behaviors within a single reservoir or formation.

The purpose of this Section is to construct a mechanical stratigraphic model for a specific unconventional reservoir, the Eagle Ford Formation. To do so, the results of two companion experimental rock deformation studies of the Eagle Ford Formation (Sections 2 and 3) provide the mechanical data to construct a model of the Eagle Ford Formation in a west Texas outcrop, and a producing reservoir in the subsurface in south Texas. Samples were collected from both localities to represent the range and variation in lithostratigraphic units comprising the Eagle Ford Formation. Twenty-two samples were tested to determine elastic properties and their relationship to the sample mineralogy and texture (Section 2). A fifteen-sample subset was deformed triaxially to determine inelastic mechanical properties such as ultimate strength and sliding friction, and mode of failure in terms of relative ductility and the orientation of fractures (Section 3). In addition, several brittleness indices are determined directly from the mechanical response displayed in the triaxial tests.

The elastic and inelastic properties determine from the experimental studies (Sections 2 and 3) are summarized herein and are used to construct a mechanical stratigraphic model of the two study locations from detailed lithostratigraphic descriptions at each location. Using the models, upscaling the mechanical properties to several length scales explores the effects of lithostratigraphic layering on bulk mechanical behavior including mechanical anisotropy. The model predictions of mechanical properties and deformation behaviors (brittleness) are compared to mechanical descriptions determined directly from geophysical logs taken at both study sites as a means to evaluate consistency between methods, and to confirm the potential to apply the present mechanical stratigraphic model to subsurface Eagle Ford reservoirs throughout the geographical extent of the Eagle Ford Formation on the basis of only geophysical logging data or lithostratigraphic information determined by core samples, mud logging and drilling data.

This Section demonstrates that the mechanical stratigraphic model of the Eagle Ford Formation provides a detailed and reasonable accurate description of the elastic and inelastic mechanical properties and behaviors at the two study sites. The model is based on detailed lithostratigraphic descriptions of the Eagle Ford Formation using visual observations and a relatively simple lithologic classification scheme, and then applying average mechanical properties for each lithology, combined with simple averaging schemes, to determine the effective behavior of the multilayered formation. The experimental rock deformation study presented in Sections 2 and 3 illustrate that the mechanical properties vary systematically with mineralogy, composition and textural

characteristics (recrystallized grains, grain fraction), and effective confining pressure, which can be expressed with quantitative relationships. The experimental data also supports robust quantitative relationships between elastic and inelastic mechanical properties. Accordingly, a mechanical stratigraphic model describing inelastic behaviors including brittleness can be constructed from elastic properties determined by geophysical measurements of seismic velocity. Alternatively, given a detailed characterization of rock characteristics such as mineralogy, composition and texture, without using visual inspection of lithofacies as done in this work but provided indirectly through rock physics interpretation of geophysical logging data, a mechanical stratigraphic model could be determined using the quantitative relationships between mechanical properties, brittleness and rock characteristics (Sections 2 and 3).

4.2. Direct Determination of a Mechanical Stratigraphic Model

4.2.1. Method

The lithostratigraphic sections at the two study sites, outcrop in west Texas and subsurface core from south Texas, were characterized using visual descriptive techniques based on color, bed thickness, grain size, laminations, and other sedimentary structures to identify lithology. Lithology was recorded at ~30 cm intervals for the outcrop, and at centimeter resolution for the subsurface core. Lithology characterization is based on Dunham's (1962) carbonate rock classification and sedimentary structures were described following Campbell's (1967) classification. Here the observed lithologic

types at both sites are classified as a member of the mudstone, wackestone, packstone, grainstone, or crystalline carbonate facies, or as a bentonite bed.

The experiments that determined the elastic and inelastic properties of representative samples were conducted at relatively low confining pressures 1 to 40 MPa to simulate the typical effective pressure observed in producing subsurface Eagle Ford reservoirs (Sections 2 and 3). A pore pressure of a gradient for the Eagle Ford of 14.7 to 15.8 MPa/km is typical across south Texas basin (Basu et al., 2012), which implies effective stress of about 20 MPa for the subsurface study site where core samples were collected. On the basis of organic maturity and other information, the Eagle Ford Formation in the outcrop study site was likely buried and lithified at similar conditions prior to uplift and exhumation. Accordingly, for the purposes of constructing the mechanical stratigraphic model, mechanical properties and brittleness indices used herein are taken from the experiments conducted at an effective confining pressure of 15 MPa, and the parameters defining the Coulomb failure criteria were determined from experiments conducted at 1, 7 and 15 MPa effective pressure.

For the carbonate samples, the measured values of Young's modulus, Poisson's ratio, ultimate strength, ductility, and brittleness indices (BI_{yield} and BI_{energy}, Section 3) are averaged for each lithologic type (carbonate facies) to determine a single representative value (Table 4.1). Elastic and strength properties are directly measured from cyclic loading tests (Section 2). Directional dependence of elastic properties was determined directly by measuring stress vs strain response in cyclic triaxial loading tests perpendicular and parallel to the plane of bedding and lamination to characterize

anisotropy of Young's modulus for each lithofacies. Ductility and brittleness indices are derived directly from the stress versus strain behavior observed in the triaxial fracture tests (Section 3). Coulomb failure parameters for each sample is determined from the triaxial compression fracture tests conducted at three confining pressures by best-fitting the Coulomb criterion,

$$\sigma_1 = m\ \sigma_3 + Co$$

to the stress at ultimate strength on the differential stress versus stress axial strain curve, where σ_1 is the maximum (axial) stress, σ_3 is the minimum stress (equal to the confining pressure), *Co* is the Coulomb parameter equivalent to the differential stress at 0 confining pressure (i.e., the Unconfined Compressive Strength, UCS, which is related to the cohesion), and *m* is the Coulomb parameter defining the pressure dependence of strength (related to the angle of internal friction).

Conducting experiments on samples from Bentonite beds is challenging due to the severe fissility and fragility. There are abundant bentonite beds with varying thickness from 1-20 cm in the Eagle Ford Formation, so a determination of their mechanical properties is important. Elastic properties perpendicular to the lamination was successfully measured using a sample of a dolomite-rich, reworked bentonite bed (Table 4.1). Using this measurement as a reference, the elastic properties parallel to lamination, and inelastic properties of bentonite beds are determined from documented relationships between Young's modulus and mechanical properties of the other lithologies tested (Sections 2 and 3).

The mechanical stratigraphic model is constructed by assigning the mechanical properties (summarized in Table 4.1) to lithologic intervals (bed thicknesses) on the basis of the bentonite and carbonate lithofacies defined in the lithostratigraphic sections for the outcrop and subsurface core study locations. In general, the inaccuracy of the mechanical stratigraphic model results from 1) the grouping of lithologies and averaging mechanical properties to just six lithofacies, 2) the resolution of lithostratigraphy in the characterization of the outcrop site of ~30 cm (the resolution in the subsurface core is ~1 cm), and 3) ignoring mechanical effects of natural fractures and bedding interfaces. However, at the scale of the reservoir and for purposes of geomechanical modeling and hydraulic fracturing operations, the mechanical stratigraphic model is constructed at a relatively fine scale.

The mean property of a composite stratigraphic interval may be estimated at various scales by appropriate averaging of the mechanical properties of different included units of varying thickness and lithology. In the case of the Eagle Ford Formation at the two study sites, and for many unconventional reservoirs in general, the stratigraphic layering is laterally uniform and continuous to length scales much greater than the layer thicknesses, and the layering is horizontal. In basins with minor tectonism, the in situ principal stress directions are parallel and perpendicular to the layering, and the stress magnitudes are within the elastic field, and deformations are small. In this case, arithmetic averaging methods of the Voigt iso-strain model and harmonic averaging of the Reuss iso-stress model may be applied to estimate the effective elastic modulus in the directions parallel and perpendicular to the layering, respectively (Voigt,

1889; Reuss, 1929), and a reasonable estimate of the behavior for an intermediate loading condition may be approximated as the Hill average modulus (Hill, 1952). The Reuss model determines a lower bound and the Voigt an upper bound for the effective elastic modulus for intermediate loading conditions. In representing the mechanical stratigraphic model, the degree of anisotropy is characterized by the ratio of the iso-strain model over the iso-stress model, and the effective modulus for general loading conditions is represented by the average of the iso-strain and iso-stress models, i.e., the Hill average modulus.

The documentation of elastic anisotropy associated with greater clay content and laminations (e.g., mudstone and wackestone (Table 4.1), by direct triaxial testing (Section 2), will add to the effective anisotropy of multilayers of different lithologies with different isotropic properties. Accordingly, the directional dependence of modulus of the facies that make up individual layers is included in the determination of the elastic anisotropy resulting from interbedded lithologies for the mechanical stratigraphic model.

For incorporating the inelastic mechanical properties into the mechanical stratigraphic model, a Reuss iso-stress model is used for determining the behavior of multilayers over different stratigraphic interval thicknesses. The mechanical data for ultimate strength, *Co*, *m*, relative ductility, and the brittleness indices were collected from triaxial compression tests of samples with the maximum compression directed perpendicular to lamination and bedding orientation (Section 3). As such the testing configuration is close to an idealized iso-stress assumption, and thus a similar assumption was used for determining the average behavior for multilayers.

For each property in the mechanical stratigraphic model, the effective value at a position, *z*, is determined by appropriate averaging as described above for a stratigraphic interval between $z+d/2$ and $z-d/2$, where d is the thickness of the stratigraphic interval. For the diagrams presented herein, the step between adjacent measurements, i.e., the resolution of the model, is 0.06 m (0.2 ft). Upscaling is investigated by using d values of 0.9 m, 1.5 m, and 3 m.

4.2.2. Results

The model is illustrated by plotting profiles of mechanical properties as a function of stratigraphic position (depth) for the outcrop (Figure 4.1) and the subsurface (Figure 4.2) study sites. Properties shown include Young's modulus, Poisson's ratio, *Co* (UCS), frictional related parameter m, ductility, ultimate strength, BI_{yield}, and BI_{energy}. The averaging window, *d*, is 0.9 m and relatively small so there is high variability because the thickness of individual lithologic units is generally smaller than 1 m.

The Eagle Ford Formation is highly variable in lithology and consists of interbeds of different carbonate facies with thickness varying from cm to m scale. It also contains bentonite beds up to 20 cm thick, though usually significantly thinner, throughout the Eagle Ford Formation. As would be expected based on properties of the different lithologic units, the mechanical stratigraphic model shows that intervals of predominantly mud-supported facies have low Young's modulus, Poisson's ratio, ultimate strength, *Co*, *m*, and brittleness, and high ductility. In contrast, intervals of predominantly packstone and grainstone layers display high Young's modulus,

Poisson's ratio, ultimate strength, brittleness, and low ductility. The plots of the different properties also illustrate that all the mechanical properties are positively correlated except for ductility, which is inversely correlated. Most of these correlations are illustrated in Sections 2 and 3.

A thick stratigraphic interval with mostly uniform lithology shows a blocky shaped curve whereas an isolated unit of contrasting properties shows a spike-shaped curve. Sharp lithologic variation (e.g., at ~15 m in the outcrop, Fig. 4.1, and at the top of the subsurface sites, Fig.4.2) is reflected by large variation in all mechanical properties and it occurs at where a thick interval of a dominant mudstone is bounded next to a thick interval of dominantly packstone/grainstone. Lithologic variation within thinner bedded units (e.g., 3-30 cm skeletal wackestone/packstone facies interbedded with mudstone, at 40 m in the outcrop site, Fig. 4.1) is indicated by frequent changes in mechanical properties plots. If the thickness of lithologic units is small relative to the stratigraphic interval for averaging, or the lithology is relatively similar the variation in mechanical properties shown by the model is relatively small. If the frequency of lithologic variations occurs at a larger scale (e.g., interbedded mudstone and packstone of 0.5 - 1m, as in the subsurface reservoir, Fig. 4.2), then profiles of mechanical properties show isolated spiky and blocky patterns. Overall, the mechanical stratigraphic mode of the Eagle Ford Formation at both study sites show significant variation over both small and large length scales, indicating that the Eagle Ford Formation is mechanically anisotropic at all length scales.

Table 4.1 Average values for mudstone, wackestone, packstone, grainstone, crystalline (recrystallized samples).

Facies	$E \perp$ (Gpa)	$v \perp$	$E //$ (Gpa)	$v //$	Co (MPa)	m	Ductility (%)	Ultimate Strength (MPa)	BI yield	BI energy
	Pc=15 MPa	Pc=15 MPa	Pc=15 MPa	Pc=15 MPa	Pc =1-15 MPa	Pc =1-15 MPa	Pc = 15 MPa			
Bentonite	12.0	0.20	12.6	0.26	110	3.8	0.57%	136	0.58	0.43
Mudstone	22.5	0.19	31.4	0.28	130	4.0	0.45%	168	0.60	0.49
Wackestone	35.4	0.21	41.1	0.30	167	4.2	0.33%	187	0.70	0.50
Packstone	52.2	0.26	57.3	0.30	197	4.5	0.23%	240	0.71	0.58
Grainstone	62.8	0.28	63.5	0.28	264	4.4	0.18%	316	0.75	0.64
Crystalline	58.1	0.27	60.5	0.29	230	4.4	0.15%	192	0.71	0.57

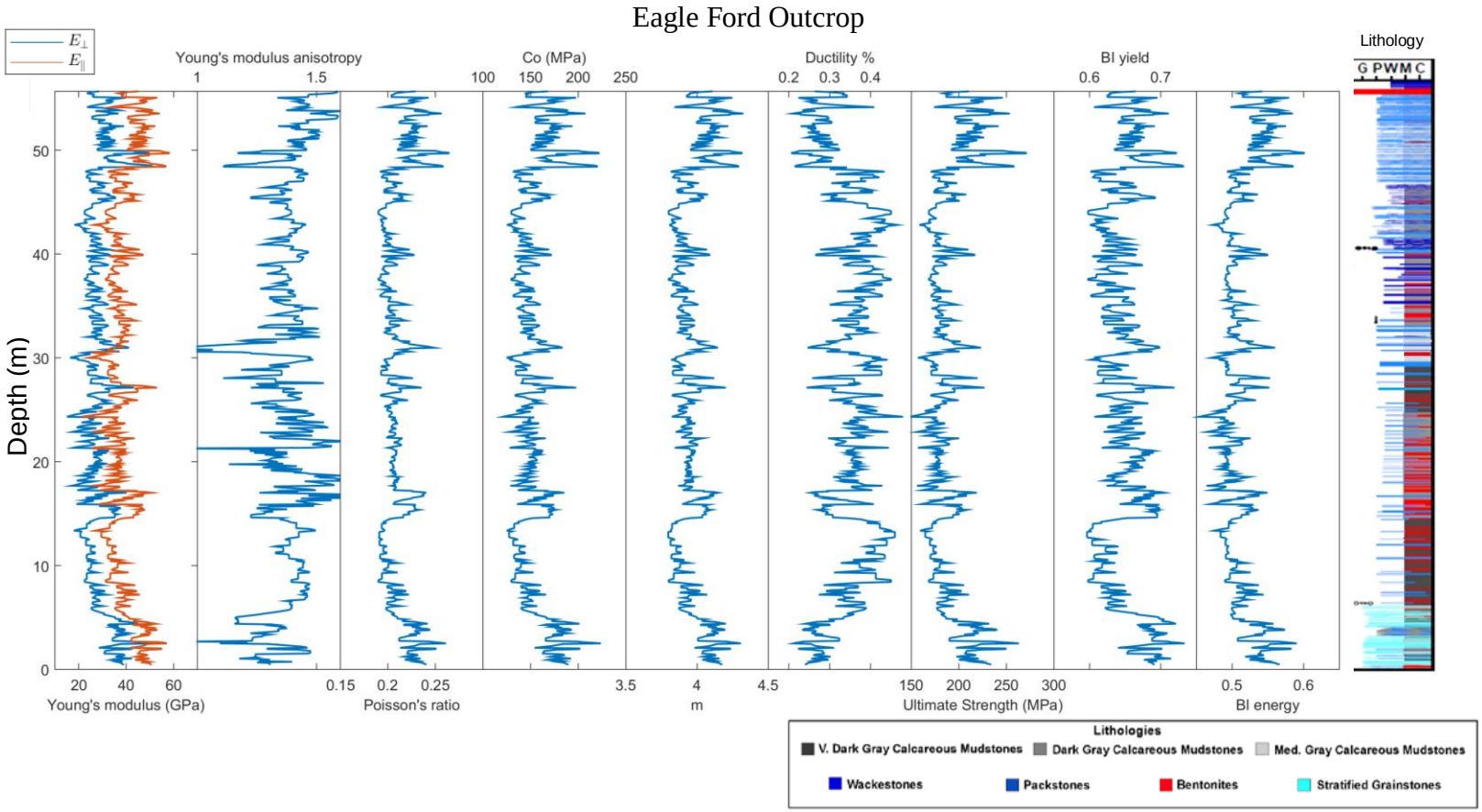

Figure 4.1 Mechanical stratigraphic model of the Eagle Ford Formation from the outcrop with an averaging window of ~0.9m (3ft). The lithostratigraphic column is based on a description of the borehole (Gardner et al., 2013). The Young's modulus was averaged using Reuss (blue) and Voigt (orange) model. Elastic anisotropy is assessed using the ratio of the Voigt/Reuss model. Poisson's ratio, UCS (Co), m, ductility, strength, and brittleness indices are averaged based on Reuss model.

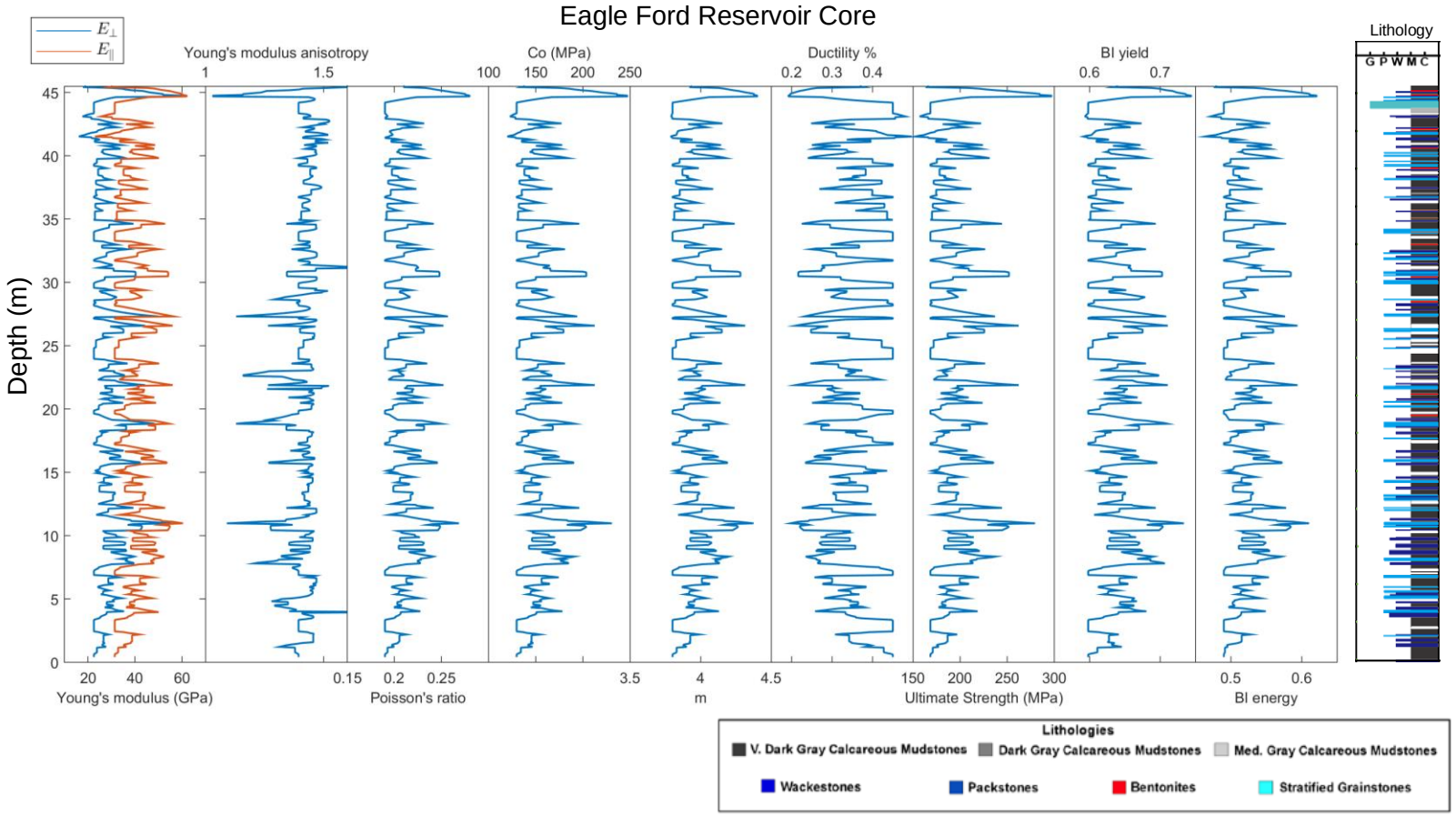

Figure 4.2 Mechanical stratigraphic model of the Eagle Ford Formation from Swenson Core with an average window of ~0.9m (3ft). The Young's modulus was averaged using Reuss (blue) and Voigt (orange) model. Elastic anisotropy is assessed using the ratio of the Voigt/Reuss model. Poisson's ratio, UCS (Co), m, ductility, strength, and brittleness indices are averaged based on Reuss model.

4.2.3. Up-scaling and Validating the Mechanical Stratigraphic Model

The experimental and lithostratigraphic based mechanical stratigraphic model is checked by comparing the model-predicted, static elastic properties with and dynamic elastic properties determined directly at each study site from sonic logging data collected in a borehole through the outcrop and in the well from which the subsurface core was acquired. At the same time, the model predicted effective elastic properties of the different stratigraphic thickness intervals is compared as a means to investigate up-scaling the mechanical model.

Young's modulus of the samples of the Eagle Ford Formation was measured at quasi-static conditions under triaxial loading at various confining pressures (Section 2). The static elastic moduli determined from the experiments suggest a strong positive correlation between Young's modulus and Poisson's ratio (Fig 2.11b).

Dynamic Young's modulus of the Eagle Ford Formation has been determined from the sonic logging data taken at in-situ conditions in the shallow borehole at the outcrop and in the deep borehole into the subsurface reservoir. The comparison of the mechanical stratigraphic model prediction of elastic modulus with sonic log data is facilitated by up-scaling the mechanical model because sonic data measurements also reflect an averaging over a greater length scale than individual lithologic units. A moving average function of elastic properties, described in the methods section, determines effective Young's

modulus for an averaging window size of 0.9 m, 1.5 m, and 3 m (Fig. 4.3, Fig. 4.4). Modulus is determined for both perpendicular and parallel to the stratigraphic layering and the different scales, and the Voigt-Reuss-Hill average modulus is determined for comparison with the sonic log.

At the finer averaging interval of ~0.9 m, changes in elastic properties of the rock are greater and more frequent compared to bulk properties at 3 m scale, especially when adjacent lithologies has larger contrast in elastic properties. At 3 m scale, the variation in elastic properties is smoothed out by averaging and thus shows very small change.

The pattern of the static Reuss-Voigt-Hill average Young's modulus determined at a 0.9 m and 1.5 m averaging window overall agree well with the dynamic Young's modulus model as the resolution of the sonic logging is around 1 m. In the sonic log data, the lower part of the Lower Eagle Ford Formation has a greater Young's modulus than the upper part. In general, the dynamic Young's modulus is greater than laboratory derived static Young's modulus in most cases, which is consistent with relationships found in the literature (Mavko et al., 2009; Sone and Zoback, 2013a).

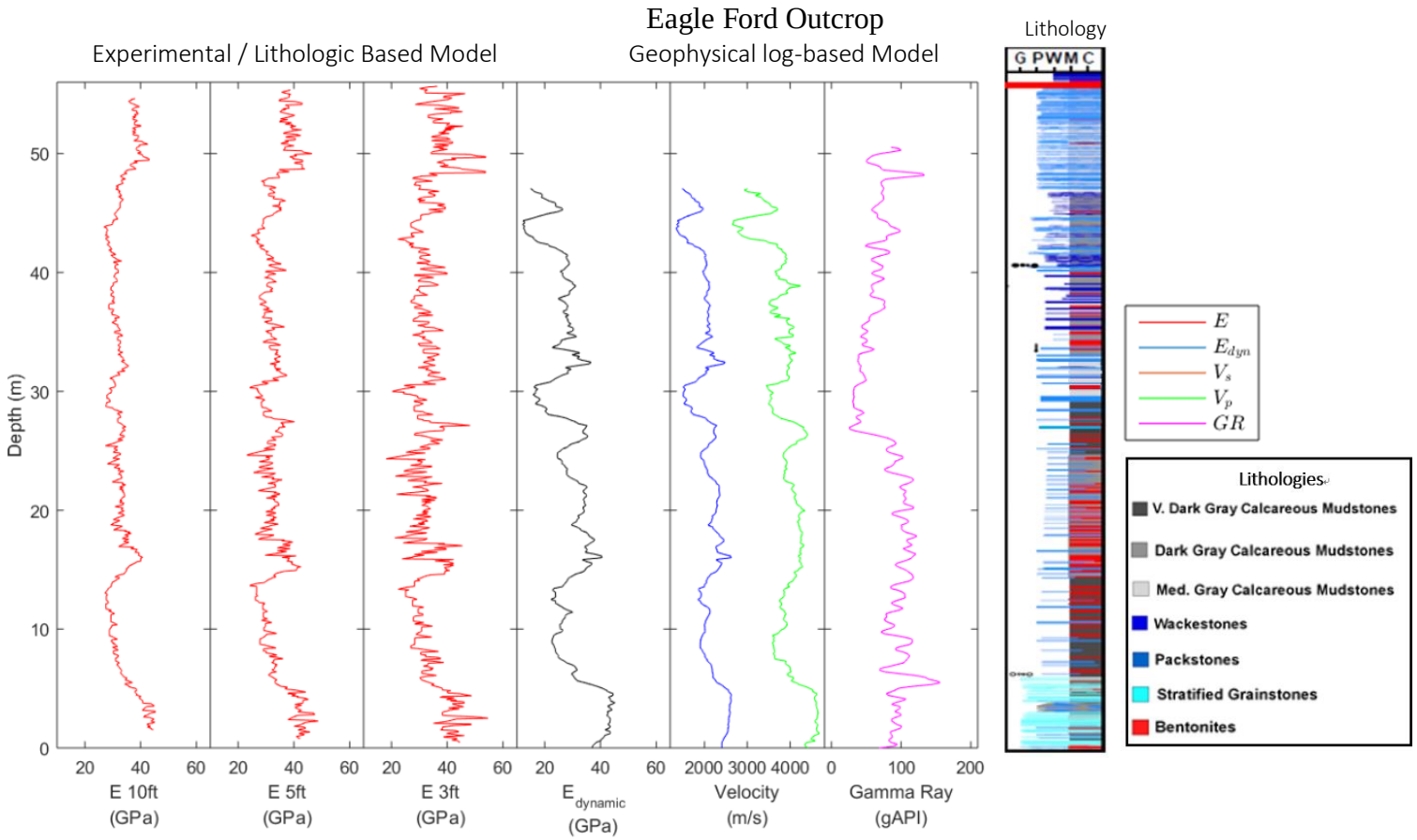

Figure 4.3 Example of the mechanical stratigraphic model of elastic properties of the Eagle Ford Formation from outcrop based on lithologic descriptions and experiment data compared to determinations from sonic logs. Young's modulus based on Voigt-Reuss-Hill model is averaged at every 3 m, 1.5 m, and 0.9 m from left to right. Young's modulus averaged at 0.9 m is compared with dynamic Young's modulus from sonic logs.

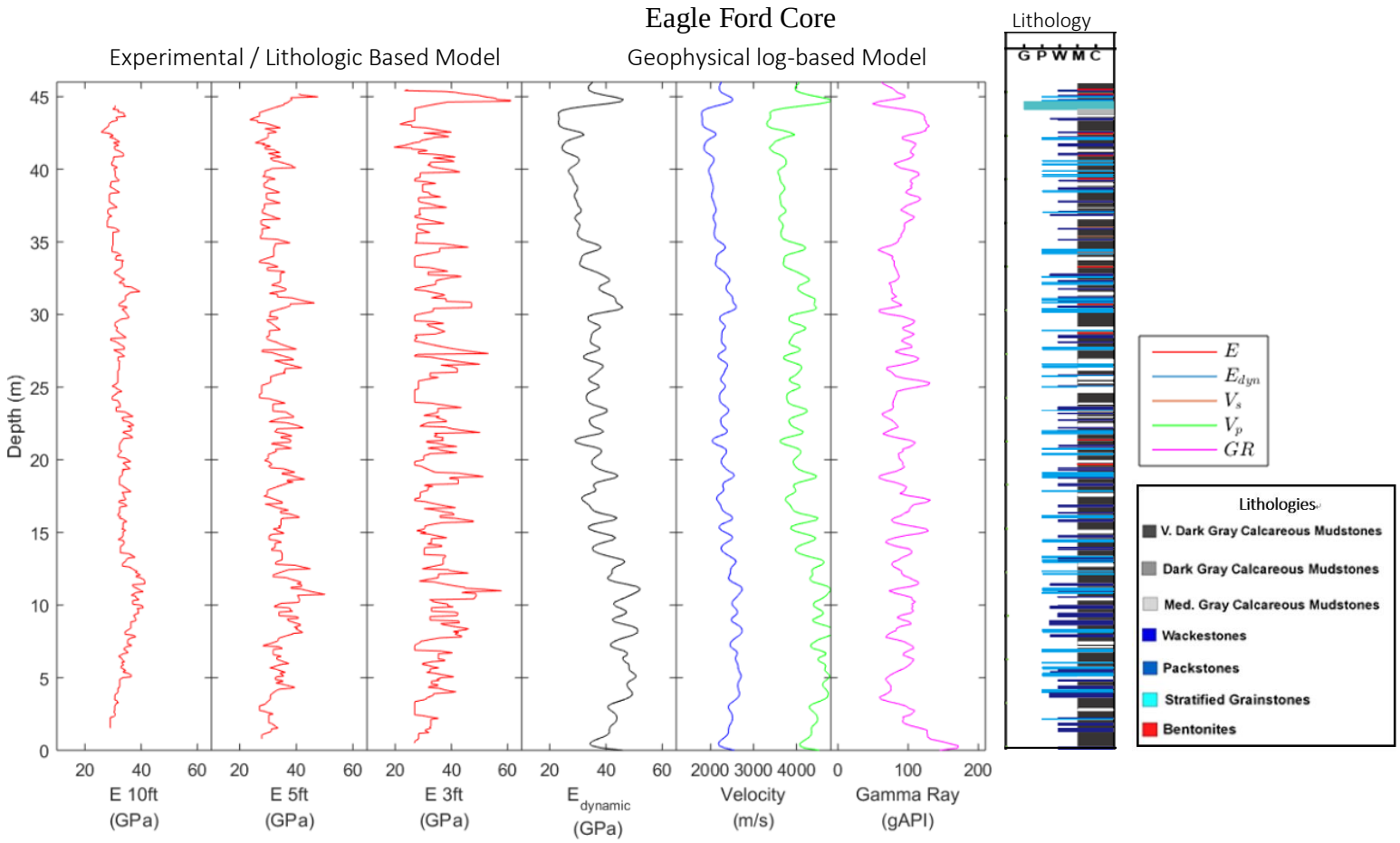

Figure 4.4 Example of the mechanical stratigraphic model of elastic properties of the Eagle Ford Formation from Swenson Core based on lithologic descriptions and experiment data compared to determinations from sonic logs. Young's modulus based on Voigt and Reuss model is averaged at every 0.9 m, 1.5 m, and 3 m. Young's modulus averaged at 0.9 m is compared with dynamic Young's modulus from sonic logs.

The plotted variation in Young's modulus predicted by the mechanical stratigraphic model overall agrees very well with the log-based plot of dynamic Young's modulus. This result supports the validity of the mechanical stratigraphic model determined from experimental rock deformation data and averaging schemes to describe properties of the multilayer at various scales. Furthermore, it supports the use of elastic moduli from sonic logging data to predict variations in static Young's modulus, as well as inelastic mechanical properties that correlate with Young's modulus of rocks as documented in Section 3.

4.3. Evaluation of Direct and Indirect Determinations of Brittleness

As presented previously, triaxial rock deformation experiments document inelastic deformation response culminating in fracture for loading under various pressure, temperature, and strain rates such that brittleness can be directly quantified. BI_{yield}, BI_{energy}, and $BI_{post\text{-}failure}$ are laboratory-based brittleness indices that are reported for triaxial rock deformation tests on Eagle Ford Formation samples in Section 3. Brittleness indices also may be determined indirectly, such as from geophysical logging data or laboratory data. $BI_{mineral}$ and $BI_{elastic}$ are examples of indirect brittleness indices because they attempt to describe inelastic deformation response from mineralogy or elastic behavior. $BI_{mineral}$ and $BI_{elastic}$ can be determined from both logging data and from laboratory data. For example, elastic moduli based brittleness index $BI_{elastic}$ can be derived from measured static elastic properties in the laboratory or dynamic elastic properties from sonic logs. Also, $BI_{mineral}$ may be determined from XRD measurements

of rock samples in the laboratory, or from determinations of mineralogy from combined analysis of several geophysical logs.

4.3.1. Methods

For direct calculations of brittleness, the stress-strain behavior of the sample allows calculation of the different brittleness indices using strain ratio, energy ratio, strength ratio, elastic properties, and frictional properties (Section 3). They capture the pre-failure and post-failure elastic deformation relative to plastic deformation of the sample.

Mineralogy is considered to be related to brittleness of polymineralic rocks because component minerals can have widely varying mechanical properties and failure behaviors, and a number of brittleness indices have proposed based on the composition of the rock (Glorioso and Rattia, 2012; Jarvie et al., 2007; Rybacki et al., 2016; Wang and Gale, 2009). The Eagle Ford Formation is calcareous rich shale, so BI_{mineral} may be determined by the weight fraction of "stiff" components which typically includes carbonates, quartz, and pyrite, assuming the brittleness of the rock results from the fraction of stiff grains comprising the rock (Rybacki et al., 2016). Yet quartz content does not show an obvious relationship with mechanical properties (Section 2, Section 3). Carbonate is considered as the only phase that contributes to the brittleness of the rock (Equation 4.1) When BI_{mineral} index has a magnitude approaching 1, the rock is regarded as brittle, and when BI_{mineral} approaches 0, the rock is predominantly soft components and thus behaves ductile.

Brittleness index $BI_{mineral}$ of the laboratory deformed samples is calculated from mineralogy determined by X-Ray Diffraction (XRD) measurements (Section 2). Brittleness of the subsurface core of the Eagle Ford Formation in south Texas, $BI_{mineral, c}$, is determined on the basis of a petrophysical evaluation of wireline logging data that gives estimates mineral abundances (Data from Apache). Brittleness of the outcrop site in west Texas, $BI_{mineral, o}$, is determined from XRD measurements on samples collected every 1-3 feet along the borehole drilled into the Lozier Canyon outcrop of the Eagle Ford Formation.

$$BI_{mineral} = \frac{Carbonate}{Calrbonate+Quartz+Clay} \quad \text{(Eq. 4.1)}$$

$$BI_{elastic} = \frac{1}{2}\left(\frac{E_{dynamic}\,(0.8-\emptyset)}{8-1} + \frac{\nu_{dynamic}-0.4}{0.15-0.4}\right) \cdot 100 \quad \text{(Eq. 4.2)}$$

Elastic moduli-based brittleness indices are calculated from the elastic moduli, either from Young's modulus or from a combination of Young's modulus and Poisson's ratio (Eqs. 4.2a and 4.2b; Tarasov and Potvin, 2013; Rybacki et al., 2016; Luan et al., 2014; Rickman et al., 2008). In this study, $BI_{elastic}$ (Eq. 4.2; Rickman et al., 2008) of Eagle Ford samples uses elastic moduli from laboratory static measurement at room temperature (Section 2). Since porosity is included in the equation and is not directly measured, it is assumed as 7% for all carbonate facies. Wireline log-derived $BI_{elastic, o}$ and $BI_{elastic, c}$ for the outcrop wellbore and subsurface core are determined using thermal neutron porosity, dynamic Young's modulus, and Poisson's ratio that has been derived from logs measured every ~ 15 cm (Eq 4.2).

4.3.2. Brittleness of the Eagle Ford Formation

Brittleness indices of the Eagle Ford Formation determined by indirect methods (elastic and mineralogy) vary from 0.47 to 0.96 (Table 4.2), depending on the definitions and pressure conditions. Instead of focusing on absolute numbers of the brittleness indices, the relationship between brittleness and rock mechanical properties has more application to shale gas recovery through hydraulic fracturing.

BI_{mineral} is determined from the bulk mineralogy using XRD, measured at the same area as linear strain gauge coverage on elastically deformed Eagle Ford samples. BI_{mineral} does not take into account the total organic content in the total weight of the rock in this study. Because most Eagle Ford Shale samples tested contains abundant calcite and quartz minerals regardless of carbonate facies, the variation of BI_{mineral} is limited toward the most brittle values among all brittleness indices, varying from 0.72 to 0.96. Most wackestone and grain-supported facies have BI_{mineral} over 0.8. The most brittle rock with a BI_{mineral} of 1 is made up of 95.72% calcite minerals, 3.13% quartz mineral, and less than 1.14% pyrite. $BI_{\text{mineral,c}}$ is determined from bulk mineralogy using XRD, and it is well correlated with the composition of the Eagle Ford Formation as expected. BI_{elastic} of the Eagle Ford samples, ranging from 0.53 to 0.72. BI_{elastic} gradually increases from mudstone to wackestone but does not show much variation in packstone/grainstone facies. Elastic moduli based brittleness indices show a positive correlation with carbonate content (calcite plus dolomite) and a negative trend with clay content (Fig. 4.5 a-d). Triaxial experiments based brittleness indices BI_{yield}, BI_{energy}, and $BI_{\text{post-failure}}$ are also found to be related to clay and carbonate content (Section 3).

Table 4.2 Summary of brittleness indices of the Eagle Ford Formation determined by indirect methods.

Name	facies	BI_{elastic}	BI_{elastic}	BI_{mineral}	BI_{mineral}
Outcrop		dynamic	static	Logs	XRD
H1B1-2	mudstone	0.34	0.60	0.83	0.63
H1B1//	mudstone		0.64		
AC_B70	mudstone		0.70		
AC_B1-27	wackestone		0.62	0.76	0.79
AC_B1-27//	wackestone	0.64	0.50		
AC_B4-83	packstone	0.75	0.64	0.84	0.89
AC_B-47	packstone	0.86	0.69		
AC_D-139	packstone	0.88	0.62	0.91	0.94
AC_D-139//	packstone	0.29	0.56		
AC_B-60	packstone	0.86	0.69	0.90	0.81
AC_E2	packstone	0.92	0.70	0.98	0.95
AC_E2//	packstone	0.62	0.73		
AC_C-109	packstone	0.95	0.73		
AC_C98	packstone	0.79	0.70	0.89	
AC_C98//	packstone	0.75	0.69		
AC_B-35	packstone	0.69	0.66	0.91	0.91
AC_B35//	packstone		0.69		
AC_C-110	grainstone	0.77	0.72	0.87	0.95
AC_C-110//	grainstone	0.76	0.71		
AC_B-50	grainstone	0.72	0.71	0.90	0.91
AC_B-50//	grainstone	0.75	0.71		
AC_A-1	grainstone	0.78		0.82	0.86
AC_A-1//	grainstone	0.68	0.67		

Table 4.2 Continued

Name	facies	BI_{elastic}	BI_{elastic}	BI_{mineral}	BI_{mineral}
Core					
SC473	mudstone		0.56	0.81	0.60
SC473//	mudstone		0.53		
SC387	mudstone		0.53	0.76	0.58
SC387//	mudstone		0.47		
SC506	mudstone		0.55	0.83	
SC513	wackestone		0.60	0.88	0.71
SC427	wackestone	0.84		0.91	0.92
SC477	packstone	0.63		0.83	0.84
SC430	packstone	0.53	0.68	0.94	0.91
SC423	packstone	0.80	0.63	0.87	0.96
SC423//	packstone	0.82	0.70		

Brittleness index BI_{elastic} is calculated based on dynamic elastic moduli using ultrasonic measurements (BI_{elastic} dynamic) or triaxial experiment data (BI_{elastic} static).
Brittleness index BI_{mineral} is calculated based on XRD measurements for laboratory deformed samples or borehole mineralogy data. For the Eagle Ford Formation from outcrop, BI_{mineral} (borehole) is based on XRD result from the same or nearby horizon as deformed samples. BI_{mineral} (borehole) for reservoir samples is based on petrophysical mineralogy model.

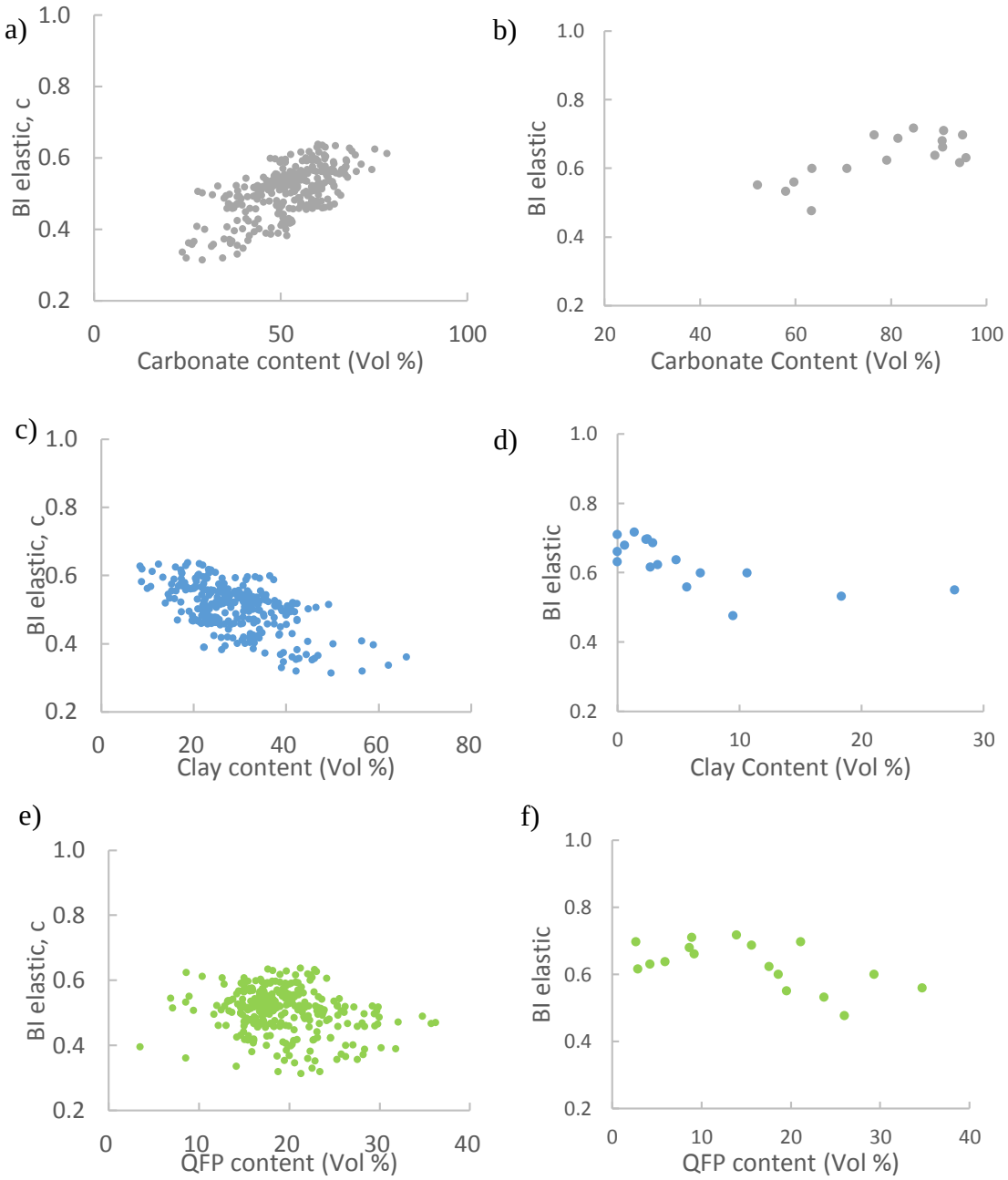

Figure 4.5 Relationship between elastic moduli related brittleness and composition. *BI* $_{\text{elastic, c}}$ is derived from thermo neutron porosity log, dynamic Young's modulus, and Poisson's ratio from sonic logs. Carbonate, clay, and QFP content (a,c,e) are from petrophysical model of formation composition. *BI* $_{\text{elastic}}$ is based on static elastic properties measured in the lab under 1 MPa confining pressure. Carbonate, clay, and QFP content (b,d,f) are from XRD composition result.

4.3.3. Evaluation of Indirect Brittleness Indices

The composition-based brittleness index $BI_{mineral}$ of the Eagle Ford Formation represents the stiff components in the samples, a strong correlation between $BI_{mineral}$ and Young's modulus is expected with the assumption that the stiff material in the shale contributes most to elastic behavior. $BI_{mineral}$ shows an increasing trend with increasing Young's modulus until the transition when Young's modulus reaches about ~ 35 GPa (Fig. 4.6a). Beyond the transition, $BI_{mineral}$ does not vary with Young's modulus. The transition point corresponds to the carbonate facies boundary from mud-supported to grain-supported rock. It is also noticeable that most grain-supported facies only contain less than 5 vol% clay. When clay fraction in the grain-supported facies is low and the samples are predominantly composed of stiff minerals (e.g., carbonate), mineralogical impact on Young's modulus becomes minimal.

$BI_{mineral, c}$ and $BI_{mineral, o}$ of the subsurface and outcrop wellbores are determined from mineralogical petrophysical logs based on wireline data and ranges from 0.29 to 0.97. Both brittleness indices are positively related to dynamic Young's modulus (Fig. 4.6b). $BI_{mineral, o}$ is also determined from XRD measurements of samples taken from the borehole at the outcrop site, yet XRD based $BI_{mineral, o}$ does not correlate well with Young's modulus, which may result from the resolution of different measurements. $BI_{mineral, o}$ determined from XRD of a sample measures composition within few cm intervals, whereas the Dynamic Young's modulus is measured over a meter interval and thus averages multiple lithologies.

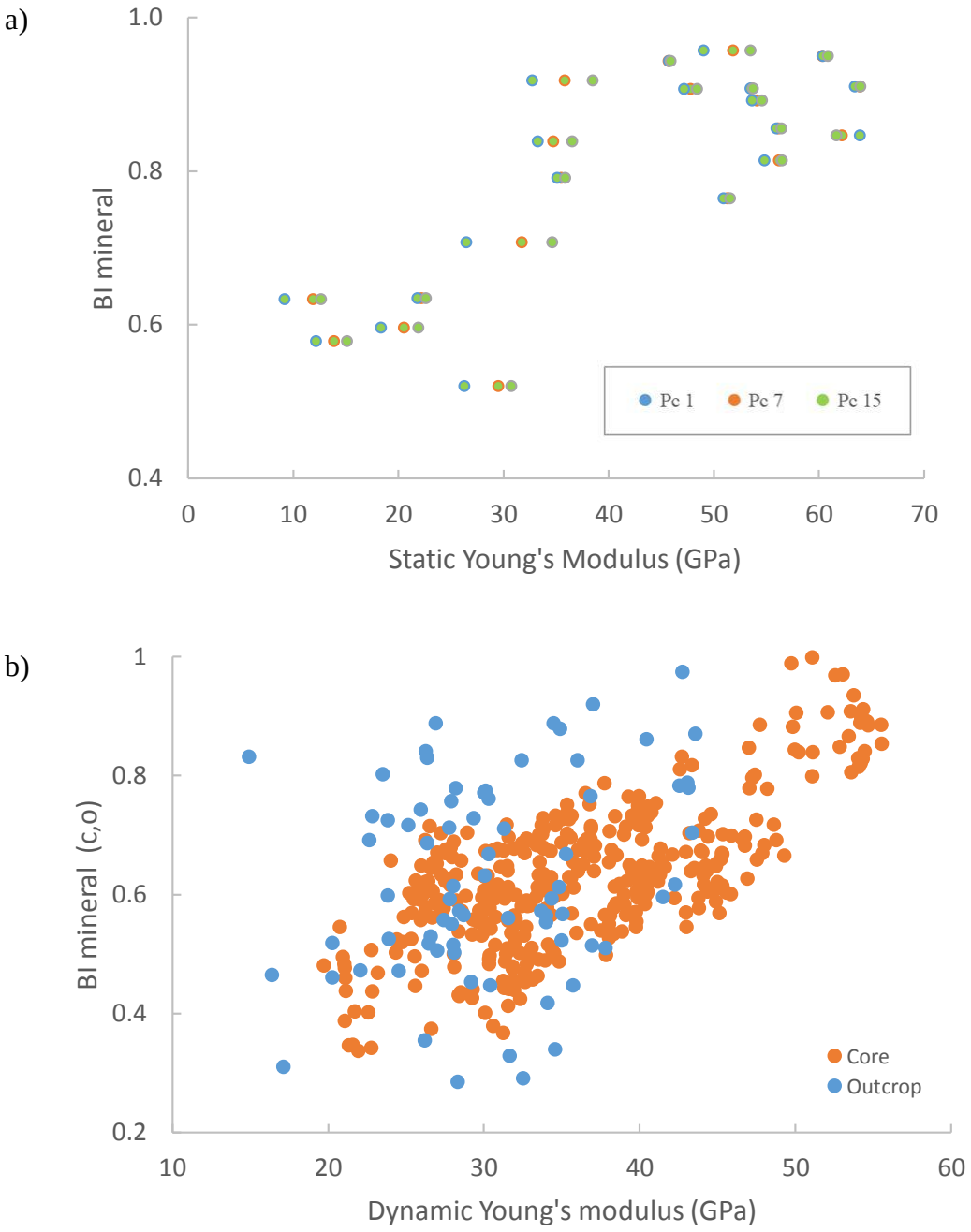

Figure 4.6 Mineralogic based brittleness index $BI_{mineral}$ as a function of Young's modulus. **a.** $BI_{mineral}$ of Eagle Ford samples is determined from Eq 4.1 based on XRD result. Static Young's modulus is determined from laboratory rock deformation tests. **b.** $BI_{mineral,c,o}$ is brittleness determined from a petrophysical model of core and outcrop borehole logs. Static Young's modulus is derived from sonic logs.

4.4. Discussion

4.4.1. Evaluating Indirect Determinations of Rock Strength

Unconfined compressive strength (UCS) of a rock is an important parameter that influences many engineering problems such as borehole instability, hydraulic fracture stimulation, reservoir production. Many studies have utilized geophysical logging data such as velocity to predict UCS or rocks. In this study, UCS is inferred from a series of triaxial experiments from 1 MPa to 15 MPa confining pressure assuming a linear relationship between a maximum stress and minimum stress (confining pressure). The relationship between UCS and mechanical properties from lab tests are explored. Compared to ductile rocks, one of the characteristics of brittle rocks is higher strength and higher Young's modulus. Therefore a correlation between brittleness and strength of the rock is expected. A positive correlation is found between static Young's modulus measured in the lab and UCS of samples. Mudstone facies with higher clay fraction show lower Young's modulus of ~22 GPa under 1 MPa confining pressure and a UCS of ~ 130 MPa. Packstone/grainstone facies with mostly carbonate minerals and few clay minerals has Young's modulus and UCS up to 65 GPa and 260 MPa, 3 times and 2 times greater than mudstone facies. Similarly, a positive relationship between elastic moduli based brittleness BI_{elastic} and UCS is also observed. When BI_{elastic} increases from 0.5 to 0.7, UCS or samples increases greatly from ~130 MPa to ~270 MPa (Fig. 4.7 a).

UCS can also be determined from geophysical borehole logs such as Vp (interval transit time), dynamic Young's modulus, and porosity (Horsrud, 2001; Lal, 1999). Lab-

based UCS profile can also be used to compare to log-based UCS to validate the use of lab-based mechanical stratigraphic model as well as and calibrate the log-derived UCS profiles.

a)

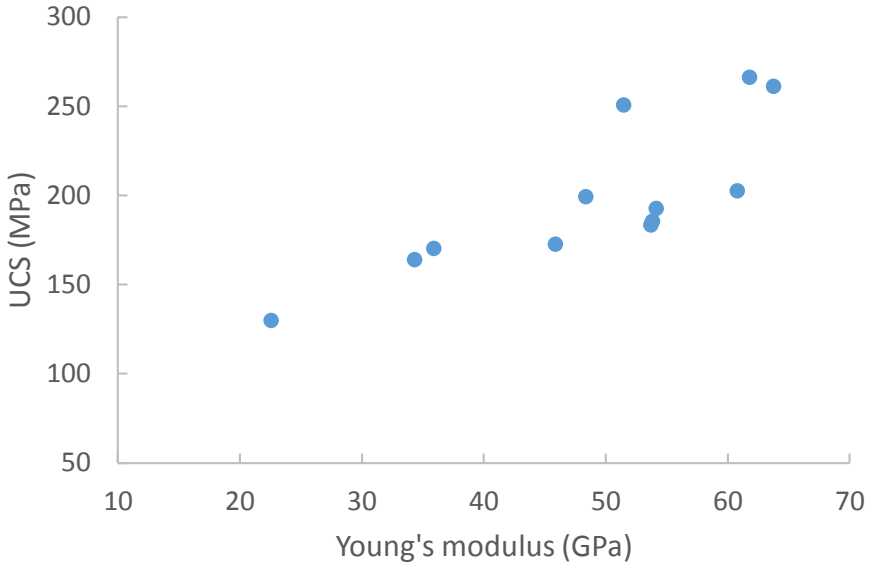

b)

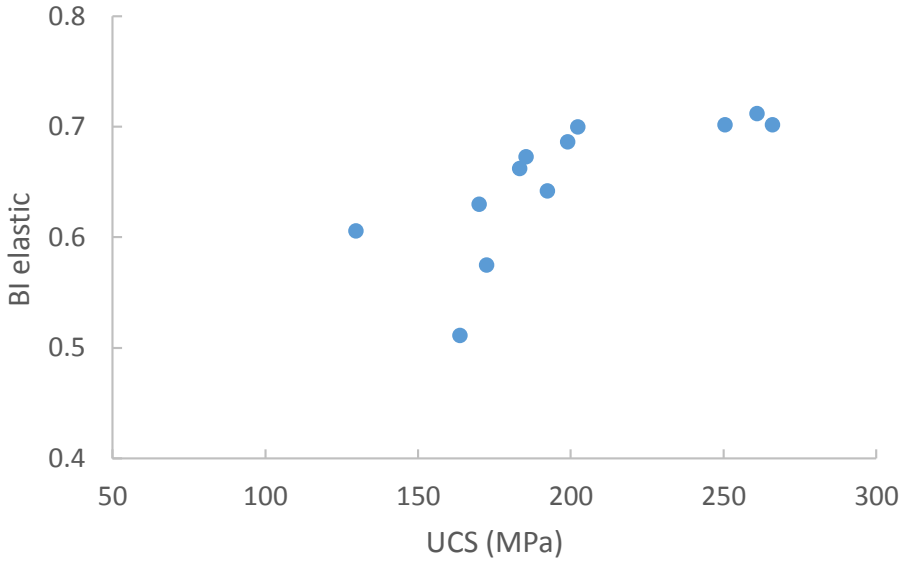

Figure 4.7 Relationship between Young's modulus and UCS of samples (**a**) and relationship between brittleness index $BI_{elastic}$ and rock strength of the samples (**b**).

4.4.2. Comparison of Brittleness Indices

Composition-based brittleness index BI_{mineral} of the Eagle Ford Formation used weight fraction of the stiff components calcite and quartz minerals relative to all components. The advantage of using a composition-based brittleness index BI_{mineral} is to get a continuous log for brittleness by using rock mineralogical logs (e.g., ECS™, Litho Scanner™), composition model derived from petrophysical well-log evaluation, or XRD measurements. It could also capture characteristics of rocks that are not accessible for laboratory testing such as samples that are too fragile to test. However, as discussed above in section 4.3.2, the BI_{mineral} indices do not appear particularly effective for providing a unique or accurate definition of brittleness, modulus or other mechanical parameters. This is partly because the indices treat the quartz component as a stiffening mineral; however, it is clearly demonstrated herein that increasing quartz fraction actually reduces strength (Fig. 2.12b), modulus (Fig. 2.12b) and brittleness (Fig. 4.5 e,f) for the Eagle Ford Formation.

Elastic property-based brittleness *BI* elastic is more widely used in industry than triaxial test-based brittleness because it is easier to obtain a continuous measurement of elastic properties in situ with logging tools, and thus brittleness indices may be easily determined. Moreover, triaxial experiments show that for the Eagle Ford Formation, elastic moduli are well correlated with each other, and to inelastic mechanical properties such as *Co* (*UCS*), ductility, ultimate strength, BI_{yield}, and BI_{energy}.

Laboratory determined Young's modulus, and both BI_{elastic} and $BI_{\text{elastic, c}}$ determined for the Eagle Ford Formation show a positive correlation with rock carbonate content and are negatively related to rock clay content (Fig. 4.5a-d). It is consistent with the observation that Young's modulus and Poisson's ratio of the Eagle Ford Formation increase from mud-supported facies to grain-supported facies, associated with an increase in carbonate content and a decrease in clay content. QFP is the common component in the Eagle Ford Formation and it is often considered as the stiff phase for many reservoir rocks. However, in the Eagle Ford, feldspar is rare and content of pyrite is much less than quartz content. Quartz mineral is more abundant in mud-supported facies than grain-supported facies. In mudstone and wackestone, quartz commonly exists as authigenic cements or microcrystalline cements that fill porosity in the rock matrix in the Eagle Ford samples (McAllister, 2017). Apparently, for the Eagle Ford, quartz cement that is associated with clays or among coccolith fragments do not serve as a load-bearing framework. Thus, with increasing quartz cements distributing throughout the matrix, stiff phase in the rock such as carbonate decreases, elastic moduli based brittleness index therefore decreases.

Mineralogy is important to elastic moduli based rock brittleness and BI_{elastic} shows a positive relationship with BI_{mineral} (Fig. 4.8a, b). The pitfall of using an elastic moduli based brittleness is that it does not truly identify rock brittle behavior relative to its ductile deformation. In addition, BI_{elastic} uses the empirical relation of brittleness and

elastic moduli (Eq. 4.2) is based on biogenic quartz-rich Barnett Shale and the Eagle Ford is a calcareous rich formation.

BI_{yield}, BI_{energy}, and $BI_{\text{post-failure}}$ are indices that correctly capture the pressure dependence of brittleness as shown in triaxial compression tests. With increasing confining pressure, rock ductility increases and brittleness indices decrease. The disadvantage of using laboratory tests based brittleness is that these inelastic properties are not easily obtained for routine application in industry. With the correlation of mechanical properties with lab-based brittleness indices and other brittleness indices, inelastic properties can be determined from elastic properties. These brittleness indices reveal rock brittle deformation relative to its ductile deformation under varying pressure conditions. BI_{yield} and BI_{energy} are based on pre-failure elastic and plastic deformation of the rock, using strain and energy consumption of the rock, respectively. BI_{yield} is thus positively correlated with BI_{energy} as expected (Fig. 4.8c). These two brittleness indices are also related to carbonate facies. From mud-supported facies to grain-supported facies, rock carbonates content increase, clay, and organic matter decrease, and plastic deformation relative to elastic deformation of the rock decreases. The brittleness of the rock, therefore, increases. However, BI_{yield} and BI_{energy} are not found to directly relate to existing mineralogy-based brittleness indices as discussed above. $BI_{\text{post-failure}}$ is based on post-failure stress drop of the rock, which captures varying degrees of ductile behavior after rock fails. Brittle rocks tend to have higher rock fracture strength, less inelastic strain prior to and after fracturing, and larger stress drop after rock failure. Therefore, *BI*

$_{\text{post-failure}}$ is also positively correlated with BI_{yield} (Fig. 4.8d). $BI_{\text{post-failure}}$ is most sensitive to pressure change compared to BI_{yield} and BI_{energy}. More distributed ductile deformation occurs after rock fails at higher confining pressure, which represented as high residual strength and strain hardening from the stress-strain curve. The pressure dependency of $BI_{\text{post-failure}}$ is about the same for different types of shales. As respect to carbonate facies, $BI_{\text{post-failure}}$ does not show any correlation with lithology. Therefore, $BI_{\text{post-failure}}$ is not an ideal brittleness index to compare different carbonate facies under various certain pressure conditions.

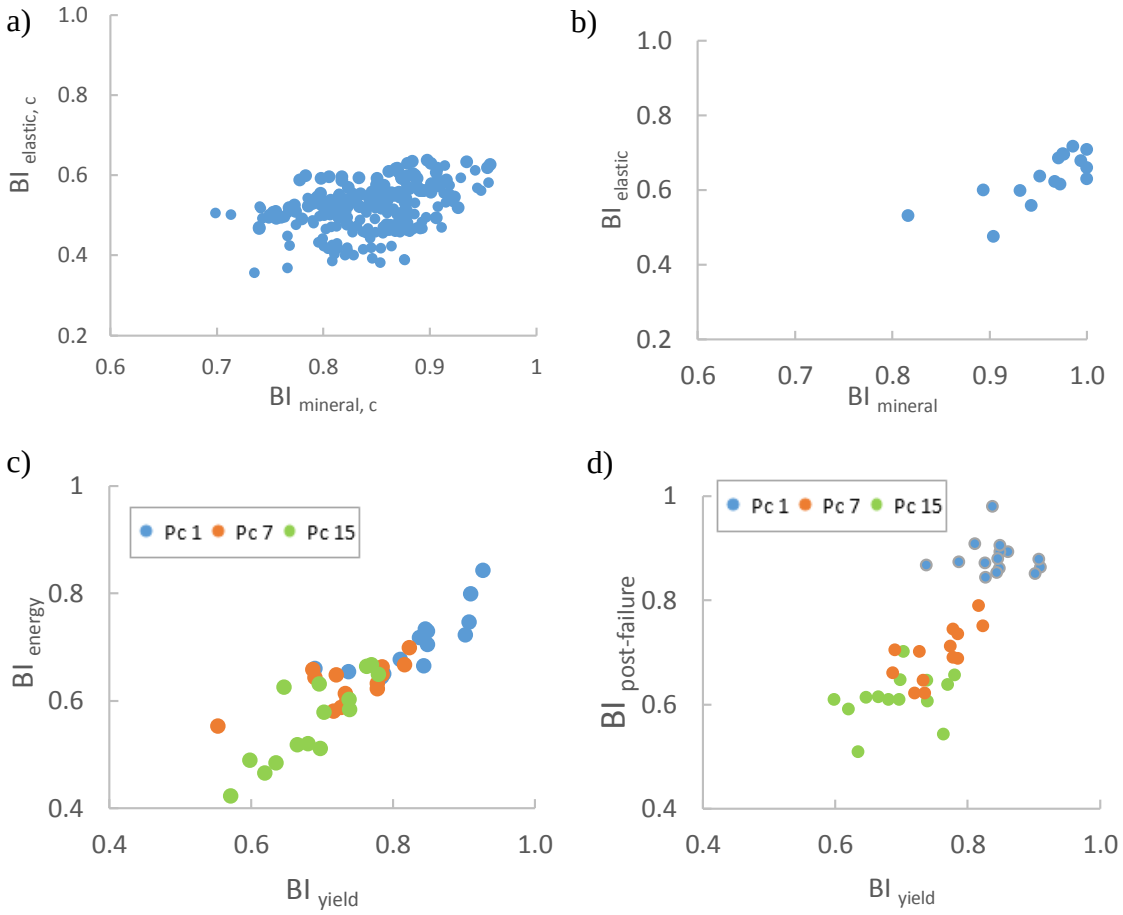

Figure 4.8 Relationship between different brittleness indices. **a, b.** A relationship between $BI_{elastic}$ and $BI_{mineral}$ for subsurface core and lab deformed samples. **c.** The relationship between BI_{yield} and BI_{energy} of the samples. **d.** A relationship between BI_{yield} and $BI_{post\text{-}failure}$ of the samples.

4.4.3. Correlation Between Brittleness and Other Rock Mechanical Properties

One of the characteristics of brittle rocks is high Young's modulus and low Poisson's ratio which corresponds to stronger ability to maintain a new fracture (Hucka and Das, 1974). It is supported by a positive correlation observed between Young's modulus and rock brittleness (Rickman et al., 2008). Since elastic moduli based

brittleness index is derived from Young's modulus and Poisson's ratio. A strong correlation between $BI_{elastic}$ and Young's modulus is observed as expected (Fig. 4.9), and the correlation yields the following equation:

$$BI_{elastic} = 0.287\ E^{0.213} \quad R^2=0.81,$$

$BI_{elastic}$ also correlates well with rock fracture strength (Fig. 4.10a), with a correlation as：

$$BI_{elastic} = 0.0623\ \sigma^{0.437} \quad R^2=0.87,$$

Composition based brittleness also shows a positive relationship with Young's Modulus for mud-supported facies (mudstones and wackestones), indicating that the stiff component of the rock contributes to its brittle nature (Fig. 4.9). At the transition point where rock Young's modulus is around ~37 GPa, the volume fraction of stiff material has the biggest change. Beyond the transition of carbonate facies, the correlation between $BI_{mineral}$ and Young's modulus diminishes for packstones and grainstones facies. Factors other than mineralogy could play a more important role in rock Young's modulus for grain-supported carbonate rocks. The correlation between $BI_{mineral}$ and Young's modulus is not very strong and is not even observed in some studies (Yang et al., 2013). Rock composition derived brittleness is also not directly correlated to rock inelastic properties such as rock compressive strength. However, with a modified definition of composition based brittleness that includes TOC and porosity of the rock, a stronger correlation between $BI_{mineral}$ and Young's modulus is observed (Fig. 4.9, Rybacki et al., 2016).

Triaxial tests based brittleness BI_{yield} captures features of rock brittle behavior relative to its ductile deformation. It shows a positive trend with both rock Young's modulus and fracture strength (Fig. 4.9, 4.10b). Since BI_{yield} is pressure dependent, the correlation is performed under each confining pressure as below:

For Pc =7 MPa

$BI_{yield} = 0.268\ E^{0.267}$ $R^2=0.91$

$BI_{yield} = 0.223\ \sigma^{0.233}$ $R^2=0.7$

For Pc =15 MPa,

$BI_{yield} = 0.279\ E^{0.234}$ $R^2=0.81$

$BI_{yield} = 0.175\ \sigma^{0.257}$ $R^2=0.66$

The data at 1 MPa confining pressure shows a larger uncertainty and the relationship is thus not included here. The relationship between Young's modulus and BI_{energy} that is on the basis of energy/work prior to rock failure is not observed in this study, yet a strong correlation is observed in other black shales (Fig. 4.9, Rybacki et al., 2016). Besides, $BI_{post\text{-}failure}$ has shown relationships with rock compressive strength. Similar to BI_{yield}, with increasing confining pressure, the strength dependence of rock brittleness increases. $BI_{post\text{-}failure}$ is more sensitive to pressure change than BI_{yield}.

Overall, power-law relationships are found between rock brittleness and rock elastic properties (Young's modulus) and inelastic properties (compressive strength). The correlation between different rock brittleness and Young's modulus are consistent with observations in other shale formation (Rybacki et al., 2016). The correlation of $BI_{elastic}$, and BI_{yield} relative to rock Young's modulus is similar. On the other hand, the

correlation of brittleness indices and rock compressive strength shows a larger variation. The general trends are overall similar.

4.4.4. Application in Production and Completion of Eagle Ford Reservoirs

Economically viable production from the low permeable shale gas reservoirs relies on horizontal drilling and hydraulic fracturing. Key processes of successful hydraulic fracture stimulation include effective initiation of multi-stages of hydrofracture along the well, propagation of new fractures and reactivation of pre-existing fractures, and preservation of fracture conductivity during long-term production. Rock mechanical properties, in-situ stress, and engineering parameters are the primary control on the result of hydrofracture stimulation. Brittleness indices are thus used to differentiate brittle/ductile deformation of formation rocks and assist in determining the position of lateral well. Various types of brittleness indices would help evaluate easy of initiation, the ability of a rock to resist fracture propagation, and healing of fractures.

Initiation of hydraulic induced fractures requires fracture toughness to be overcome by break down pressures, which depend on in-situ stress states and rock tensile strength. Favorable conditions for fracture initiation are low stress, low toughness, and low tensile strength. The primary stress that affects break down pressure is the least horizontal stress (S_{hmin}). The magnitude of S_{hmin} is constrained by elastic and inelastic deformation of formation rock. Mode I fracture toughness is related to rock tensile strength and ductility. Rock with high tensile strength suggests high toughness and high break down pressure. Based on Griffith failure criteria, rock tensile strength is

positively correlated with Young's Modulus and Poisson's Ratio. However, pre-existing natural fractures are very likely present in the reservoir as rock volume increases, leading to a decrease in rock tensile strength. In addition, the magnitude of in-situ stress increases with depth, then tensile strength of the rock is negligible. Therefore, fracture toughness is the primary control of fracture initiation. Fracture toughness is related to critical energy, Young's Modulus, and Poisson's ratio. BI_{yield}, BI_{energy}, and $BI_{elastic}$ are indicators for evaluating a favorable condition of fracture initiation. *BI* elastic includes Young's modulus and Poisson's ratio. BI_{yield} and BI_{energy} describe ductility of the rock before failure in compression tests. It is similar to fracture toughness in a way that toughness also captures the ability of the material to deform plastically before fracture although toughness is measured in tension. A rock with higher brittleness would have large elastic energy before failure and low toughness.

Propagation of hydraulic induced fractures is predominantly controlled by the in-situ stress states of the reservoir, mainly minimum horizontal stress (S_{hmin}) as the fracture is propagating perpendicular to the minimum stress in a basinal setting. S_{hmin} is influenced by Young's modulus and Poisson's ratio of the rock, and burial/lithification history, and is likely correlated locally with the mechanical stratigraphic properties of stratigraphic multilayer units at different scales. Propagation within a layered sequence of sedimentary reservoir rocks would also depend on lithology variation and interface properties (i.e. frictional strength), which could result in locally large contrast of S_{hmin} in adjacent layers. Fracture growth in the vertical direction is influenced by the presence of

a high-stress zone. A layer with high-stress can serve as a fracture barrier and will limit the fracture height. The adjacent layer with low-stress, on the other hand, will trap the fracture. The fracture will contain in the low stress layer and grow laterally into the formation. The width of the fracture is related to Young's modulus. Lower Young's modulus would imply a larger fracture width and shorter fracture length and height. Since $B_{elastic}$ depends on Young's modulus, it can provide insights into fracture geometry and pattern in different layers during fracture propagation. $BI_{post\text{-}failure}$ may also be useful to assess post-failure energy release after rock propagates. With increasing ductility, energy is released through more plastic deformation after rock fails. This can be used to assess the efficiency of hydraulic fracture propagation in different types of shales.

From the geologic aspect, long-term production of the shale gas reservoir is influenced by stress change through time and healing of induced fractures, which is associated with proppant embedment and creep behavior of rocks. Time-dependent long-term creep behavior of the shale depends on the mineralogy of the rock (i.e. clay content) and is very sensitive to temperature and anisotropy of the rock. Shales with high clay content has shown more creep deformation. Therefore, $BI_{mineral} / (1\text{-}BI_{mineral})$ may be a good indicator of long-term preservation of hydraulic fracture conductivity as $BI_{mineral}$ includes minerals other than clay. Relationship between shale creep behavior and elastic properties has been studied as elastic moduli are easier to obtain from well-log data (Sone and Zoback, 2013a, 2013b). Young's modulus is negatively correlated with

the creep compliance of the shale. Elastic property derived brittleness BI_{elastic} could also be a good assessor to compare healing of fractures in different types of shale.

In the context of hydraulic fracture treatment design, some brittleness indices are more critical than others to assess controls on different stages of hydraulic fracturing process: initiation, propagation, and preservation of hydraulic induced fractures. A comprehensive analysis of brittleness indices can lead to a successful hydraulic fracture treatment plan.

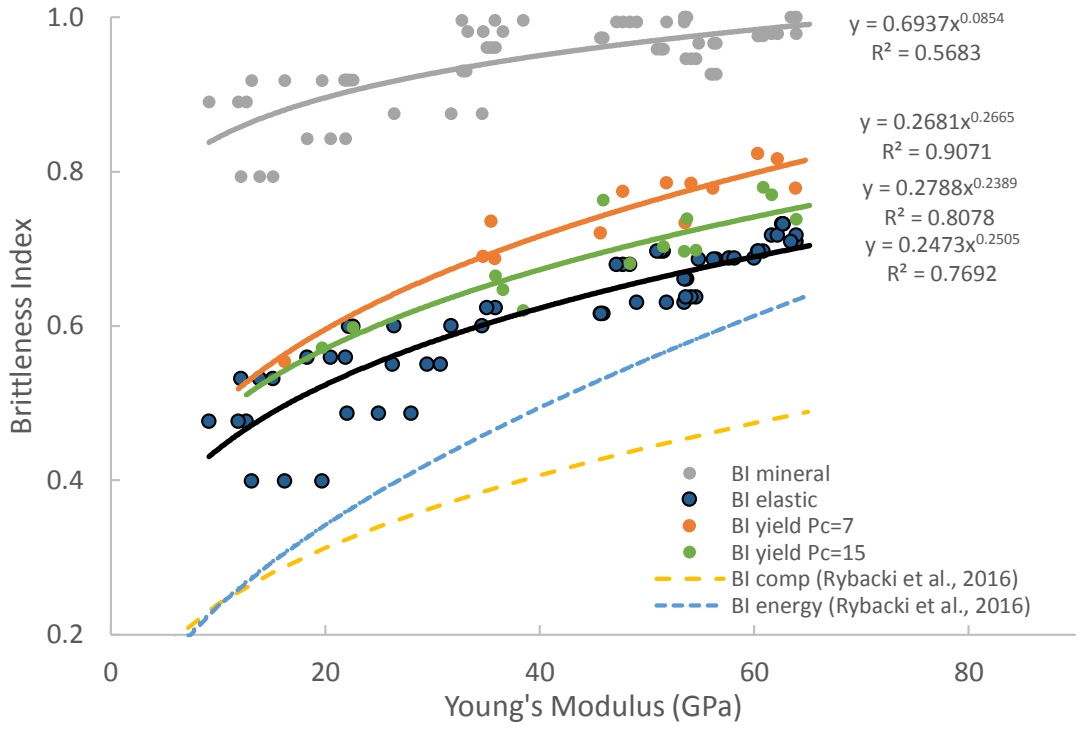

Figure 4.9 A comparison of brittleness indices BI_{mineral}, BI_{elastic}, and BI_{yield} as a function of Young's modulus. Correlation of pressure dependent brittleness index BI_{yield} and Young's modulus is fitted for 7 MPa and 15 MPa confining pressures, respectively. The correlation between composition and energy based brittleness indices and Young's modulus are plotted for comparison (based on Rybacki et al., 2016).

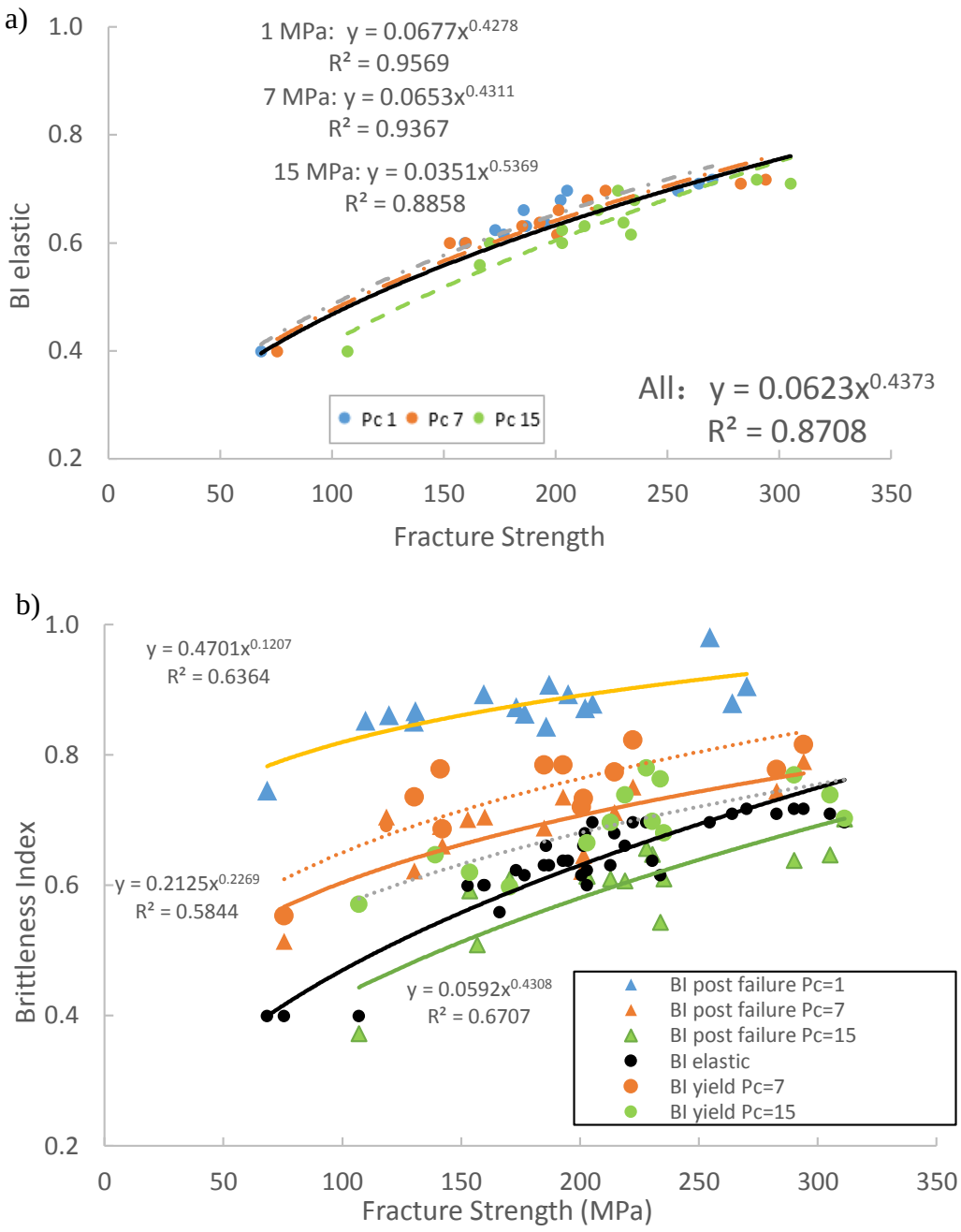

Figure 4.10 Relationship between brittleness indices and fracture strength. **a.** Relationship between BI_{elastic} with rock fracture strength. **b.** A summary of rock brittleness and its relation to rock fracture strength. Correlations of $BI_{\text{post-failure}}$ and rock fracture strength are fitted with power law for tests performed under 1 MPa, 7 MPa, and 15 MPa confining pressure.

4.5. Conclusions

A wide range of elastic and inelastic properties of the Eagle Ford Formation is observed based on laboratory rock deformation tests. Combined with lithologic, mineralogical, and textural analyses, several empirical relationships are built between geomechanical properties and physical properties. The Young's modulus and rock strength are strongly affected by rock composition and texture. Empirical relationships established between laboratory mechanical properties and geophysical logs overall agrees with shales trend worldwide despite uncertainties due to the sample conditions and scale of measurement. In order to apply laboratory data to exploration and production of shale gas reservoir, mechanical stratigraphic models of the Eagle Ford Formation are established and formation brittleness is assessed to address many field applications including wellbore stability, hydraulic fracture stimulation, shale gas recovery through fracturing.

Mechanical stratigraphic models are built based on laboratory geomechanical properties of individual lithologies and lithostratigraphic characterization. The model is also made on the basis of empirical relationships between physical (geophysical logs) and geomechanical properties. Based on the specific rock mechanical properties, they are upscaled to bulk behavior of layered units using different models. The variation of static Young's modulus upscaled using Ruess iso-stress model is mostly consistent with geophysical derived dynamic Young's modulus. Considering the uncertainty, the variation of a single rock mechanical properties within a section provides more insights

into reservoir production compared to values of upscaled properties. The mechanical stratigraphic model of the Eagle Ford Formation shows that the formation has great heterogeneous and anisotropic from micro- to field scale.

Brittleness indices of the Eagle Ford Formation are obtained based on triaxial experiment data, geophysical logs, and rock composition. Values of BI_{mineral} is much higher for all rock types than the other brittleness due to its definition. BI_{mineral}, BI_{elastic}, BI_{yield}, and BI_{energy} increases from mud-supported facies to grain supported facies. Among these, BI_{elastic} is more closely related to mineralogy and porosity. Generally, brittleness increases with an increase in carbonate content, and with a decrease in clay, porosity, and content of quartz. The relationship between brittleness and rock mechanical properties of the Eagle Ford Formation can be represented as power-law functions. Young's modulus is positively correlated with the stiff phase of the rock (BI_{mineral}) and pre-failure elastic strain relative to total strain (BI_{yield}). Rock compressive strength is correlated with elastic property related brittleness (BI_{mineral}) and brittleness indices that capture brittle versus ductile deformation such as BI_{yield} and $BI_{\text{post-failure}}$.

Although brittleness is not a true measure of rock mechanical properties. Based on a variety of definitions, brittleness could capture certain mechanical behavior during rock deformation from a different aspect. An assessment of a series of brittleness could help to apply brittleness indices to the determination of favorable conditions for shale gas exploration and production. BI_{elastic}, BI_{yield}, and $BI_{\text{post-failure}}$ are good indicators for evaluating a favorable condition of fracture initiation and growth of the fractures.

4.6. References

Baroni, A., Delorme, M., and Khvoenkova, N., 2015. Forecasting production in shale and tight reservoirs: a practical simulation method capturing the complex hydraulic fracturing physics. In SPE Middle East Oil and Gas Show and Conference. Society of Petroleum Engineers. 10.2118/172831-MS.

Basu, N., Barzola, G., Bello, H., Clarke, P., & Viloria, O., 2012. Eagle Ford reservoir characterization from multisource data integration. AAPG Search and Discovery. Article #80234

Campbell, C. V., 1967. Lamina, laminaset, bed and bedset. Sedimentology, 8(1), 7-26.

Dunham, R. J., 1962. Classification of carbonate rocks according to depositional texture, in W. E. Ham, ed., Classification of carbonate rocks—A symposium: American Association of Petroleum Geologists Memoir 1, p. 108–121.

Gardner, R.D., Pope, M.C., Wehner, M.P., and Donovan, A., 2013. Comparative Stratigraphy of the Eagle Ford Group Strata in Lozier Canyon and Antonio Creek, Terrell County, Texas. GCAGS Journal, v. 2, p. 42–52.

Glorioso, J. C., and Rattia, A., 2012. Unconventional reservoirs: basic petrophysical concepts for shale gas. In SPE/EAGE European Unconventional Resources Conference and Exhibition-From Potential to Production. 10.2118/153004-MS.

Griggs, D., & Handin, J., 1960. Rock deformation. Geological Society of America NY 382pp.

Gu, H., and Siebrits, E., 2006. Effect of formation modulus contrast on hydraulic fracture height containment. In International Oil and Gas Conference and Exhibition in China. Society of Petroleum Engineers. 10.2523/103822-MS.

Hajiabdolmajid, V., and Kaiser, P., 2003. Brittleness of rock and stability assessment in hard rock tunneling. Tunnelling and Underground Space Technology, 18(1), 35-48.

Handin, J., and Hager Jr, R. V., 1957. Experimental deformation of sedimentary rocks under confining pressure: Tests at room temperature on dry samples. AAPG Bulletin, 41(1), 1-50.

Heard, H. C., 1960. Transition from Brittle to Ductile Flow in Solenhofen Limestone as a Function of Temperature. Confining Pressure, and Interstitial Fluid Pressure, Rock Deformation, 193-22.

Hill, R., 1952. The elastic behaviour of a crystalline aggregate. Proceedings of the Physical Society. Section A, 65(5), 349.

Hucka, V., and B. Das., 1974. Brittleness determination of rocks by different methods, International Journal of Rock Mechanics and Mining Sciences and Geomechanics Abstracts, 11(10), 389–392.

Holt, R. M., Fjaer, E., Nes, O. M., and Alassi, H. T., 2011. A shaly look at brittleness. In 45th US Rock Mechanics/Geomechanics Symposium. American Rock Mechanics Association.

Horsrud, P., 2001. Estimating mechanical properties of shale from empirical correlations. SPE Drilling and Completion, 16(02), 68-73.

Jarvie, D. M., Hill, R. J., Ruble, T. E., and Pollastro, R. M, 2007. Unconventional shale-gas systems: The Mississippian Barnett Shale of north-central Texas as one model for thermogenic shale-gas assessment. AAPG bulletin, 91(4), 475-499.

Lal, M., 1999. Shale stability: drilling fluid interaction and shale strength. In SPE Asia Pacific Oil and Gas Conference and Exhibition. Society of Petroleum Engineers. SPE 54356

Luan, X., Di, B., Wei, J., Li, X., Qian, K., Xie, J., and Ding, P., 2014. Laboratory measurements of brittleness anisotropy in synthetic shale with different cementation. In SEG Technical Program Expanded Abstracts Society of Exploration Geophysicists. pp. 3005-3009

Mavko G, Mukerji T, Dovrkin J., 2009. The Rock Physics Handbook: Tools for Analysis of Porous Media. Cambridge: Cambridge University Press. p. 185–90.

Maxwell, S. C., and Cipolla, C. L., 2011. What does microseismicity tell us about hydraulic fracturing? In SPE Annual Technical Conference and Exhibition. Society of Petroleum Engineers. 4. 10.2118/146932-MS.

Mcallister, R. 2017. Diagenetic modifications of the Eagle Ford Formation: implications on chemical and physical properties. Doctoral Dissertation, University of Manchester.

Reuss, A., & Angnew, Z., 1929. A calculation of the bulk modulus of polycrystalline materials. Math Meth, 9, 55.

Rickman, R., Mullen, M., Petre, E., Grieser, B. and Kundert, D., 2008. A practical use of shale petrophysics for stimulation design optimization: all shale plays are not clones of the Barnett Shale. SPE 115258.

Rybacki, E., Meier, T., and Dresen, G., 2016. What controls the mechanical properties of shale rocks?–Part II: Brittleness. Journal of Petroleum Science and Engineering, 144, 39-58.

Sone, H., and Zoback, M. D., 2013. Mechanical properties of shale-gas reservoir rocks—Part 1: Static and dynamic elastic properties and anisotropy. Geophysics, 78(5), D381-D392.

Sone, H. and Zoback, M.D., 2013. Mechanical properties of shale-gas reservoir rocks—Part 2: Ductile creep, brittle strength, and their relation to the elastic modulus. Geophysics, 78(5), pp. D393-D402.

Tarasov, B., and Potvin, Y., 2013. Universal criteria for rock brittleness estimation under triaxial compression. International Journal of Rock Mechanics and Mining Sciences, 59, 57-69.

Teufel, L. W., Hart, C. M., Sattler, A. R., and Clark, J. A., 1984. Determination of hydraulic fracture azimuth by geophysical, geological, and oriented-core methods at the Multiwell Experiment Site, Rifle, CO. In SPE Annual Technical Conference and Exhibition. Society of Petroleum Engineers. SPE 13226

Van Der Baan, M., Eaton, D., and Dusseault, M., 2013. Microseismic monitoring developments in hydraulic fracture stimulation. In ISRM International Conference for Effective and Sustainable Hydraulic Fracturing. International Society for Rock Mechanics and Rock Engineering. 10.5772/56444.

Voigt, W. (1889). Ueber die Beziehung zwischen den beiden Elasticitätsconstanten isotroper Körper. Annalen Der Physik, 274(12), 573-587.

Yao, Y., 2012. Linear elastic and cohesive fracture analysis to model hydraulic fracture in brittle and ductile rocks. Rock Mechanics and Rock Engineering, 45(3), 375-387.

Wang, F.P., and Gale J.F.W., 2009. Screening criteria for shale-gas systems: GCAGS Transactions, v. 59, p. 779-793.

Zhang, D., Ranjith, P. G., and Perera, M. S. A., 2016. The brittleness indices used in rock mechanics and their application in shale hydraulic fracturing: A review. Journal of Petroleum Science and Engineering, 143, 158-170.

5. SUMMARY

Mechanical stratigraphy strongly impacts the growth of hydraulic fractures in shale reservoirs. Without a complete understanding of the properties of the target and surrounding intervals, it is hard to predict the bulk mechanical response of these zones, including the surrounding layers. Due to limited access to the core from productive fields, a complete mechanical characterization often is lacking. Outcrop and core from a condensate producing reservoir provide a great opportunity to characterize the geomechanical properties of individual and composite lithologic units of the Cretaceous carbonaceous Eagle Ford Formation over length scales of a decimeter to tens of meters. This study employs extensive triaxial deformation experiments on samples of the Eagle Ford Formation, as well as detailed lithostratigraphic characterizations of the sampled outcrop and subsurface well site, to define the elastic and inelastic properties and relate them to lithologic characteristics.

The Eagle Ford Formation exhibits a wide variation in elastic modulus as a function of carbonate facies. The reservoir rock samples also show a moderate pressure dependency when compared to the outcrop samples, especially under low-pressure conditions. The latter difference is likely related to crack-like pores and microcracks in the reservoir rocks that result from decompression. Under reservoir conditions, Young's modulus and Poisson's ratio increase by a factor of 4 and 1.5, respectively. Young's modulus and Poison's ratio increase similarly with an increase in carbonate content, and a decrease in organic matter and clay mineral fraction. Young's modulus also increases

with an increase in the ratio of grains to mud-size particles, quantified by the grain fraction. This latter relation is most significant for the mudstone and wackestone facies with relatively large mud matrix. Both Young's modulus and Poisson's ratio of the Eagle Ford Formation can display anisotropy with a directional variation of ~40%, most notably in micro-laminated and clay-rich rocks. The degree of anisotropy is positively correlated with clay mineral content, with the greatest change occurring in mud-supported facies.

The inelastic strength properties of yield strength, ultimate strength, and coefficient of sliding friction are determined as a function of confining pressure to quantify failure criteria and a fracture mode criterion appropriate to hydrofracture. The ultimate strength increases by a factor of 2 from the mudstone to packstone/grainstone facies. Ultimate strength increases gradually with confining pressure. All carbonate facies deformed by formation of brittle failure macroscopic faulting displaying the greatest localization under low-stress conditions. The angle of the failure plane is not sensitive to facies type, yet it does increase with confining pressure. Clay minerals have a significant impact on ultimate strength and decrease by 50% for clay contents ranging from 0 to ~10%. Yet increasing clay mineral content does not promote an increase in ductility over the conditions tested. The ultimate strength increases with increasing grain fraction for samples with 0-50% grain fraction with more subtle changes above 50%.

Based on the laboratory mechanical data, six brittleness indices are derived and compared with the mechanical properties. Most of the brittleness indices increase from

the mud-supported to grain-supported facies. Young's modulus and ultimate strength show a positive trend with the composition-based brittleness and pre-fracture strain based brittleness indices, suggesting that Young's modulus could be used to estimate brittleness of the formation if the rock fails in a predominantly brittle manner.

A mechanical stratigraphic model of the Eagle Ford Formation is constructed based on detailed lithostratigraphic descriptions of the Eagle Ford Formation using visual observations and a relatively simple lithologic classification scheme, and then applying average mechanical properties for each lithology, combined with simple averaging schemes, to determine the effective behavior of the multilayered formation. The mechanical properties of the Eagle Ford Formation vary systematically with mineralogy, composition, and textural characteristics (i.e., recrystallized grains, grain fraction), and effective confining pressure, which can be expressed with quantitative relationships. The experimental data also supports robust quantitative relationships between elastic and inelastic mechanical properties. Accordingly, a mechanical stratigraphic model describing inelastic behaviors including brittleness can be constructed indirectly from geophysical and rock physics interpretation of logging data.